



Technische Universität München

The present work was submitted to the Chair of Space Propulsion and Mobility

presented by

Martin Bernat

Student ID No.: 03741047

Master's Thesis

System Analysis of a Novel Water Electrolysis Propulsion System for a Satellite Mission in Low Earth Orbit

Munich, July 28, 2023

Supervising professor: Prof. Dr.-Ing. Chiara Manfretti

Assistant supervisor: Sören Heizmann, M.Sc.

Eidesstattliche Erklärung

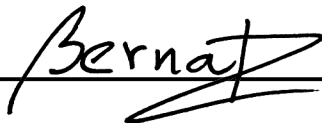
Hiermit erkläre ich, dass die vorliegende Arbeit von mir selbstständig verfasst wurde, und dass keine anderen als die angegebenen Hilfsmittel benutzt wurden. Die Stellen der Arbeit, die anderen Werken dem Wortlaut oder Sinn nach entnommen sind, sind in jedem einzelnen Fall unter Angabe der Quelle als Entlehnung kenntlich gemacht. Diese Erklärung erstreckt sich auch auf in der Arbeit enthaltene Grafiken, Zeichnungen, Kartenskizzen und bildliche Darstellungen.

Ich erkläre mich außerdem damit einverstanden, dass meine Master-, Bachelor- oder Semesterarbeit vom Lehrstuhl auf Anfrage fachlich interessierten Personen, auch über eine Bibliothek, zugänglich gemacht wird, und dass darin enthaltene Ergebnisse sowie dabei entstandene Entwicklungen und Programme vom Lehrstuhl für Raumfahrtantriebe und -mobilität uneingeschränkt genutzt werden dürfen. (Rechte an evtl. entstehenden Programmen und Erfindungen müssen im Vorfeld geklärt werden.)

Ottobrunn, 18/07/2023

Ort, Datum

Unterschrift



Name: Martin Bernat

Matrikelnummer: 03741047

Abstract

Growing demand for deployment of satellites on Low Earth Orbit (LEO), where either drag needs to be compensated for at lower altitudes or de-orbit manoeuvre is necessary for higher altitudes, is a driving force behind efforts to develop a propulsion system that can deal with these challenges while overcoming issues of currently used propulsion subsystems. With most commonly used LEO propulsion subsystem using toxic hydrazine which is unsustainable, expensive and unsafe to handle, an alternative is searched. One candidate is Water Electrolysis Propulsion (WEP) which utilizes water as a propellant that is split on orbit using an electrolyser to provide hydrogen and oxygen which can then be combined to produce higher performance than conventional storable propellants.

Market analysis was performed to find a satellite representative of LEO. This search produced a reference satellite which is yet to be launched - FLuorescence EXplorer (FLEX). To analyse performance of WEP on LEO preliminary design was done which implemented WEP on FLEX to compare its capabilities to the original - hydrazine propulsion. Focus of the preliminary design was on matching their performance while reducing wet mass. To do preliminary design experimental electrolyser data was analysed and mathematical model of an electrolyser was created to enable simulation of operation of a WEP system. This enabled determining areas which are crucial for successful implementation of WEP on LEO and which were explored - setting of electrolyser operating range, pressure effects, hydrogen permeation and thermal management of electrolyser.

Two delta-v budgets for missions in altitudes of 705 and 814 km, similar to FLEX target altitude, were considered and results show the need for optimized delta-v budget as it affects mass of a satellite that uses WEP. Compared to a satellite with conventional propulsion with wet mass of 460 kg WEP provides savings of 1.47 %, leading to a satellite wet mass of 453.25 kg, for a delta-v budget designed for conventional propulsion with possibility of further mass reduction upon delta-v budget optimization for WEP application. This optimization consists of providing sufficient time between manoeuvres to make an electrolyser small and minimize maximum delta-v manoeuvre to reduce size and mass of intermediate tanks.

This research identified critical areas that need to be further explored for implementation of WEP. Minimization of hydrogen leakage - permeation, ensuring compatibility of materials with gaseous hydrogen and optimization of operating range to balance satellite mass, thermal management and efficiency.

Contents

List of Figures	I
List of Tables	III
List of Symbols	V
1. Introduction	1
2. Technological background	3
2.1. Electrolysis	3
2.1.1. Electrolyser types	3
2.1.2. Electrolyser performance	5
2.2. Space propulsion	7
2.2.1. Specific impulse	7
2.2.2. Tsiolkovski rocket equation	8
2.3. Water electrolysis propulsion	8
2.4. Orbital manoeuvres	9
2.4.1. One impulse manoeuvre	9
2.4.2. Hohmann transfer	9
3. Mission analysis	11
3.1. Market Research	11
3.1.1. Selection criteria	11
3.1.2. Satellite analysis	12
3.2. Reference mission selection	17
3.2.1. Validation of the analysis	20
3.3. Reference mission	22
3.3.1. Propulsion requirements	23
4. Preliminary design	31
4.1. List of assumptions	31
4.1.1. Operating temperatures	31
4.1.2. Operating pressures	32
4.1.3. Thruster	32
4.2. Propulsion subsystem	33
4.2.1. Propulsion operation	33
4.2.2. Propulsion subsystem layout	34
4.2.3. Propulsion components mass budget	35

4.3. Tank selection	35
4.3.1. Water tank	38
4.3.2. Intermediate tanks	39
4.4. Electrolyser	43
4.4.1. Electrolyser performance	44
4.4.2. Electrolyser operation modelling	51
4.4.3. Electrolyser thermals	53
4.5. Power subsystem	60
4.6. De-orbit	60
4.7. Mathematical model solver	61
5. Optimization	63
5.1. Current density optimization	63
6. System performance	67
6.1. Nominal performance	67
6.1.1. Tanks	67
6.1.2. Electrolyser	68
6.1.3. Power subsystem and thermals	68
6.1.4. De-orbit	69
6.1.5. Propellant charging cycles	69
6.1.6. System nominal mass	69
6.2. Sensitivity analysis	70
6.2.1. Specific impulse	71
6.2.2. Pressure	72
6.2.3. Permeation	74
6.3. SWOT analysis	74
6.3.1. Strengths	75
6.3.2. Weaknesses	75
6.3.3. Opportunities	76
6.3.4. Threats	76
7. Outlook	79
8. Conclusion	81
Bibliography	83
A. Appendix	87
A.1. Market research data	87

List of Figures

2.1. Diagram of operation of a Proton Exchange Membrane (PEM) cathode vapour feed electrolyser with Water Feed Barrier (WFB)	5
2.2. Electrolyser efficiencies for complete operating range	7
2.3. Diagram of the simplified WEP operation	8
2.4. Hohmann transfer sequence	10
3.1. Distribution of mission types and mission orbits of current and future missions on LEO .	15
3.2. Distribution of average altitudes of LEO satellites	16
3.3. Distribution of launch masses of LEO satellites	17
3.4. Orbital data for satellites CALIPSO and Sentinel-3	24
3.5. Normalized semi-major axis evolution for considered orbits	26
3.6. Inclination evolution for considered orbits	26
3.7. Delta-v manoeuvre timing chart	30
4.1. Proposed fluid diagram for WEP	36
4.2. Mass factors for tank sizing	38
4.3. Electrolyser current densities for voltage settings at different temperatures	44
4.4. Electrolyser performance at different temperatures	45
4.5. Process of extraction of data for experimental measurements	46
4.6. Electrolyser performance dependency on pressure	47
4.7. Dependency of maximum available current density on pressure: pressure-current density curve	48
4.8. Pressure-current density curve for the nominal electrolyser	49
4.9. Effect of pressure on electrolyser performance	50
4.10. Flowchart of simulation of electrolyser operation	52
4.11. Performance of electrolyser represented by charging curves for varying number of cells . .	52
4.12. Sizing of the electrolyser depending on delta-v requirement	53
4.13. Effect of charging cycles on propellants in intermediate tanks	54
4.14. Operating points considered for thermal analysis on current density curve	55
4.15. Evolution of temperatures during electrolyser heat up for different operating points	57
4.16. Heat dissipation rate dependence on electrolyser performance and pressure	58
4.17. Heat dissipation rate (blue) with satellite absorbed heat rate (orange) at different pressures for operating case of maximum available current density. Thermal resistance R_λ was set for maximum current density at 1 bar. Intersection of surfaces shows equilibrium temperature.	59
4.18. Iterative cycle for mass estimation	62

5.1. Satellite mass optimisation via electrolyser operating voltage with constant voltage operation	65
5.2. Power and heat dissipation rate for different voltage settings (left). Power and heat dissipation rate for different voltage settings per cell (right).	65
5.3. Operating ranges for maximum voltage, maximum efficiency and optimum mass cases in voltage (left) and cell efficiency (right)	66
6.1. Intermediate tank capacity during nominal mission lifetime for the two considered delta-v budgets	70
6.2. Sensitivity analysis results for specific impulse	71
6.3. Sensitivity analysis for pressure case 1 - variation of intermediate tank outlet pressure with intermediate tank storage pressure of 10 bar	73
6.4. Sensitivity analysis for pressure case 2 - variation of intermediate tank outlet pressure with intermediate tank storage pressure equal to it	73
6.5. Sensitivity analysis for pressure case 3 - variation of intermediate tank outlet and storage pressures	74
6.6. Sensitivity analysis results for permeation	75
6.7. Results of SWOT analysis	77

List of Tables

3.1. Catalogues of satellites on Earth orbit.	12
3.2. Number of LEO satellites according to different databases.	13
3.3. Countries of origin for satellites with insufficient information available.	14
3.4. Insufficient information for satellites based on mission type.	14
3.5. Properties chosen for the reference satellite.	17
3.6. Increments and decrements to the rating coefficient for propulsion use	18
3.7. Results of the second iteration of the reference mission selection	19
3.8. Comparison of relative performance of all satellites for all combinations of weighting factor assignments	20
3.9. Results of validation of performance in different categories of launch mass	21
3.10. Absolute deviation of satellite properties from the reference values	22
3.11. Known properties of the satellite FLEX	23
3.12. Commissioning delta-v budget for considered orbits	25
3.13. Maintenance delta-v budget for considered orbits	26
3.14. Initial conditions for considered orbits for de-orbit analysis	27
3.15. Natural decay duration for different solar activity predictions	28
3.16. Required delta-v for active de-orbit scenarios	28
3.17. Complete delta-v budget for considered orbits	29
3.18. Critical aspects of the considered delta-v budgets for the two orbits	30
4.1. List of assumptions for preliminary design	33
4.2. Description of component tasks for WEP	35
4.3. Mass budget for propulsion components of considered systems	36
4.4. Hydrogen permeation rates determined from literature search	41
4.5. Hydrogen losses due to permeation for different storage pressures	42
4.6. Properties of considered materials for tanks	43
4.7. Electrolyser components	44
4.8. Coefficients for pressure-current density curve	47
4.9. Maximum available current densities for various pressures	48
4.10. Performance of electrolyser during heat up with varying number of cells	57
4.11. Masses of components used in power subsystem of FLEX	60
5.1. Satellite properties for extreme operating points for Sentinel-3 delta-v budget	64
5.2. Satellite properties for different operating ranges for Sentinel-3 delta-v budget	66
6.1. Properties of tanks chosen for WEP	67

6.2. Electrolyser properties for considered delta-v budgets	68
6.3. Power subsystem and thermal properties for electrolyser for considered delta-v budgets . .	68
6.4. De-orbit performance of considered orbits	69
6.5. Comparison of mass budget of FLEX with WEP and conventional propulsion system . . .	70

List of Symbols

General Symbols

ΔH_R	[J/mol]	Reaction enthalpy
Δi	[°]	Change in inclination
ΔT	[K]	Change in temperature
Δv	[m/s]	Velocity increment delta-v
\dot{m}	[g/s]	Gas generation rate
\dot{Q}_{abs}	[W]	Absorbed heat rate
\dot{Q}_{diss}	[W]	Heat dissipation rate
a	[km]	Semi-major axis
A_{act}	[m ²]	Electrolyser active area
c_p	[J/kgK]	Specific heat capacity
d	[mm]	Thickness
e^-	[-]	Electron
F	[N]	Thrust
F_c	[C/mol]	Faraday constant ($F_c = 96485C/mol$)
g	[m/s ²]	Gravitational acceleration
H^+	[-]	Hydrogen ion
H_2	[-]	Molecular hydrogen
H_2O	[-]	Molecular water
I	[A]	Current
i	[°]	Inclination
I_{sp}	[s]	Specific impulse
j	[A/cm ²]	Current density
M	[g/mol]	Molar mass

m	[kg]	Mass
O_2	[-]	Molecular oxygen
p	[Bar]	Pressure
P	[W]	Power
q_n	[-]	Curve denominator coefficient
Q_{el}	[As]	Electric charge
Q_{th}	[J]	Thermal energy
r	[mm]	Radius
R_λ	[K/W]	Thermal resistance
$R_{specific}$	[J/kgK]	Specific gas constant
s_N	[-]	Curve numerator coefficient
T	[K]	Temperature
t	[s]	Time
T_{OP}	[K]	Electrolyser operating temperature
T_{SAT}	[K]	Satellite structure temperature
U	[V]	Voltage
U_{real}	[V]	Actual electrolyser voltage
U_{th}	[V]	Thermoneutral voltage
v	[m/s]	Velocity
V	[m ³]	Volume
z	[-]	Charge number

Greek Symbols

η_F	[-]	Faraday efficiency
η_U	[-]	Voltage efficiency
η_{cell}	[-]	Cell efficiency
Γ	[mol/cm ² s]	Specific gas generation rate
Φ	[°]	Transition angle
Ψ	[W/cm ²]	Power density
ρ	[kg/m ³]	Density
σ	[MPa]	Yield stress

Abbreviations

AC	Attitude control.
AIT	Assembly, Integration and Testing.
CalPoly	California Polytechnic State University.
CFRP	Carbon-Fiber-Reinforced Polymer.
DRAMA	Debris Risk Assessment And Mitigation Analysis.
ECSS	European Cooperation for Space Standardization.
EoL	End of Life.
ESA	European Space Agency.
FDV	Fill and Drain Valve.
FLEX	FLuorescence EXplorer.
ISO	International Organization for Standardization.
ISRU	In-Situ Resource Utilization.
LEO	Low Earth Orbit.
LV	Latch valve.
MAINT	Maintenance.
NASA	National Aeronautics and Space Administration.
OC	Orbit control.
OCO-2	Orbiting Carbon Observatory 2.
OSCAR	Observing Systems Capability Analysis and Review tool.
PCDU	Power Conditioning and Distribution Unit.
PEM	Proton Exchange Membrane.
PR	Pressure regulator.
PT	Pressure transducer.
PVNO	Normally open pyro-valve.
RAAN	Right Ascension of the Ascending Node.
RGB	Red-Green-Blue.
SSO	Sun-Synchronous Orbit.
T	Thruster.
UCS	Union of Concerned Scientist.
UN/ECE	Economic Commission for Europe of the United Nations.
USSPACECOM	United States Space Command.
WEP	Water Electrolysis Propulsion.
WFB	Water Feed Barrier.

1. Introduction

Ever since first human-made objects have reached space Low Earth Orbit (LEO) has been of particular interest due to favourable conditions it provides for Earth observation, communications and human missions. With the increasing demand of small satellites LEO is the primary target due to easy accessibility and wide variety of orbits for different types of missions.

Due to constantly increasing number of satellites in LEO regulations have been put in place requiring removal of a satellite within 25 years after end of its active operations. This is to reduce number of objects in orbit to decrease collisions and provide space for other satellites [1]. This creates requirements for satellites propulsion subsystem because unlike other orbits not all LEO missions have propulsion subsystem. This depends on satellite altitude as atmospheric drag due to Earth's atmosphere can be beneficial for de-orbiting without need for propulsion but also negative if a certain altitude needs to be maintained during operational lifetime.

Conventional propulsion subsystems generally used in space depend on chemical storable propellants which in both mono- and bi- propellant configurations usually contain hydrazine. Hydrazine is chosen due its long storage capabilities and hypergolic properties which simplify design of the propulsion subsystem. Its use, however, is problematic due to its properties. Hydrazine has been on the list of substances of very high concern of European Chemicals Agency since 2011 due to its carcinogenic effects on humans [2]. Its high toxicity provides challenges for handling during satellite assembly to protect humans from the risks of exposure. This increases complexity of operations and increases costs. Furthermore, failed launch or de-orbiting with residual propellants still on board can contribute to environmental disasters. This is why steps towards alternative fuels are currently being made.

Such low toxicity alternative fuels are generally referred to as green propellants. With many green propellants in development to provide less hazardous alternatives to hydrazine there is one substance present on Earth in high abundance which can be considered as the ultimate green propellant - water. Water in its pure form is not feasible for use in conventional propulsion. Instead, electrolysis can be used to separate atoms of oxygen and hydrogen from molecules of water which can then be used in a bi-propellant configuration.

Combination of hydrogen and oxygen provides good performance and it is typically used for propulsion in lower stages of rockets rather than in satellite applications. This is due to the low density of hydrogen which requires large tanks and the two substances in these applications are stored cryogenically which adds complexity into the system. As a result storable propellants such as hydrazine are a better alternative for satellite applications.

However, an alternative way of use of hydrogen and oxygen in satellites is being developed and implementation of such an approach is done within a Water Electrolysis Propulsion (WEP) system. This

propulsion subsystem uses water as a primary propellant for long term storage due to its high density and lower storage demands. With an electrolyser present on board of a satellite hydrogen and oxygen can be obtained from water on demand to generate thrust. Not only is this propellant non-toxic and non-expensive but its performance, with the theoretical specific impulse values above 400 seconds [3] compared to hydrazine which has specific impulse below 240 seconds, results in smaller mass of propellants required.

The concept of WEP has been intensively explored in recent years and such propulsion subsystem is currently being developed at the Chair of Space propulsion and Mobility of the Technical University of Munich. With past experiences being in the area of WEP for CubeSat applications [4] and focus on development of PEM electrolyser suitable for space applications this thesis comes as a first step towards development of the proposed propulsion subsystem for larger satellites.

This thesis aims to build on the findings of capabilities and downsides of WEP to determine the feasibility of the proposed concept for satellites in LEO. To do so reference mission representative of LEO is chosen for which WEP is developed to compare its performance to conventional propulsion subsystem. The target of this thesis is to match the performance of the conventional propulsion while minimizing wet mass of the chosen satellite. Wet mass quantifies whether WEP provides improvement for given satellite.

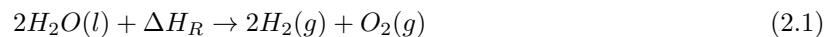
In Chapter 2 basics necessary for understanding of operation of WEP are introduced. Chapter 3 focuses on analysis of LEO to determine what types of missions are the most typical for such orbit to aid in selection of a reference mission to which a WEP can be implemented. Preliminary design of WEP implemented for the chosen mission is done in Chapter 4 where all considerations are presented so that they can be implemented into a tool which automates the preliminary design for any satellite. Chapter 5 uses this tool to perform optimization to ensure achieving the desired optimization target. Results of the preliminary design are shown in Chapter 6 which focuses on nominal performance of the WEP satellite but also includes sensitivity analysis of input parameters to indicate the result variation. Finally, outlook and summary of this thesis are included in Chapter 7 and 8 respectively.

2. Technological background

2.1. Electrolysis

Electrolysis is a process that utilizes electric current to initiate and perform a chemical reaction which results in release of electrons from a reactant and their acceptance by another specie. This chemical reaction takes place in a medium - electrolyte which in the case of water electrolysis is the subject of the chemical reaction - water. Current for the reaction is applied at electrodes. One with negative electrical potential - cathode, and one with positive electrical potential - anode. An assembly of an electrolyte and electrodes make up an electrolysis cell which can then be stacked to size the electrolyser.

Overall reaction used for electrolysis of water is in Equation (2.1) where ΔH_R is reaction enthalpy that represents energy that needs to be supplied to split the molecule of water into hydrogen and oxygen.



2.1.1. Electrolyser types

Even though this thesis is part of development of a PEM electrolyser for space applications there are other types of electrolyser applicable for use in water electrolysis. This section introduces all options to describe their operation and justifies the final use of PEM. The available electrolyser types are:

- Alkaline electrolyser
- Solid oxide electrolyser
- PEM electrolyser

Alkaline electrolyser

Alkaline electrolyser is an electrolyser that uses a porous diaphragm that separates anode and cathode through which hydroxyl ions, that are left after separation of gaseous hydrogen at cathode, and isolates generated gases. It is operated at temperatures below 80°C, however, its disadvantage lies in lower operating pressures [5]. Furthermore, presence of water in both sections of the electrolyser introduces the need to separate generated gases from water, which result in higher complexity of the system and are unsuitable for use in micro-gravity environment.

Solid oxide electrolyser

Solid oxide electrolyser utilizes water in the form of steam and as such requires temperatures of up to 1000°C for operation [6]. This results in operation at high working pressures and high efficiency. However, even though highest possible efficiency for an electrolyser for space applications is desirable high operating temperatures create a challenge for providing sufficient thermal energy for its operation and for thermal management of a satellite to reduce the heat transfer to other subsystems. This makes this type of electrolyser unfeasible for intended use with additional factor being its ongoing development [5].

PEM electrolyser

PEM electrolyser utilizes a proton exchange membrane that is placed between the electrodes as an electrolyte through which hydrogen protons diffuse. It is operated at temperatures below 80°C and provides high gas generation at high efficiency [5]. PEM electrolyser design enables elimination of all moving parts, such as pumps, thanks to which high pressure gases can be generated from low pressure water [7]. These are known as "static feed" electrolysers. This provides an advantage over other electrolyser types for space applications. In fact PEM technology was already used in space in the Gemini mission for fuel cells [7]. Nowadays, in combination with electrolyser reversible fuel cells can be utilized.

Operation of PEM electrolyser leads to reactions at anode, shown in Equation (2.2), and cathode, shown in Equation (2.3). Electrons are separated from liquid water at the anode which leads to generation of gaseous oxygen and hydrogen ions. The electrons flow to the cathode where they are absorbed by hydrogen ions that permeate through the membrane and form gaseous hydrogen.

Anode reaction:



Cathode reaction:



There are two types of PEM electrolyser depending on where the water is fed into the electrolyser - anode and cathode feed.

Anode feed electrolyser has water feed on the anode side. The hydrogen ions, which result from the reaction at anode, travel through the membrane while carrying water across. Both sides of the electrolyser have liquid water in them which results in necessity of separation of the gases from water. However, water passage across the membrane via protons is beneficial for reducing ohmic resistance to provide the highest gas generation rates possible with PEM technology [7].

Cathode feed electrolysers feed water from the cathode side. While the reactions remain the same as in the case of anode feed, travel of water across the membrane is caused by diffusion [7]. Once the anode reaction occurs hydrogen protons travel back across the membrane while carrying some of the water back. This electrolyser design leads to a water-free anode side of the electrolyser so no separation mechanism is necessary for it. However, gas generation rate is reduced in comparison with anode feed [7].

Cathode feed can be further modified to remove the need for separation of water and gases on the cathode side. Achieving this reduces mass of additional components to perform the separation and

reduces complexity of the system. To do this semi-permeable membrane can be added to the cathode side, Water Feed Barrier (WFB), that lets through only as much water as is utilized during electrolysis [7]. Such system is called cathode vapour feed and it provides the same performance as cathode feed while simplifying the system and making it suitable for use in space. To prevent diffusion of hydrogen through WFB from cathode side to water side additional anode can be installed on the water side to prevent blocking of water diffusion by hydrogen [8].

As the cathode vapour feed electrolyser is the most suitable for use in space applications it is considered in this thesis. Diagram of the electrolyser operation is shown in Figure 2.1.

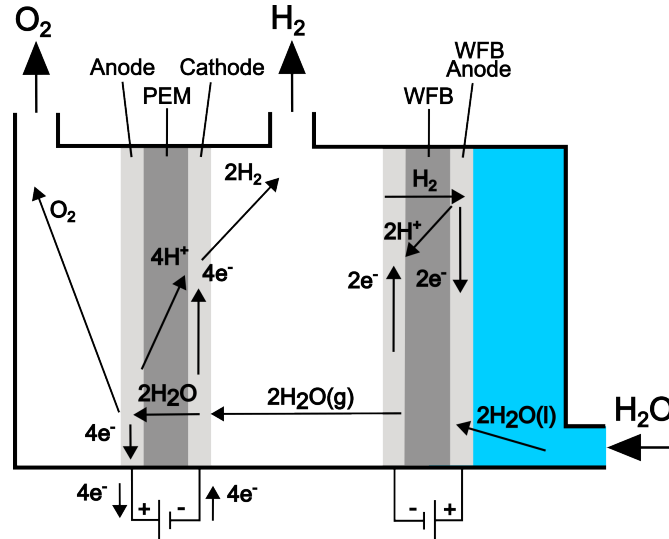


Figure 2.1.: Diagram of operation of a PEM cathode vapour feed electrolyser with WFB [7][8].

2.1.2. Electrolyser performance

According to Faraday's first law of electrolysis mass deposited at an electrode is directly proportional to electric charge that runs through it. This is shown mathematically in Equation (2.4). Therefore, electric charge Q_{el} represents the energy, shown in Equation (2.1) as reaction enthalpy ΔH_R , that is required for electrolysis to happen. Electric charge Q_{el} , defined as Equation (2.5), here I is current and t is time, sets the amount of electric current for the electrolyser operation.

$$m \propto Q_{el} \quad (2.4)$$

$$Q_{el} = I \cdot t \quad (2.5)$$

To see the effect that that electric current has on mass generated during electrolysis Equation (2.6), which was derived by Heizmann [8] from Faraday law, can be used.

$$m = \frac{Q_{el} \cdot M}{z \cdot F_c} = \frac{I \cdot t \cdot M}{z \cdot F} \quad (2.6)$$

where, m is generated gas, Q_{el} is electric charge, M is molar mass of generated gas, z is charge number and F_c is Faraday constant.

This equation enables determination of current flow to achieve certain amount of hydrogen and oxygen and it makes current the primary driver behind electrolyser performance as the only variable in the equation. Additionally, voltage needs to be maintained during electrolyser operation given by current-voltage relation specific to each electrolyser.

To enable comparison of electrolysers of different sizes current density is used for measuring electrolyser performance rather than current. Current density j can be calculated via Equation (2.7) where I is current and A_{act} is the electrolyser active area.

$$j = \frac{I}{A_{act}} \quad (2.7)$$

Similarly, as the product of current I and voltage U is power P it can be normalized with respect to active area to obtain power density Ψ to enable comparison between different electrolysers. This is shown in Equation (2.8).

$$\Psi = \frac{I \cdot U}{A_{act}} = \frac{P}{A_{act}} \quad (2.8)$$

Electrolyser efficiencies

Electrolyser can be operated at wide range of current densities but selection of the operating point/range needs to be carefully considered due to varying efficiencies which affect the performance. There are two efficiencies which need to be considered; voltage efficiency and Faraday efficiency.

Voltage efficiency relates the actual voltage U at which the electrolyser is operated with thermoneutral voltage U_{th} . Thermoneutral voltage results directly from reaction enthalpy ΔH_R which sets the energy required for water molecule dissolution and it describes minimum electrolysis voltage for operation without heat supply [8]. Calculation of voltage efficiency is shown in Equation (2.9) where η_U is the voltage efficiency, U_{th} is thermoneutral voltage and U_{real} is the actual electrolyser voltage.

$$\eta_U = \frac{U_{th}}{U_{real}} \quad (2.9)$$

Faraday efficiency, sometimes referred to as current efficiency, compares the amount of generated hydrogen with theoretically achievable value to determine losses that are not related to voltage. These losses are caused mainly by generated gas crossover across the membrane and current losses [9]. Electrolyser parameters affecting the loss are the membrane thickness, temperature and pressure [10]. Calculation of Faraday efficiency can be done via Equation (2.10) where \dot{m}_{H_2-th} is the theoretically achievable hydrogen generation rate and \dot{m}_{H_2-real} is the actual hydrogen generation rate.

$$\eta_F = \frac{\dot{m}_{H_2-real}}{\dot{m}_{H_2-th}} \quad (2.10)$$

Overall electrolyser cell efficiency can be determined by taking a product of the two efficiencies which results in cell efficiency as shown in Equation (2.11).

$$\eta_{cell} = \eta_U \cdot \eta_F \quad (2.11)$$

Efficiency also varies depending on temperature, voltage and current density of the electrolyser. This makes efficiency a parameter for optimization in later sections. Variation of the efficiencies with respect to current is shown in Figure 2.2 showing that highest voltage efficiency occurs at high temperatures and low voltage setting while for Faraday efficiency high temperatures and high voltage are required. Their combination, shown as cell efficiency, shows that the highest overall efficiency occurs at low current density where gas generation is small.

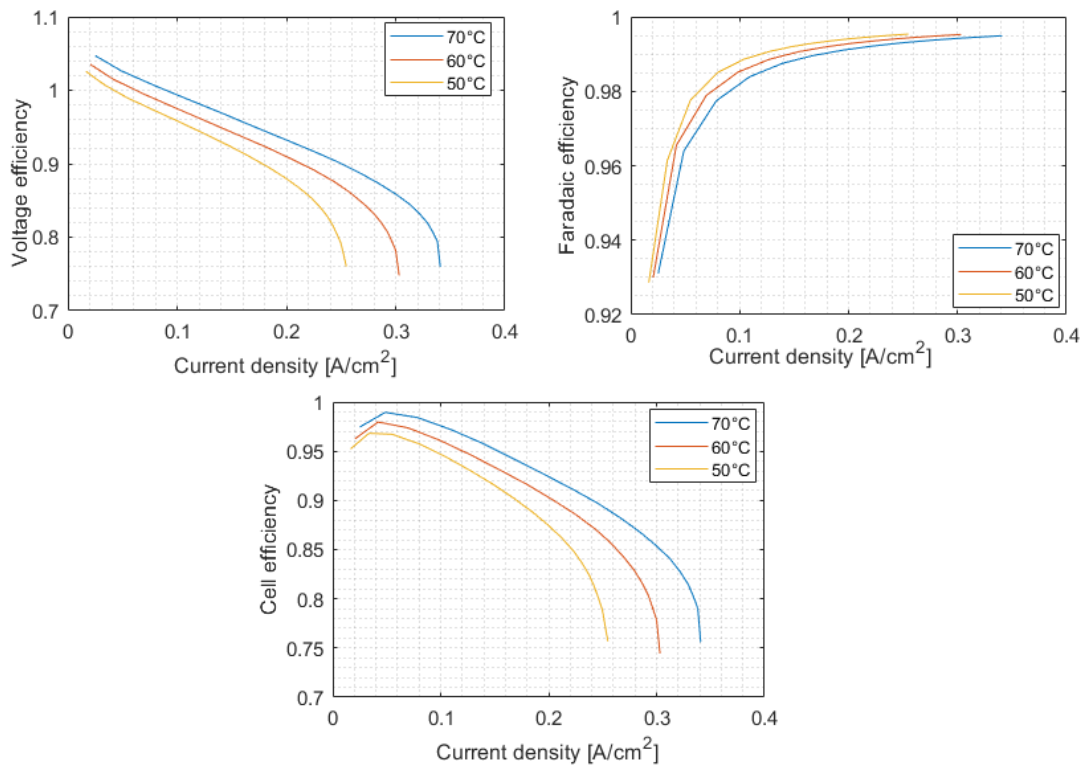


Figure 2.2.: Electrolyser efficiencies for complete operating range [11].

2.2. Space propulsion

This section aims to introduce the basic concepts of space propulsion that will be considered in later sections of this thesis.

2.2.1. Specific impulse

Specific impulse quantifies how efficiently a propulsion subsystem generates thrust. Equation (2.12) indicates the relationship of specific impulse I_{SP} with thrust T and propellant mass flow rate \dot{m} . Symbol

g is a gravitational acceleration. The higher the I_{SP} the more efficient the propulsion subsystem is as more thrust can be generated for lower expended propellant mass.

$$I_{SP} = \frac{T}{\dot{m} \cdot g} \tag{2.12}$$

2.2.2. Tsiolkovski rocket equation

The Tsiolkovski rocket equation provides simplified approach, that assumes thrust as the only force acting on a vehicle, to calculate capability of a spacecraft to produce velocity increment while expending propellant to generate thrust. As can be seen in Equation (2.13) it relates performance of the propulsion subsystem represented via I_{SP} with the initial and final masses of the spacecraft m_0 and m_f . Symbol g stands for gravitational acceleration and Δv is the velocity increment.

$$\Delta v = I_{SP} \cdot g \cdot \ln\left(\frac{m_0}{m_f}\right) \tag{2.13}$$

Parameter Δv is important for determining the performance of a spacecraft. Orbital manoeuvres are quantified by ΔV which does not account for mass of a spacecraft that performs the manoeuvres. By using Tsiolkovski rocket equation propellant masses corresponding to Δv for each manoeuvre can be found. Propellant mass varies based on the initial mass of the spacecraft which means that a manoeuvre performed at the beginning of a mission requires more propellant than the same manoeuvre performed at the end of the mission for the same Δv .

For simplicity Δv will be referred to as delta-v in later sections.

2.3. Water electrolysis propulsion

Water electrolysis propulsion system is a novel propulsion type that utilizes water as the primary propellant. Compared to conventional pressure-fed propulsion it is more complex due to the inclusion of an electrolyser, which needs to be supplied with power to generate hydrogen and oxygen gases, and two tanks for intermediate storage of gases before they can be used for thrust generation. This provides a benefit of using a single, non-toxic propellant while achieving better I_{SP} similar to the one found in conventional bi-propellant propulsion. Figure 2.3 shows simplified structure of the WEP system. Determining ideal sizing and layout of WEP to optimize it for application on LEO is the subject of this thesis and more detailed description of individual components is included in later sections.

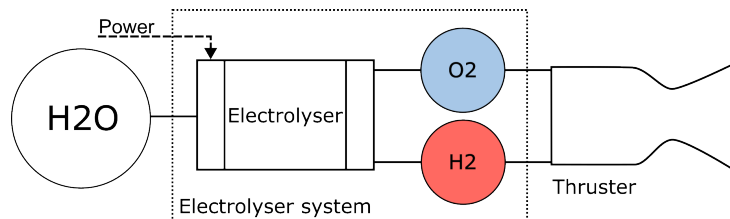


Figure 2.3.: Diagram of the simplified WEP operation

2.4. Orbital manoeuvres

2.4.1. One impulse manoeuvre

Single impulse manoeuvre can be utilized to adjust orbital parameters. To calculate velocity increment Δv required for such an adjustment Equation (2.14) can be used. This equation uses initial and final orbital velocities v_1 and v_2 along with angle between the velocity directions - transition angle ϕ .

$$\Delta v = \sqrt{v_1^2 + v_2^2 - 2 \cdot v_1 \cdot v_2 \cdot \cos \phi} \quad (2.14)$$

This manoeuvre can be utilized for tangent plane manoeuvres to change orbit inclination or Right Ascension of the Ascending Node (RAAN). To achieve most efficient plane transfer such manoeuvre should be carried at the point of minimum orbital velocity - apoapsis. It is desirable to adjust inclination while keeping the orbital velocity constant to prevent variation of other orbital parameters. When considering $v_1 = v_2 = v$ Equation (2.14) can be rearranged as shown in Equation (2.15) where Δi is change in inclination.

$$\Delta v = 2 \cdot v \cdot \sin \frac{\Delta i}{2} \quad (2.15)$$

2.4.2. Hohmann transfer

Hohmann transfer is two impulse manoeuvre which requires the lower propulsion demand - lowest Δv to transfer between two orbits in the same plane when two body problem is considered.

The simplest case is transfer between two circular orbits. In the following example subscript notation in refers to the initial - inner orbit, subscript fin refers to the final - outer orbit and H refers to the Hohmann transfer orbit.

Hohmann transfer is performed by an initial impulse which propels the spacecraft on a Hohmann transfer orbit which touches both initial and final orbit. Second impulse is added at the apoapsis of the Hohmann transfer orbit, where it touches the final orbit, to raise the periapsis. This sequence is shown in Figure 2.4 where dark circle represents inner and light circle outer orbit. Symbols a_{in} , a_{fin} and a_H are initial, final and Hohmann transfer orbit semi-major axis respectively. Symbols v_{in} and v_{fin} are initial and final orbit velocity and t_H is Hohmann transfer orbit period. Finally, $\Delta v_{in \rightarrow H}$ is the velocity increment to achieve Hohmann transfer orbit and $\Delta v_{H \rightarrow fin}$ is velocity increment to transfer from Hohmann transfer orbit to the final orbit.

Calculation of total velocity impulse to perform Hohmann transfer is shown in Equation (2.16) [12].

$$\Delta v = \Delta v_{in \rightarrow H} + \Delta v_{H \rightarrow fin} = (v_{in} - v_{fin}) \cdot \left(\frac{\sqrt{a_{in}} + \sqrt{a_{fin}}}{\sqrt{a_H}} - 1 \right) \quad (2.16)$$

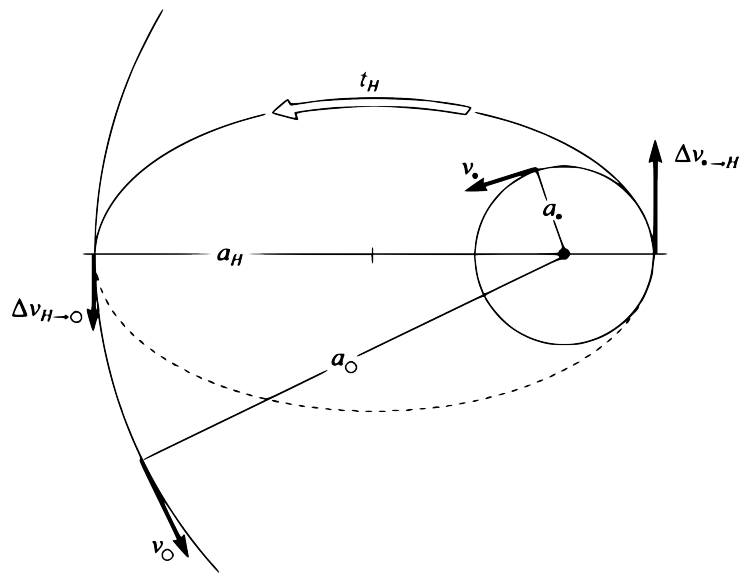


Figure 2.4.: Hohmann transfer sequence, taken from [12].

3. Mission analysis

3.1. Market Research

Prior to performing feasibility analysis it is necessary to determine what satellites are already on LEO. This information will serve as a basis for setting up a reference mission considered in later stages.

3.1.1. Selection criteria

There are currently thousands of objects on Earth orbit, including active and inactive satellites, remnants of rocket stages and debris. That is why it is necessary to classify what objects are included in this analysis. The following list consists of properties that are required for each satellite to be considered:

- On LEO
- Operational
- Launched after 31/12/1999
- Not part of a large constellation
- Mass larger than 24 kg
- Not purely military purpose

Inactive satellites are not be considered as they utilized technology of the past which is lacking in performance compared to novel technologies used nowadays. As this feasibility analysis tries to demonstrate that the WEP is a prospective propulsion of the future which can compete with conventional propulsion subsystems only operational satellites that are currently on LEO and were launched after 31/12/1999 are included. Future missions, where available information allows, are also be considered.

Majority of satellites currently on LEO is part of a constellation. Satellite constellations consist of satellites in numbers ranging from tens to hundreds and are defined by their cooperation and interaction to achieve a common goal. Their architecture is common for all satellites within the constellation which differs from non-constellation satellites. This usually means that they are mass produced, smaller than regular satellites and their life-time is usually shorter due to a degree of redundancy within the constellation.

For the reasons of different architecture and their high number the large constellations are excluded from this analysis because they would introduce a bias to the research. There are, however, constellations which consist of only a few satellites which architecturally resemble non-constellation satellites – such as the SkyMed constellation consisting of 4 satellites. The satellites of these constellations are considered as

long as they contain small number of satellites, majority of the constellation is already in orbit and they are not planned to be expanded further. This resulted in consideration of 47 satellites in constellations.

This analysis does not consider CubeSats. Their size causes that their architecture is different to that of satellites in different mass categories. Furthermore, propulsion subsystem availability for CubeSats is currently limited and it would be difficult to design a propulsion subsystem that would be scalable for satellites from few kilograms to tons.

As there is a large quantity of objects on orbit manual validation of each satellite is not possible due to time constraints. Based on the CubeSat design specification document by California Polytechnic State University (CalPoly) the largest specified CubeSat form factor is 12U [13] which has a maximum launch mass of 24 kg. However, there are even larger form factors such as 16U, which have not yet been launched but are considered for future missions. Even though mass does not define whether satellite is CubeSat or not, and considering that majority of CubeSats is in the 3U form factor with a maximum launch mass of 6 kg, the limit of 24 kg is considered as a cut-off point for this analysis [14]. No matter whether a satellite below 24 kg is a CubeSat or not, the propulsion subsystem for such missions will be different than propulsion subsystem for larger satellites.

The number of military satellites on orbit is not negligible but information about these satellites is usually limited due to the nature of their mission. There are, however, satellites which serve both civil/governmental and military purposes. Typically these are imaging satellites which have sufficient information about their bus and payload. These, unlike purely military satellites, are considered in the thesis.

3.1.2. Satellite analysis

Current missions

Even after the selection criteria from previous section are applied individual analysis of each satellite introduces significant time constraint. Fortunately, there are databases available, which collect information about objects on orbit. Two of these databases were used: Union of Concerned Scientist (UCS) satellite database and United States Space Command (USSPACECOM) database.

UCS database keeps track of all operational satellites LEO [15]. The limiting factor is the update frequency because at the time of writing of this thesis the only data that is available is 7 months old. The other database, which is published by USSPACECOM, lists real time orbital information about all objects in space but it enables filtering to show only objects which are a payload and are on LEO [16].

Prior to applying the selection criteria both databases contained 20640 objects around Earth. Table 3.1 indicates the individual contributions of each database.

Table 3.1.: Catalogues of satellites on Earth orbit.

Source	LEO Objects	LEO satellites	Reference
UCS	5464	4700	[15]
USSPACECOM	20640	7740	[16]

Applying constraints is complicated by the fact that not both databases contain identical properties of satellites. USSPACECOM data is general and contains only orbital information while UCS database

contains concrete data about satellite platforms. Due to this the constraints on mass and non-military purpose were applied on data from the UCS database and MATLAB was utilized to compare both databases using COSPAR ID, which is an international designator assigned to each satellite, to find satellites from UCS database in the USSPACECOM database. The remaining satellites in the USSPACECOM database had to be analysed manually as their status is unknown due to the fact that they were omitted in the UCS database or they were launched after the database was last updated.

The number of satellites at each stage of constraint application is shown in Table 3.2. Where satellites in smaller constellations fulfilling the requirements stated in the previous section are included in the non-constellation category. As can be seen majority of satellites are part of large constellations. With more than 3200 of satellites in this category being part of Starlink constellation neglecting constellation satellites is justified as a feasibility analysis focused on the needs of constellation satellites must be performed separately. The total number of satellites considered for this thesis is 377.

Table 3.2.: Number of LEO satellites according to different databases.

Source	Fulfilling requirements	Constellation	Non-constellation	Reference
UCS	3328	3017	310	[15]
USSPACECOM	5454	5077	377	[16]

Each of the 377 satellites needed to be analysed individually to find their properties for further processing. Two approaches were considered. Either find parameters for all missions to obtain all relevant data, which is time constraining, or find the most occurring mission type and find parameters for all satellites of this type to speed the process up. Even though there is one mission type predominant among the LEO satellites, it is not sufficiently high to justify the loss of information if other mission types were discarded. The decision was made to find information of each satellite individually.

Properties that was searched for each satellite consisted of the following categories:

- Physical dimensions
 - Launch mass
 - Payload mass
 - Satellite dimensions
- Available power
- Design life
- Propulsion subsystem
 - Propulsion type and use cases
 - Propellant and its mass
 - Number of thrusters and thrust

It was not possible to find all information for each satellite. Mainly because a significant number of them are commercial satellites whose capabilities are proprietary. Decision was made that if no information can be found from at least 2 out of the 4 information categories, the satellite can be considered irrelevant

for the analysis. Information about origin of satellites with insufficient information is shown in Table 3.3 and it shows that majority of satellites with insufficient data is from China.

This analysis concluded that out of the 377 considered satellites insufficient data is present for 34.16 % of the satellites. If Chinese satellites were omitted altogether, the insufficient data would be present only for 14.34 % of satellites which would increase accuracy of this analysis. But although the data is insufficient it is still considered. This means that the analysis that is performed in the following sections is applicable to 65.84 % of all current satellites on LEO.

Table 3.3.: Countries of origin for satellites with insufficient information available.

Country	Insufficient data satellites	Percentage of all insufficient data satellites
China	84	67.74 %
United States	13	10.48 %
Other	27	21.78 %

During the manual analysis some satellites were found to be inactive, due to cessation of operation between the date of publishing and present day, and were removed. Some objects which were considered to be satellites by UCS were freight modules on resupply missions for the International Space Station and they were also removed. This caused that the final number of satellites considered for the analysis was 363.

To analyse satellites on LEO mission types were categorized in the following groups:

- **Earth Observation** - Including Earth science
- **Technology** - Missions to demonstrate or develop technologies
- **Space Science** - Including space observation and on-orbit experiments
- **Space Logistics** - Satellites used for deployment of other satellites
- **Communications**

Using this classification it was determined that Earth observation missions not only are the most occurring mission type but they also have the smallest percentage of satellites with insufficient data as shown in Table 3.4. This indicates another advantage of consideration of this mission type for the reference mission. In contrast communications satellites have insufficient information available for all but one satellite due to their commercial origin.

Table 3.4.: Insufficient information for satellites based on mission type.

Mission type	Insufficient data	Total	% of insufficient data satellites
Earth Observation	47	237	19.8 %
Technology	31	50	62.0 %
Communications	33	34	97.1 %
Space Science	7	32	21.9 %
Space Logistics	6	10	60.0 %

Future missions

Consideration of future missions is just as important because the aim of this thesis is to propose a propulsion subsystem that is competitive with current conventional propulsion subsystems and is also perspective for future use. Decision has been made that all missions on LEO whose development is further than mission concept shall be considered.

Unlike in the case of current missions no databases listing future missions were found. To give an order to a manual search that needed to be performed, the decision was made that future missions of all major governmental agencies should be searched first as they are transparent and provide sufficient information.

Future commercial missions are more difficult to find. As in the case of current satellites commercial satellites tend not to have sufficient information about them available often due to their proprietary nature. During the search it was determined that significant portion of commercial projects are constellations which as in the case of current missions are neglected. In total 34 commercial missions and 108 governmental and inter-governmental missions were found. Compared to current satellites number of satellites for which there is insufficient information is larger. This leads to a conclusion that sufficient information is available - the research is valid for 44.37 % of all the future LEO missions.

Results of the analysis

This section provides an overview and results of the analysis that was performed on the data collected in previous sections. Due to high number of data collected only the results of the analysis are shown. In total 505 current and future satellites were considered and properties found in the previous sections are used to set up requirements for the reference mission.

From the previously introduced mission types the most reoccurring, with 71 % of satellites, was found to be Earth observation as shown in Figure 3.1 indicating that it is the best choice for the reference mission. The same figure indicates the best choice for orbit selection as orbital information is set by two parameters, orbit type, for which best choice is shown in Figure 3.1 as Sun-Synchronous Orbit (SSO) with 80.2 % of all considered satellites, and the second parameter is altitude. Figure 3.2 shows that majority of satellites in LEO is located between 423 km and 871 km of altitude with curve resembling normal distribution. The median value of 616 km was chosen as a reference mission target. Selection of altitude in LEO is of the highest importance because it sets mass of the propellant that will be required for orbit maintenance and for possible de-orbit.

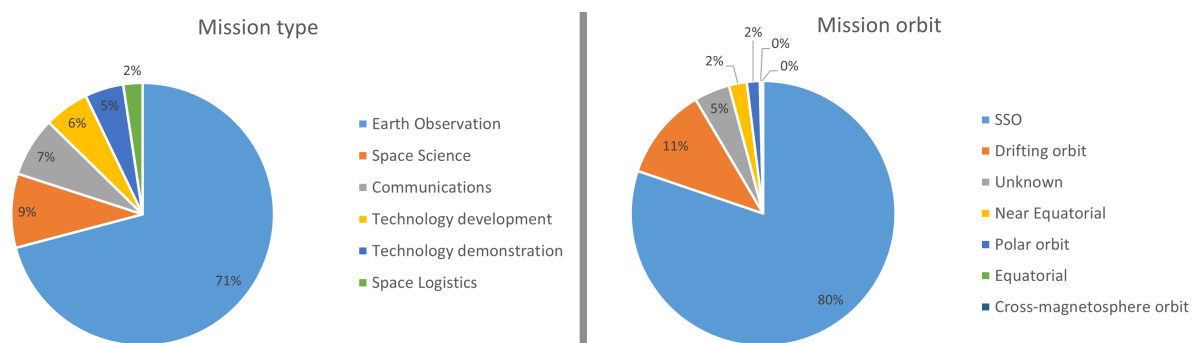


Figure 3.1.: Distribution of mission types and mission orbits of current and future LEO missions [15, 16].

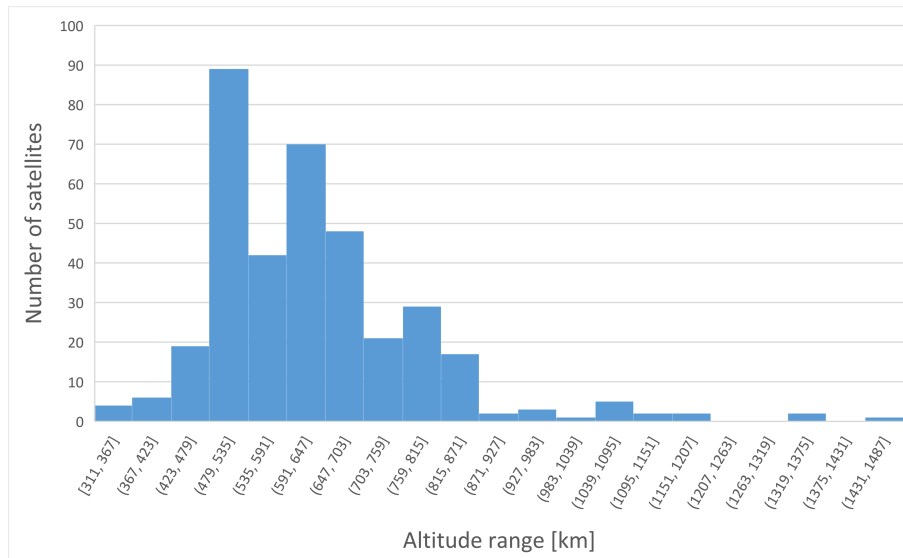


Figure 3.2.: Distribution of average altitudes of LEO satellites [16].

To determine requirements for propulsion subsystem of the reference satellite, analysis of all satellites' propulsion subsystems was performed. This category proved to be the most challenging as information availability was limited. Propulsion subsystem type is unknown in 55.84 % of missions with further 10.89 % of missions utilizing no propulsion subsystem. Even though the chosen conventional propulsion subsystem represents only 44.16 % of all non-constellation LEO satellites data collected indicate that the most used, in 22.38 % of all satellites but 54.7 % of satellites with known propulsion, conventional propulsion subsystem is chemical monopropellant propulsion which is set as the primary WEP competitor. Propulsion subsystem use cases for LEO were divided into the following categories:

- **Orbital control** - Orbit adjustment against perturbations. In-plane (altitude) and out-of-plane (ground track) adjustments.
- **Attitude control** - Orientation adjustments
- **Manoeuvres** - Orbit changes. Including space observation and on-orbit experiments
- **Maintenance** - Attitude control system momentum dump, de-orbit, collision avoidance, orbit insertion

Each propulsion subsystem can be utilised for any number of the use cases but they were only considered for satellites which had their propulsion subsystem specified. Satellites for which propulsion subsystem used was known, 93 % of them use propulsion subsystem for orbit control. Furthermore, 42.1 % of the of satellites uses propulsion for maintenance. This is mainly for de-orbiting if the satellite is in high altitudes, which require longer time for natural orbit decay, and for collision avoidance. Attitude control and manoeuvres are both used for 21 % of satellites. Based on this an assumption is made that the reference satellite should use propulsion subsystem for orbit control and for maintenance.

The last section of the analysis is dedicated to satellite properties. This is done to understand design choices for each satellite and to find trends which could be applied for the reference satellite. As the spread of the data is wide and single most occurring value cannot be determined median values can be used instead. This was not the case for mission design life where median value coincided with the most

reoccurring number - 60 months which occurred for 37 % of satellites. Figure 3.3 shows the distribution of satellite masses on LEO. Even though highest number of satellites is included in masses of up to 429 kg median value of 473 kg was chosen due to large variation of masses within that category.

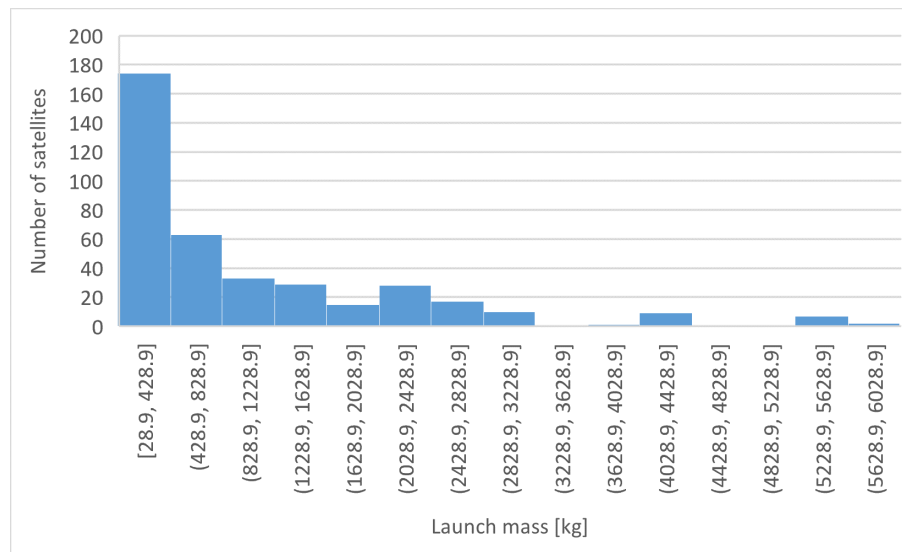


Figure 3.3.: Distribution of launch masses of LEO satellites.

Some properties considered for the reference mission are dependent on launch mass and they were normalized for all satellites with respect to their launch mass to enable determination of their median value. This includes End of Life (EoL) power - median value of 1.56 W/kg and satellite area perpendicular to the direction of motion - median value of 0.006 m²/kg. Using the reference launch mass of 473 kg reference values for these two parameters can then be calculated. Final target parameters for the reference mission are shown in Table 3.5. Additional requirement that was considered in search of the reference mission was data availability. This was quantified by percentage of parameters that were available for given satellite. The higher the percentage the more information about satellite is available.

Table 3.5.: Properties chosen for the reference satellite.

Criteria	Value	% of all satellites
Mission type	Earth Observation	70.9 %
Orbit	Sun-synchronous	80.2 %
Propulsion	Chemical propulsion (Monopropellant)	54.7 %
Propulsion use	Orbit control	93.0 %
	Maintenance	42.1 %
Median launch mass	473 kg	-
Median average altitude	616 km	-
Median mission duration	60 months	-
Median normalized power (Power)	1.56 W/kg (736.4 W)	-
Median normalized area (Area)	0.006 m ² /kg (2.83 m ²)	-

3.2. Reference mission selection

With all relevant LEO satellites found and the analysis of satellite properties completed a reference mission shall be found that fulfils the reference values. Not all target values for the considered properties

can be achieved but an attempt is made to find a satellite with the best combination of all properties.

To initiate the search for reference satellite only Earth observation satellites on SSO were taken. Satellites with insufficient data were removed because finding a reference satellite with as much information as possible is desirable. Similarly, satellites which do not have any propulsion subsystem onboard were not considered either because they are not relevant for this research. Lastly, duplicate satellite buses were removed. This was done to simplify the analysis as some satellites were part of a small constellation or series and there were multiple identical satellites.

To rank performance of a satellite with respect to target values linear utility function, labelled as ϕ is used which uses two parameters for each explored property - weighting factor w and rating coefficient y . The linear utility function equation is shown in Equation (3.1).

$$\phi = \sum_{i=1}^n w_i \cdot y_i \quad (3.1)$$

Weighting factor enables expression of a preference for desired properties. Weighting range of 1 to 10 was chosen arbitrarily to have a large range of weights to explore. Rating coefficient is obtained by comparing actual property value with a reference value and depending on how far away from the target the actual value is the rating coefficient is set. Rating coefficient value is set in a range of 0 to 1. Value of 1 is set for a property whose actual value is equal to target value. The lowest value - 0 relies on the maximum deviation of the property from the target value among considered satellites. This means that a satellite with a property value furthest away from the target has a rating coefficient of that property 0 and other satellites have a rating coefficient between 0 and 1 depending on linear distribution. This indicates that the wider property variation is the more inefficient the ranking gets and one satellite with property value completely different than the rest can jeopardize the rating coefficient.

For this reason launch mass was set as the main design driver, as it is responsible for all other satellite properties, and satellites in a limited mass range should be considered for the ranking to avoid the issues mentioned above. Rating coefficient of each property, labelled as y , can be calculated using Equation (3.2).

$$y = 1 - \frac{|x_{ref} - x|}{\Delta x_{max}} \quad (3.2)$$

where x_{ref} is the reference value, x is the actual value and Δx_{max} is the maximum deviation between the reference and actual value of all considered satellites.

Selection of rating for non-numerical properties was handled in another way. Chemical monopropellant propulsion, as the most occurring solution, was given a rating value of 1, whilst other propulsion types were assigned 0.5. For use of the propulsion subsystem increments and decrements to the rating coefficient are used which based on the percentage of satellites that utilize that use case. These are shown in Table 3.6.

Table 3.6.: Increments and decrements to the rating coefficient for propulsion use

	Attitude control	Orbit control	Maintenance	Manoeuvres
Increment/decrement	- 0.2105	+ 0.6884	+ 0.3116	- 0.2105

Highest rating coefficient is achievable for combination of Orbit control and maintenance. If any of the

other two use cases is added the rating coefficient needs to be decremented.

However, as selection of the weighting factors expresses subjective preference of the designer usage of such ranking method is biased. In ideal case team of experts responsible for relevant subsystems discuss suitability of each weighting factor to help make the selection more objective. In the case of this analysis, no such option is available. Alternatively, to limit the bias probing iterative approach is used.

First iteration of the analysis was performed for a case of identical weighting factors for all properties. Because the number of analysed satellites was still high at this stage, this iteration aided in identifying the most prospective satellites. For the first stage of the reference satellite selection satellites which are in the range of the reference mass of 473 ± 100 kg were considered with the intention of considering different masses in next iterations.

In the second iteration weighting factors were assigned subjectively with the same mass range. As this thesis focuses on propulsion, propulsion-relevant properties have the highest weighting factor. Additionally launch mass, which is the main property according to which the satellites were picked for this analysis, and data availability have the highest weighting factor as they are equally important for future analysis. Satellite area and EoL power have the lowest weighting factor. Although they are important for design of the propulsion system, they are considered secondary. The best performing satellites along with their property values, rating coefficients and utility values (shown as weighted total) are shown in Table 3.7. To fit all the data into the table the following abbreviations are used for propulsion use: Attitude control (AC), Orbit control (OC) and Maintenance (MAINT)

Table 3.7.: Results of the second iteration of the reference mission selection

Property	Target	Weight	FLEX		OCO-2		Haiyang-1	
			Value	Rating	Value	Rating	Value	Rating
Altitude [km]	616	5	815	0.000	702.5	0.565	778	0.186
Design life [years]	5	5	3	0.600	2	0.400	5	1.000
Launch mass [kg]	473	10	460	0.866	454	0.804	442	0.680
Area [m^2]	2.83	2	1.8	0.877	1.993	0.900	1.54	0.846
EoL Power [W]	736.43	2	700	0.966	815	0.926	510	0.787
Propulsion system	Chem.	10	Chem.	1.000	Chem.	1.000	Chem.	1.000
Propulsion use	OC		OC	1.000	OC	1.000	OC	0.478
	MAINT	10	MAINT		MAINT		AC	
Data availability	100 %	10	92.9 %	0.929	92.9 %	0.929	71.4 %	0.714
Unweighted total			6.237		6.524		5.691	
Weighted total			44.631		45.806		37.920	

First two iterations indicate, that the best candidate is a satellite called Orbiting Carbon Observatory 2 (OCO-2) as its utility values are higher than the other satellites'. Final iteration was aimed at confirming this trend and looking at the overall performance of all satellites in all possible cases of weight assignments. MATLAB script was written which uses all rating coefficients along with loops which vary all weighting factors. As there are 8 parameters 10^8 iterations were run. This way, distribution of relative positions of all considered satellites can be found which indicates their general performance without subjective bias. Results of this analysis are shown in Table 3.8. They confirm the trend observed in the first two iterations as the OCO-2 has the highest utility value among the analysed satellites in 85.19 % of different weighting factor assignments. This supports the decision to make OCO-2 satellite the reference satellite

of this thesis. An alternative option for a reference satellite could be FLEX, which performs similarly well and is the best in 14.09 % of weighting factors assignment.

Table 3.8.: Comparison of relative performance of all satellites for all combinations of weighting factor assignments

Satellite	1 st position	2 nd position	3 rd position
ASNARO	0.00 %	0.16 %	1.57 %
DMC 3-FM1	0.18 %	5.49 %	9.69 %
FLEX	14.09 %	74.49 %	8.87 %
HAIYANG-1	0.33 %	5.48 %	43.98 %
KANOPUS-V	0.14 %	0.96 %	4.04 %
OCO-2	85.19 %	12.24 %	1.50 %
SARAL	0.06 %	1.17 %	30.35 %

3.2.1. Validation of the analysis

Validation of the results is performed to show that the best candidates that came out of the analysis are a global best case and not just the best case for the selected arbitrary restrictions of the design space which were introduced by considering only satellites in the range of $473 \text{ kg} \pm 100$. Disadvantage of using an evaluation approach presented in the previous section is the fact that it is a relative comparison. Which means that results of the analysis are dependent on a scope of values of individual properties in the analysis.

As such, this type of analysis is most efficient when is used for a comparison of similarly performing objects. As even one satellite with largely different performance can negatively impact the analysis by introducing a bias. For example, if all but one satellite have a mass close to a median value while the remaining one has a mass in multiples of the median, the rating coefficient becomes irrelevant. Because while the one different satellite is penalized and its coefficient is equal to zero the coefficients of other satellites will be nearly identical not enabling clear selection of the best performer.

As launch mass was used for to restrict the design space in the analysis increasing the mass range considered for the analysis can aid in seeing effects of such constraint and in validating the results. Only Earth observation missions were included and in total three different cases are considered:

1. **Case 1:** Original restriction of the launch mass - 43 satellites
2. **Case 2:** Maximum symmetrical restriction of the launch mass - 155 satellites
3. **Case 3:** No restriction of the launch mass - 359 satellites

The original restriction considers the case introduced in the previous section where the launch mass was arbitrarily constrained to $473 \pm 100 \text{ kg}$. This case can be called symmetrical as the difference between lower boundary and the reference launch mass value is equal to difference between upper boundary and launch mass.

The second case is intended to consider a maximum symmetrical restriction. By subtracting minimum satellite mass and the reference launch mass the largest range of satellites can be used for which upper and lower boundaries are the same distance from the reference value. By using this approach it results

in consideration of all satellites in the launch mass range of 473 ± 444.1 kg. Lastly all satellites are considered which leads to the launch mass range of 28.9 - 5730 kg.

Approach

To compare the three cases a MATLAB script which was used in the previous section for the sensitivity analysis was used to determine the absolute positions with any combination of weighting factors. However, as there are 10^8 of iterations it introduces a strain onto computational capabilities which can be handled if a small number of satellites is analysed but it is unable to process high numbers. Therefore, a range of weighting factors of 1 - 5 was considered instead which offers results at a reasonable processing time.

Satellites which performed well in the original restriction are closely tracked in the other two cases to see how well they perform on a more global scale. Satellites, which were not considered in the original case because they did not fit the mass restriction, that perform well in the two other considered cases are noted and then compared at the end of this validation to see how they perform compared to the original satellites.

To enable comparison of satellites in all three cases a weighting system shall be introduced that enables quantification of an absolute position of the satellite. As the MATLAB script expresses satellite's positions compared to other satellites in all iterations, which can be quantified as a percentage of all cases, weights for each position can be assigned and then multiplied by corresponding percentage and added up to rank satellite's absolute position. The larger the sum of all positions multiplied by their corresponding weight, the better the absolute position among other satellites.

As there are hundreds of satellites only the first twenty positions are considered and weighted. Weighting would then be in a range of 1 - 20, with 20 being assigned to the first position and 1 to the twentieth position.

To focus only on the best performing satellites best 3 satellites from each case are considered unless they were already present from a previous case. This resulted in a collection of 6 satellites which are shown in Table 3.9. Satellites whose mass did not meet the mass constraints for a given case are labelled as "x" as they were not present in the given case.

Results confirm suitability of OCO-2 satellite which performed the best in the first two categories. However, what is more important is performance of satellite FLEX which placed second in the original analysis but with wider array of satellites it performed the best in remaining two cases. Other satellites from the initial analysis did not perform so well and on the other hand satellite CALIPSO performed well even though it did not fit the constraints of the first case.

Table 3.9.: Results of validation of performance in different categories of launch mass

Satellite	Case 1		Case 2		Case 3	
	Total	Position	Total	Position	Total	Position
OCO-2	19.96	1	17.42	2	12.39	6
FLEX	18.99	2	19.53	1	19.15	1
HAIYANG-1	18.26	3	13.00	7	0.92	34
SARAL	17.88	4	16.10	3	6.53	17
CALIPSO	x	x	14.98	5	13.64	3
PRISMA	x	x	8.36	13	14.13	2

Final step of the verification does not focus on satellite ranking based on the weighting factors but rather focuses on absolute accuracy of their properties. Percentage deviation of each property from the reference was found and all of them were averaged to find an overall deviation which is an absolute measure of a degree of fulfilment of the requirements. Table 3.10 shows the final results. It can be seen that OCO-2 which was chosen initially has the smallest averaged deviation and is therefore the best fit for the reference satellite with satellite FLEX being close behind.

This approach is best for judging proximity of satellite values to the reference values and it was only done for validation because it does not enable prioritization, which in the analysis is done via weighting, that helps in setting priorities.

Table 3.10.: Absolute deviation of satellite properties from the reference values

Satellite name	Average deviation of properties
OCO-2	15.75 %
FLEX	16.53 %
CALIPSO	20.61 %
SARAL	21.96 %
HAIYANG 1C	24.02 %
PRISMA	29.98 %

Conclusion

Even though the OCO-2 satellite was identified as a satellite that best fits the requirements in most of the approaches availability of information about the satellite plays the most significant role when confirming it as a reference satellite. This availability was used for ranking it in the previous sections but it was judged based on variety of satellite properties. For the upcoming analysis the most important factor is the availability of the detailed information about the propulsion system itself as it is crucial for comparison to WEP system.

This was found to be a difficult task. Even though many of the best performing satellites are operated by governmental and intergovernmental agencies which publicly share information, satellite buses are usually outsourced to private companies which do not disclose such information.

Out of the best performing satellites only two of them have detailed information about propulsion available. Current mission CALIPSO, which is part of the same constellation as OCO-2, and future planned mission FLEX. As it came out as the second best option in the reference mission search satellite FLEX was chosen as a reference satellite. With FLEX being a future mission it will help show that WEP is a competitive propulsion subsystem towards the future LEO applications.

3.3. Reference mission

With the selection process done more in-depth analysis of the satellite FLEX needs to be performed. As the mission is planned to be launched in near future information available about the mission is limited. What is known about the satellite is shown in Table 3.11. The mission is designed to operate in tandem with Sentinel-3 satellite which provides an additional insight into the expected delta-v budget [17]. As it is a future mission no delta-v budget is available.

The goals of the FLEX mission, which are achieved through its single instrument - Fluorescence Imaging Spectrometer [17], are the following:

- Observe and measure fluorescence of the global vegetation
- Use vegetation fluorescence to evaluate plant stress and photosynthetic activity
- Track vegetation health and performance

Table 3.11.: Known properties of the satellite FLEX [17, 18]

Orbit type	Sun-synchronous
Average altitude [km]	814
Type	Earth Observation
Design life [months]	36
Launch mass [kg]	460
Payload mass [kg]	140
Bus dimensions [m]	1.5×1.2×1.2
EoL Power [W]	700
Propulsion system	Chemical (Monopropellant)
Propulsion use	Orbit control and Maintenance
Propulsion type	Blowdown
Propellant	Hydrazine
Propellant mass [kg]	28
Number of Thrusters	4
Thrust each [N]	1

3.3.1. Propulsion requirements

Initially, because there was no delta-v budget for FLEX available, mission that would be similar in satellite properties and orbit to FLEX was searched whose delta-v budget could be implemented for the reference mission. Market research showed no such satellite existed. In fact, the closest satellite in terms of performance is the aforementioned satellite CALIPSO which is located at an altitude of 705 km. At this altitude difference in use of delta-v is noticeable due to larger influence of atmospheric drag and it is expected that frequency of manoeuvres is higher. CALIPSO mission orbit can be taken as a conservative delta-v budget to determine, whether WEP would be feasible for use in more challenging conditions designed for conventional propulsion.

Second comparison can be made with Sentinel-3 satellite with which FLEX is supposed to be flying in tandem at the altitude of 814 km. Even though Sentinel-3 satellites are much larger and are designed for longer lifetime FLEX needs to maintain the same relative position to them and their manoeuvres can be applied to the case of FLEX. From now on when referring to CALIPSO and Sentinel-3 the orbits utilized by these two satellites are considered.

To understand distribution of the manoeuvres and to see what maintenance needs to be done to orbital parameters historical orbital data can be used for the two missions. This enables generation of a manoeuvre schedule for WEP implementation. Such historical orbital data were obtained from USSPACECOM database [16].

Unlike in the case of conventional propulsion delta-v budget for WEP needs to provide information on timings of individual manoeuvres because sufficient time needs to be allocated before each manoeuvre

to provide charging time to generate required propellant. While in the case of conventional propulsion any amount of delta-v is ready on demand. For future applications of WEP manoeuvres can be designed specifically for the system needs to provide favourable conditions for its operation. But for this application delta-v budget not optimized WEP can be used

Based on the historical data it can be stated that there are two primary parameters which are adjusted for both CALIPSO and Sentinel-3 - semi-major axis and inclination. This results in variation of other parameters which are coupled. Only parameter which is not varied through manoeuvres is RAAN. This is caused by the selected orbit - SSO, where the rate of change of RAAN has to be equal to the rotation of Earth around Sun. This results in yearly cycles of the parameter. Data for both missions are shown in Figure 3.4. Rapid decrease of semi-major axis and increase of inclination of satellite CALIPSO was an intentional change to operate it at a lower altitude in cooperation with another satellite while de-orbiting.

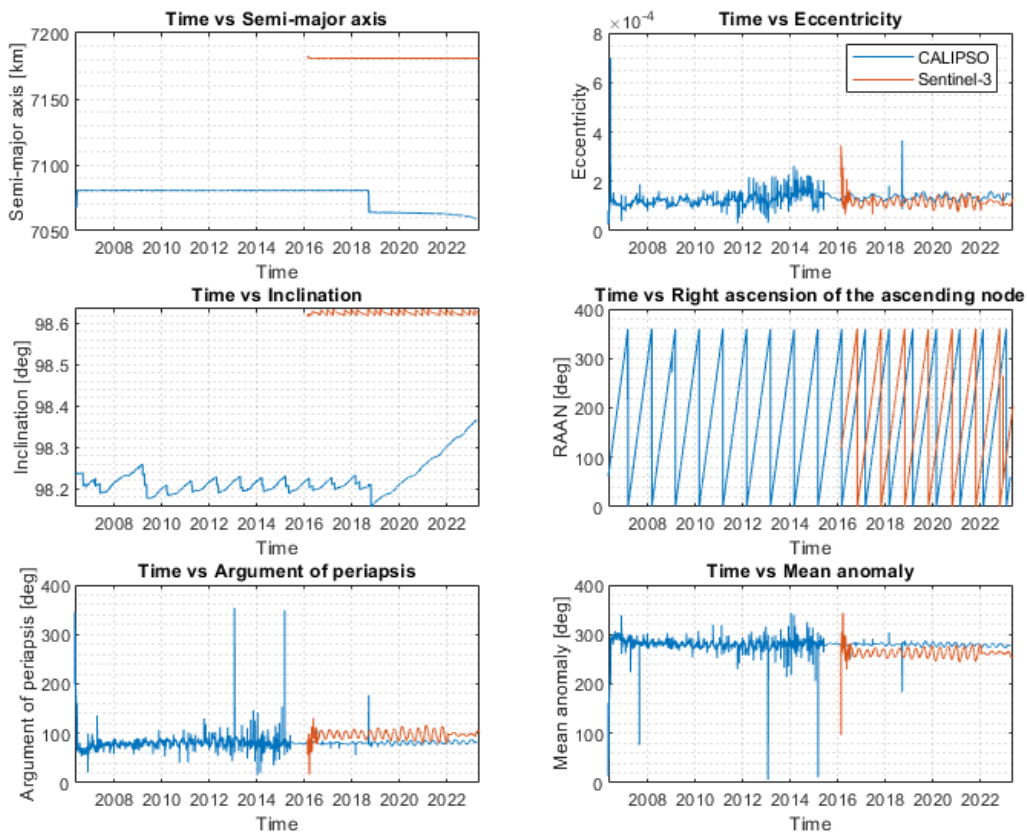


Figure 3.4.: Orbital data for satellites CALIPSO and Sentinel-3 obtained from [16].

Manoeuvre analysis for both satellites was done manually from the historical data. By taking orbital parameters before and after each manoeuvre and calculating corresponding delta-v. For determining the delta-v an assumption was made that semi-major axis corrections were adjusted using Hohmann transfer and inclination was adjusted using one impulse manoeuvre at the orbital nodes for the largest efficiency.

It is known from market research that propulsion subsystem onboard of CALIPSO and Sentinel-3 missions is used for orbit control and maintenance. In this specific case orbit control consists of adjustments to

ensure consistent ground track over the mission duration. Maintenance consists of initial orbit adjustment after separation from a launcher, collision avoidance and de-orbiting. With the purpose of the propulsion subsystem known its tasks can be separated into three phases:

1. Satellite commissioning
2. Maintenance
3. End of Life

Satellite commissioning

Phase of satellite commissioning sets requirements for initial manoeuvres of the satellite which are aimed on adjusting orbital parameters to achieve nominal orbit.

Amount of delta-v required in this phase dependent on launcher capabilities and desired orbit. In some cases this phase consists of largest delta-v manoeuvres in the whole mission lifetime. For WEP application the largest manoeuvres are the ones which set the size of intermediate tanks to provide sufficient storage of gases. However, commissioning manoeuvres can be separated into smaller manoeuvres for WEP to provide sufficient charging time without having to size the tanks larger than required for other mission phases.

In the case of the two reference missions the commissioning manoeuvres are not the ones with largest delta-v and do not set tank requirements. Total delta-v required for commissioning of each mission is shown in Table 3.12 and it indicates higher adjustment necessary for the CALIPSO orbit.

Table 3.12.: Commissioning delta-v budget for considered orbits [16]

	CALIPSO	Sentinel-3
Semi-major axis commissioning delta-v [m/s]	7.088	1.717
Inclination commissioning delta-v [m/s]	0	2.522

Maintenance - semi-major axis

Maintenance phase takes place during nominal satellite operations. By adjusting semi-major axis, altitude maintenance against atmospheric drag and collision avoidance are taken care of. Figure 3.5 shows evolution of semi-major axis during the whole maintenance phase for both missions during the same period of time. Semi-major axis was normalized in order to compare percentage deviations of both missions. It can be seen that required accuracy of Sentinel-3 is much higher while showing that the decay rate due to atmospheric drag is significantly affected by the difference in altitudes. The figure compares performance only for a two year period during which both satellites were at their nominal orbit.

Maintenance - inclination

Sun-synchronous orbits are beneficial for Earth observation missions due to the repeating ground track and consistent lighting conditions of Earth surface. This benefit comes with downsides. Due to luni-solar perturbation yearly inclination perturbation at these orbits can reach up to 0.047° which needs to be adjusted [12].

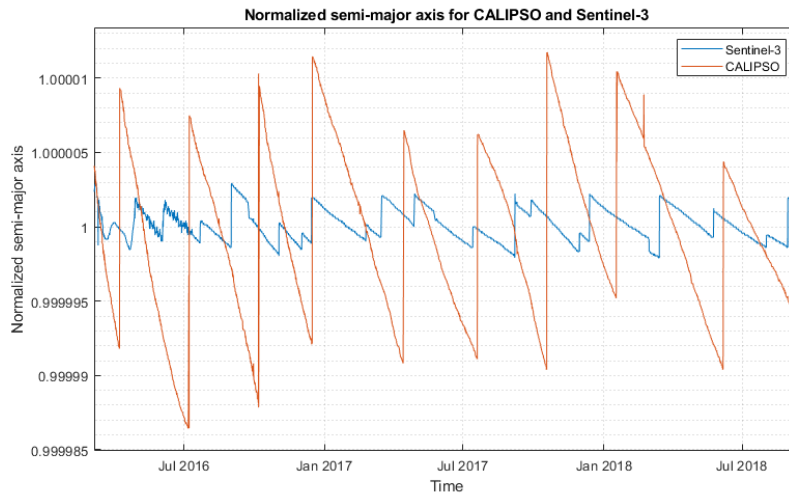


Figure 3.5.: Normalized semi-major axis evolution for considered orbits obtained from [16].

As in the case of semi-major axis inclination was normalized for both considered missions to see how the maintenance differs and it is shown in Figure 3.6. As in the previous case Sentinel-3 requires higher inclination precision at a cost of more frequent manoeuvres. By finding delta-v required for maintenance during the whole mission lifetime yearly budget can be determined and it is shown in Table 3.13. Inclination delta-v budget for both missions is similar but required delta-v to maintain semi-major axis is higher for CALIPSO by an order of magnitude. Main contributor to this difference is higher atmospheric drag which needs to be countered. This results in higher demand of delta-v and more frequent manoeuvres.

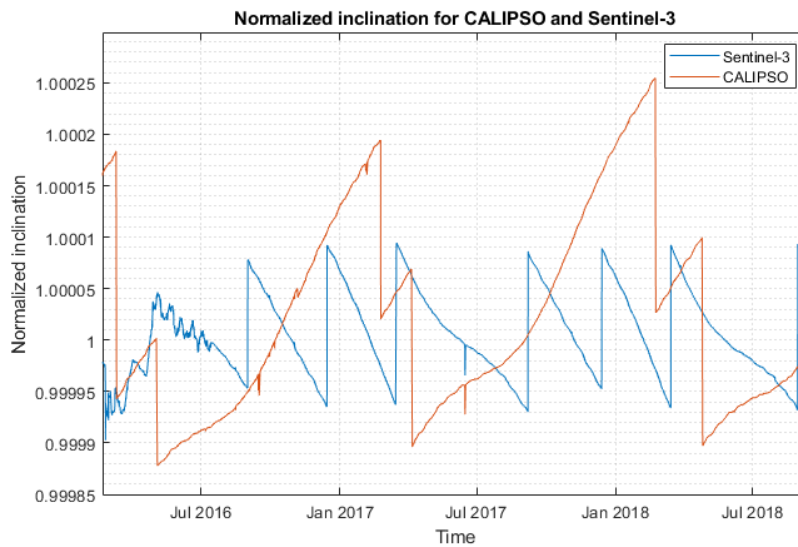


Figure 3.6.: Inclination evolution for considered orbits obtained from [16].

Table 3.13.: Maintenance delta-v budget for considered orbits derived from [16]

	CALIPSO	Sentinel-3
Semi-major axis maintenance delta-v [m/s/year]	1.299	0.119
Inclination maintenance delta-v [m/s/year]	5.612	5.757

End of life

Once nominal operations are completed, satellites in LEO are required to decay and re-enter Earth atmosphere within 25 years [1]. It is preferred that objects de-orbit directly but as will be shown later this is not a viable option for the considered orbits.

If such a condition cannot be achieved by orbital perturbations, active de-orbiting through the use of propulsion system or other de-orbiting means needs to be performed. To explore if active de-orbiting is required for considered orbits de-orbit simulations can be performed. Tool suite developed by European Space Agency (ESA) called Debris Risk Assessment And Mitigation Analysis (DRAMA) is used to perform required calculations and deduce means of de-orbiting via Observing Systems Capability Analysis and Review tool (OSCAR).

Drag coefficient is the main satellite property that affects de-orbiting along with the area orthogonal to direction of motion. If an exact value cannot be determined, it is acceptable to use value of 2.2 for the coefficient for long periods [19]. This is the case for the FLEX satellite.

To get an estimate of a satellite lifetime - time to reenter Earth atmosphere, initial conditions are important. Different approach is taken for CALIPSO and Sentinel-3 satellites. As Sentinel-3 is still operational and decommissioning date has not been decided yet, its latest position is considered as initial conditions for de-orbit analysis. CALIPSO is still operational but was moved into a lower orbit where it still performs nominal operations but de-orbits at the same time. The last position in its nominal orbit prior to altitude decrease was used for de-orbiting analysis. Starting date is another important parameter because solar activity during the year varies and it determines how high atmospheric drag is. Because CALIPSO initial conditions are from a different period to simplify the analysis start date is set for both missions as 2nd June 2023. Both initial conditions are shown in Table 3.14.

OSCAR assumes that once the altitude of the satellite reaches 120 km it can be considered as de-orbited.

Table 3.14.: Initial conditions for considered orbits for de-orbit analysis [16]

	CALIPSO orbit	Sentinel-3 orbit
Semi-major axis [km]	7080.61	7180.00
Eccentricity	1.42×10^{-4}	1.31×10^{-4}
Inclination [deg]	98.20	98.60
RAAN [deg]	191.80	202.73
Argument of perigee [deg]	79.39	103.51
Mean anomaly [deg]	280.74	256.62

Initial validation considers de-orbiting by natural decay. This orbital decay is dependant on orbital perturbations, mainly drag, which reduces altitude over time. Main factors that affect decay rate are solar activity, represented by solar radio flux, and Earth's magnetic field, represented by geomagnetic index. To assess their variation the following approaches can be taken:

1. ESA solar activity prediction
2. European Cooperation for Space Standardization (ECSS) sample solar cycle
3. Monte Carlo sampling

ESA solar activity prediction is a model developed by ESA that predicts evolution of solar and geomagnetic activity. ECSS sample solar cycle uses recommendation from ECSS-E-ST-10-04C standard which suggests repetition of a set solar cycle for the whole decay duration [20]. Monte Carlo sampling uses random assignment of parameters for each day which are in a range chosen based on desired number of previous solar cycles. To ensure credibility of the results all listed approaches are explored. It is required to use propagation time of at least 200 year unless re-entry occurs earlier [19].

Results of the considered approaches is shown in Table 3.15. It can be seen that none of the approaches indicate that FLEX would be able to de-orbit from either orbit within the required duration. So active de-orbiting is necessary. It also shows that ESA prediction provides the most conservative prediction of the solar activity out of the three cases.

Table 3.15.: Natural decay duration for different solar activity predictions

	CALIPSO orbit	Sentinel-3 orbit
ESA prediction estimated de-orbit [years]	79.17	180.20
ECSS solar cycle estimated de-orbit [years]	49.89	168.20
Monte carlo estimated de-orbit [years]	46.82	153.37

For active de-orbiting OSCAR provides different settings for de-orbit strategies. Two are relevant for LEO. These are direct and delayed de-orbit. Direct de-orbit means that a satellite de-orbits once it reaches perigee directly after de-orbit manoeuvre occurs on apogee which requires high delta-v for higher orbits. Delayed de-orbit strategy can be applied instead. It enables setting of a required remaining lifetime and a manoeuvre is performed at the beginning of a de-orbit period that enables reaching this goal by decreasing altitude at a perigee so that a satellite can decay by orbital perturbations.

When working with the remaining lifetime a requirement of 5 % margin required by International Organization for Standardization (ISO) standard ISO 27852:2016 is applied which is used for semi-analytical methods [21]. This margin serves as a buffer for potential force model and integration errors.

Because it was determined in the natural decay case that the ESA prediction model is the most conservative only that model is explored for active de-orbiting to obtain the highest delta-v that can be expected. Table 3.16 shows required delta-v for both active de-orbit strategies for both orbits. It can be seen that direct de-orbit requires more delta-v than is available for the FLEX mission and that is why it is unfeasible. Delayed de-orbit, which still results in the largest manoeuvre in the whole mission lifetime, is the best choice. The difference in required delta-v to de-orbit between the two orbits is significant and it counters the benefits of smaller semi-major axis maintenance for higher altitudes.

Table 3.16.: Required delta-v for active de-orbit scenarios

	CALIPSO orbit	Sentinel-3 orbit
Direct de-orbit delta-v [m/s]	162.41	187.84
Delayed de-orbit delta-v [m/s]	39.34	76.49

Conclusion

Total delta-v available on-board of the satellite can be found using Tsiolkovski rocket equation which was introduced in Equation (2.13).

Difficulty in estimating total delta-v lies in the fact that the satellite uses blow-down propulsion where specific impulse decreases over its lifetime. Value of specific impulse was assumed as 213 seconds which is a typical median value of specific impulse for blow-down hydrazine monopropellant propulsion systems in their complete cycle. With known propellant mass of 28 kg and launch mass of 460 kg, the total available delta-v is found to be 131.22 m/s which will be used for design of WEP.

With required nominal delta-v for the two different orbits found in previous sections it is necessary to account for uncertainties and include delta-v margins. Margin suggestions from ESA are considered [22]. Based on this margins related to delta-v budget can be split into three categories:

- Margin of 5 % shall be included for accurately calculated manoeuvres
- Margin of 100 % shall be included for general orbit maintenance manoeuvres (if they were not analytically derived)
- Margin of 100 % shall be included for attitude control and angular momentum manoeuvres

It is assumed that commissioning and maintenance manoeuvres were derived via analytical methods during the development and 5 % margin is applied. De-orbit delta-v was determined through analytical means and the same margin can be applied but it was already included within the DRAMA calculations via ISO 27852:2016 [21].

With total and yearly delta-v for individual manoeuvres known mission lifetime can be estimated and total delta-v contributions for each task calculated. This is shown in Table 3.17. Even though CALIPSO orbit altitude requires higher frequency of manoeuvres and higher delta-v for maintenance, the largest contribution - de-orbiting causes that its lifetime is longer than for Sentinel-3 orbit.

Table 3.17.: Complete delta-v budget for considered orbits

	CALIPSO orbit	Sentinel-3 orbit
Calculated lifetime [years]	11.64	8.15
Commissioning delta-v [m/s]	7.44	4.45
De-orbiting delta-v [m/s]	39.34	76.49
Semi-major axis maintenance delta-v [m/s]	15.88	1.02
Inclination maintenance delta-v [m/s]	68.57	49.26
Total delta-v [m/s]	131.22	131.22

Based on this de-orbit manoeuvre can be identified as the most demanding manoeuvre according to which the intermediate tanks should be sized to provide sufficient amount of propellants. However, sizing tanks for a manoeuvre which significantly deviates from other manoeuvres would introduce other challenges, such as high required volume and mass of the tanks, and it can be assumed that de-orbit manoeuvres will be split into series of smaller manoeuvres to accommodate required delta-v. This means de-orbit manoeuvre can be disregarded for sizing of WEP system and nominal manoeuvres will be used for sizing instead.

There are two important parameters for sizing. Maximum delta-v per manoeuvre, which sizes intermediate tanks, and highest gas generation rate manoeuvre, which sets requirements on the electrolyser. Table 3.18 shows both parameters and it indicates that Sentinel-3 delta-v budget is more feasible for application of WEP thanks to lower maximum delta-v per manoeuvre and smaller required gas generation rate which is going to lead to smaller mass of both components.

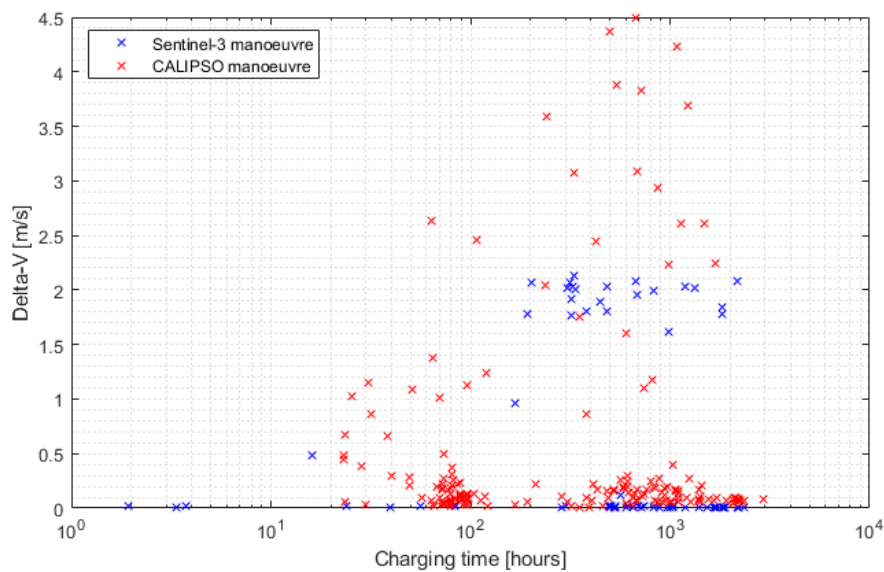
Table 3.18.: Critical aspects of the considered delta-v budgets for the two orbits [16]

	CALIPSO	Sentinel-3
Largest manoeuvre delta-v [km/s]	4.49	2.13
Largest charging rate demand [km/s/day]	0.96	0.73

Manoeuvre timing

Even though insight into the use cases of propulsion system and delta-v budget is important for general design of propulsion system to design WEP most important factor is the time between manoeuvres. To address this manoeuvres from historical data that were collected in previous sections to obtain delta-v budget were merged in a tabular form consisting of manoeuvre start, delay between manoeuvres and required delta-v. By plotting such data manoeuvre timing chart can be produced as shown in Figure 3.7 thanks to which sizing of the electrolyser can be performed by determining how many electrolyser cells are required to accommodate all manoeuvres. Electrolyser sizing using this chart is performed in later sections.

This figure indicates that Sentinel-3 delta-v budget is more feasible for application of WEP because not only is a lower maximum delta-v needed but its manoeuvres are also more organized at a similar delta-v level compared to the case of CALIPSO where large delta-v manoeuvres vary widely. Nonetheless, both cases will be explored and compared.

**Figure 3.7.:** Delta-v manoeuvre timing chart derived from data from [16].

4. Preliminary design

Preliminary design of WEP consists of determining how a satellite with conventional propulsion can be modified to be able to perform the same tasks but with WEP. Primary input to this analysis is the delta-v budget that provides required delta-v manoeuvres along with time available prior to each manoeuvre for propellant generation. With primary focus of the design on matching the performance of conventional propulsion, by achieving the same manoeuvres at the same time, the variable to minimize is the wet mass.

Sizing of individual components and subsystems along with description of their dependencies is done in the following sections.

4.1. List of assumptions

Focus of the preliminary design is mainly on parts of the propulsion subsystem which are not used in conventional propulsion subsystem. Parts of WEP system which are identical or operate similarly to conventional propulsion can be simplified at this stage to enable analysis of the whole system. Similarly, limited availability of experimental data and dedicated test bench still in development further steps need to be made to enable complete analysis. Assumptions made are listed in Table 4.1 and justification for their use is in their dedicated sections.

4.1.1. Operating temperatures

Internal satellite temperature

Operating and survival temperatures of each satellite subsystems vary widely. In depth thermal analysis is required to set these ranges, however, such analysis cannot be performed and there is no data available that would bring an insight into thermal management of the reference satellite.

More general approach is taken to explore thermal control of the satellite. Even though temperatures vary based on a mission type and technology used the most sensitive component was identified to be battery which typically operate between 0 and 30°. Other subsystems which are located in the internal structure and are not directly exposed to external influences operate in this range too [23], [24].

Therefore, for the purpose of this thesis an assumption is made that a reference temperature of all internal components of the satellite is set to 20°C. This means that as long as the tanks are located in the internal structure their temperature, along with propellants inside them, is 20°C.

Temperature of generated gases

Even though temperature of the generated gases varies based on electrolyser operating temperature, an assumption is made that due to a small flux of the generated gases their temperature decreases to the satellite internal temperature by the time they reach intermediate tanks.

4.1.2. Operating pressures

Water tank pressure

The operation of water tank is identical to the one used in conventional propulsion of FLEX - blow-down. This results in pressure variation with target maximum pressure of the water tank of 15 bar.

Combustion chamber pressure

Design and analysis of thruster is not part of this thesis. Its development is already ongoing and in current iteration the required operating pressure is 8 bar.

Intermediate tank outlet pressure

With target pressure of 8 bar set for combustion chamber pressure at intermediate tank outlets needs to account for pressure losses prior to reaching the thruster. At this stage it is assumed that pressure of 10 bar is sufficient to achieve the goal of 8 bar in combustion chamber.

Intermediate tank pressure

Intermediate tank pressure is given by performance of the electrolyser. In this stage it is assumed that the electrolyser can achieve maximum pressure of 100 bar which sets the maximum expected intermediate tank pressure.

Minimum intermediate tank pressure is given by properties of a gas that is stored inside of the tanks. Permeation, which occurs for hydrogen and will be explained in the section focusing on tanks, increases with increasing pressure so selection of long term storage pressure can negatively affect hydrogen losses. At this stage it is assumed that intermediate tank pressure for mission phases where no propulsion is necessary (minimum tank pressure) is equal to the intermediate tank outlet pressure - 10 bar. This enables thruster operation at constant pressure at all times resulting in constant specific impulse. Effects of selection of this pressure on hydrogen losses is explored in later sections.

4.1.3. Thruster

Focus on thruster is limited in this thesis as it is assumed that the thruster used for WEP is identical in performance to the one used in conventional propulsion for FLEX with the exception of specific impulse. Even though this affects other parameters of the thruster these are neglected at this stage. Intended operation of the thrusters is at a constant pressure which is achieved by pressure regulators placed downstream of intermediate tanks. With constant pressure flow into combustion chamber specific

impulse is constant too. An assumption was made that for this iteration of development specific impulse of 340 seconds is used.

List of all assumptions made is shown in Table 4.1. In later sections of this thesis effects of varying pressure and specific impulse, which were set by assumptions, are explored to determine their significance and quantify their effects on the satellite.

Table 4.1.: List of assumptions for preliminary design

ID	Assumption
Temperatures	
TEMP-1	Satellite internal temperature is held constant at 20°C
TEMP-2	Electrolyser nominal temperature is 70°C
Pressures	
PRES-1	Initial water tank pressure is 15 bar
PRES-2	Maximum intermediate tank pressure is 100 bar
PRES-3	Long term storage pressure - minimum intermediate tank pressure is 10 bar
PRES-4	Thruster combustion chamber pressure is constant at 8 bar
PRES-5	Intermediate tank outlet pressure is constant at 10 bar
Thruster performance	
THRU-1	Thruster specific impulse is 340 seconds and remains constant

4.2. Propulsion subsystem

As the type of propulsion subsystem to be implemented is given, focus of this section is on individual components which together form this system. WEP to be implemented is still in development which means that operation of such system needs to be simplified.

Primary difference between WEP and conventional propulsion is inclusion of electrolyser and intermediate tanks. These components are the main objective of this thesis as other operational considerations, such as thrusters, do not require implementation of novel technologies and are secondary. Major components are described in their dedicated sections because they require analysis for their selection. Minor components such as thrusters and valves are analysed in this section because they will be identical for every iteration of the design.

4.2.1. Propulsion operation

With WEP system still in development and focus primarily on components which are not present in conventional propulsion subsystem assumptions are made to simplify the analysis. Operation of WEP system can be divided into four steps:

1. Long term storage of water
2. Production of hydrogen and oxygen via electrolysis

3. Temporary storage of electrolysis products
4. Thrust generation

With first and fourth step being present in conventional propulsion subsystem assumptions are made to enable focusing on second and third steps which need to be analysed to provide better understanding of the system behaviour and help set requirements for future developments.

An assumption was made that thrusters which are intended for use on FLEX with hydrazine are kept the same for WEP in this analysis. Dedicated thruster will need to be developed for implementation with WEP in the future, however, at this stage a specific impulse of 340 seconds is assumed, which is a conservative assumption as higher values are achievable [3]. It is assumed that a pressure regulator is placed at the intermediate tank outlet to provide constant pressure input to thrusters and enable constant specific impulse operation.

There are several system designs available for propulsion subsystem. Simplest solution is to use the two gases in stoichiometric ratio - ratio obtained from electrolysis, in a single thruster. Alternatives require more complex design. This can range from use of secondary cold gas thruster to adjust main thruster mixture ratio, use of two different thrusters - fuel and oxidizer rich, or use of another propellant for use in tri-propellant configuration [3].

Even though these alternatives achieve lower temperatures than stoichiometric ratio, which results in combustion chamber temperatures above 3300 K, designs of thrusters that can withstand such high temperatures have already been developed [25]. The stoichiometric ratio approach is therefore chosen which reduces propulsion subsystem complexity.

4.2.2. Propulsion subsystem layout

Unlike propulsion subsystem working with hydrazine, which requires safeguards for ground operations as its release could harm personnel during ground operations, operation and handling of water enables simplifications in design of the propulsion subsystem and removal of these safeguards. Components typically used for this are a Latch valve (LV) or pyrotechnical valve which prevent leakage of propellant during filling operations. These add mass to the satellite which can be saved with WEP.

With layout of conventional propulsion of FLEX known, fluid diagram for WEP system is proposed in Figure 4.1. This diagram provides an insight into the operation of the propulsion subsystem and quantifies number of components from which mass can be the subsystem mass can be determined. Individual components used in the diagram are the following:

- Fill and Drain Valve (FDV) - for loading of propellants and unloading of gases and vapours
- Pressure transducer (PT) - measures pressure
- Normally open pyro-valve (PVNO) - for permanent closure of pipe if required
- Pressure regulator (PR) - maintains constant pressure input into thrusters
- Thruster (T) - complete thruster assembly, generates thrust
- CAP - cap that permanently closes a pipe

To ensure redundancy of the electrolyser in case of a failure, fluid system is separated into two branches with each of them holding half of the electrolyser cells. In case one cell fails PVNO in each branch can be used to close off water feed to prevent its leakage through cell membranes into the intermediate tanks. PVNO of the faulty branch behind the electrolyser is closed off too to prevent leakage and contamination of gases through the cells of the closed off branch due to effects of high pressure that acts from the second branch. This makes all cells in closed branch unusable but it enables continued safe operation of the electrolyser.

There are two FDV for both Hydrogen and Oxygen at the electrolyser outlet to enable venting of the accumulated air inside of each branch. Two FDV for water could be placed on the electrolyser for venting of the water channels. However, an assumption is made that these channels can be vented during loading of propellants and then permanently closed with caps rather than using FDV to reduce mass. The mass of the caps is assumed negligible.

Explanation of use for each component, with the exception of PT, PR and T whose purpose was already explained, is shown in Table 4.2.

Table 4.2.: Description of component tasks for WEP

Component	Primary task
FDV 1 & FDV 2	Loading of water and pressurizer gas
FDV H1 & FDV O1	Venting of each gas side in branch 1 during commissioning
FDV H2 & FDV O2	Venting of each gas side in branch 2 during commissioning
PVNO 1 & PVNO H1 & PVNO O1	Close off cell branch 1
PVNO 2 & PVNO H2 & PVNO O2	Close off cell branch 2

4.2.3. Propulsion components mass budget

With design of propulsion subsystem layout done mass of the whole subsystem can be estimated.

Because thrusters for FLEX are developed by Nammo [18], an assumption was made that all FLEX propulsion subsystem components are manufactured by Nammo where possible. For components that Nammo does not develop lightest compatible components from other manufacturers from Europe were used. For WEP the lightest compatible components available from European manufacturers were used.

Total number of components for each propulsion layout is shown in Table 4.3 [18]. Mass budget does not contain mass of tanks and electrolyser as these are analysed in later sections. As the number of components does not change during iterative design these masses are final. Mass of pipes for conventional propulsion was used based on a similar system and for electrolysis 20 % was added to account for expected increase. Total mass for both cases is comparable. If an alternative way of redundancy for electrolyser was found PVNO removal could improve WEP mass.

4.3. Tank selection

Tanks are expected to be a major contribution to mass increase in WEP compared to conventional propulsion subsystem. As not only is a tank for primary propellant required, but also tanks for each of the products of electrolysis. This provides a challenge in terms of selection of materials for tanks as each

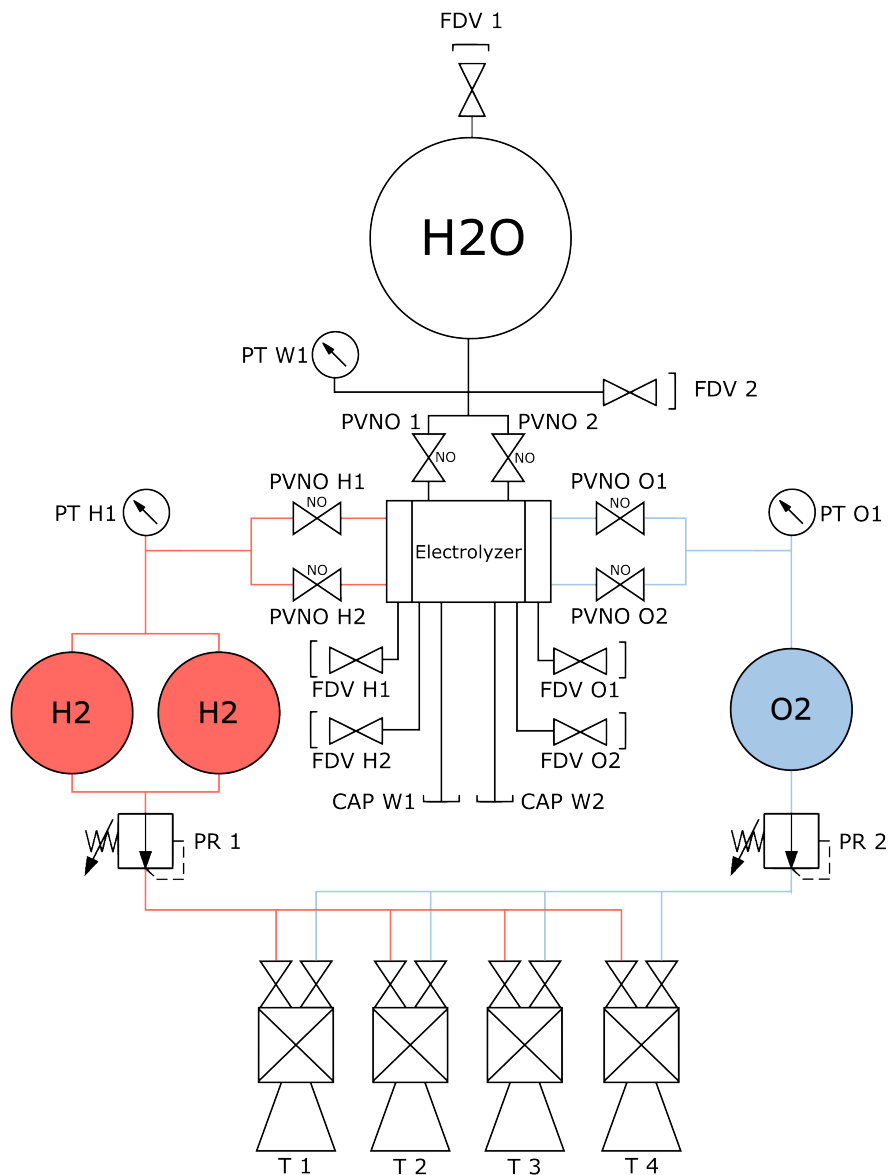


Figure 4.1.: Proposed fluid diagram for WEP

Table 4.3.: Mass budget for propulsion components of considered systems

Component	Conventional propulsion		WEP		Reference
	Number	Mass each [kg]	Number	Mass each [kg]	
FDV	3	0.05	6	0.05	[26]
PT	2	0.215	3	0.125	[27, 28]
PVNO	3	0.16	4	0.16	[29]
LV	1	0.545	-	-	[29]
T	4	0.45	4	0.45	[18]
PR	-	-	2	0.25	[30]
Pipes	1	0.6	1.2	0.72	[31]
Total [kg]		2.315		2.535	

of the species stored behaves differently. Degradation of material properties being the main concern due to effects of all three propellants along with leakage of hydrogen through tank wall due to the small size of hydrogen atoms - permeability.

Once desired volume of a tank is known sizing can be done according to Barlow's formula, shown in Equation (4.1), which relates dimensions of a spherical pressure vessel - thickness t and radius r , and its capability to withstand pressure p for given material yield stress σ [32]. Even though the equation differs depending on a shape of a pressure vessel in this case an assumption is made that only spherical tanks are used to simplify the analysis. Based on the assumptions made earlier two maximum pressure levels are explored; 15 bar for water tank and 100 bar for hydrogen and oxygen tanks.

$$p = \frac{2 \cdot t \cdot \sigma}{r} \quad (4.1)$$

Using Barlow's formula smallest theoretical thickness of a pressure vessel can be found. Resulting mass of a vessel for chosen tank radius r , tank thickness d and tank material defined by density ρ can be estimated via Equation (4.2) [32].

$$m = 4 \cdot \pi \cdot r^2 \cdot d \cdot \rho \quad (4.2)$$

However, Barlow's formula works with an ideal case - closed pressure vessel without parts which reduce stress that the pressure vessel can withstand such as orifices. Actual tank thickness needs to be higher, and correspondingly its mass, to account for these non-ideal features. As there is no way of calculating this non-ideal case market analysis of space-grade propellant tanks was performed to see deviation between calculated theoretical mass (via Barlow's formula) and actual mass to determine if there is a ratio between these two values that could be used to estimate masses of tanks of different sizes.

This market research revealed the factor between actual mass and theoretical mass calculated via Barlow's formula varies for each manufacturer. Tanks from company RAFAEL are a good benchmark because they were found to be one of few manufacturers that makes tanks in small sizes which are necessary for the reference satellite [31]. Furthermore, hydrazine tank used in satellites FLEX and CALIPSO is identical and is made by RAFAEL, making it the best reference. Factors determined from masses of their spherical tanks are considered. All these tanks are manufactured primarily from titanium alloy Ti-6Al-4V for use with hydrazine. To simplify the analysis an assumption is made that each tank is fully made out of this material to compare the two masses.

Using all their tanks Figure 4.2 can be created that shows dependence of the mass ratios on theoretical tank mass. Maximum expected operating pressure of all explored tanks is below 30 bar which is lower than intended pressure for the intermediate tanks. Inclusion of factor to account for pressure increase is disregarded because effect of pressure is already considered in Barlow's formula.

Using these values interpolation can be used to determine appropriate factor for tanks based on theoretical mass calculated via Barlow's formula to find actual tank mass. Collected data indicates that the smaller the tank is the larger the mass that needs to be added to estimate the actual mass.

Tank material is selected based on the substance that is held within it to ensure their compatibility to avoid tank/propellant degradation through mutual reactions. With most used material for tanks being

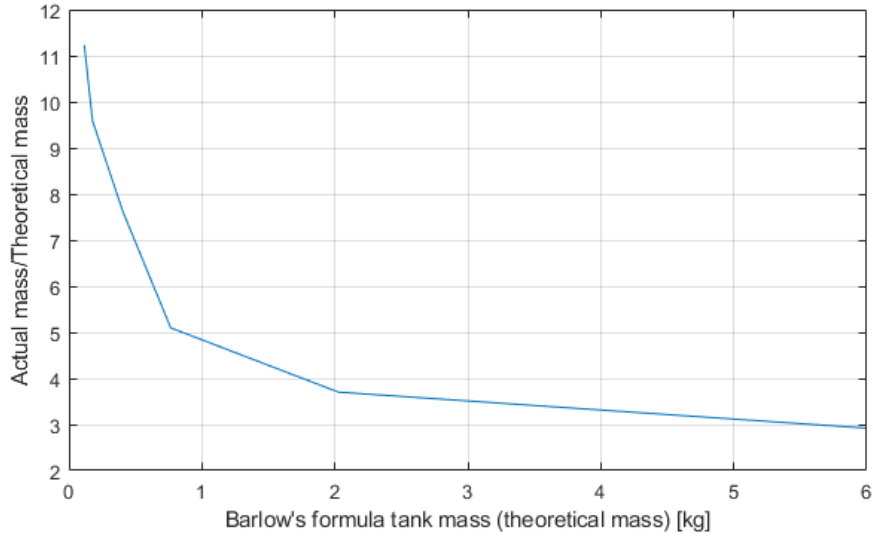


Figure 4.2.: Mass factors for tank sizing derived from [31]

titanium alloy Ti-6Al-4V it is the best candidate with a large selection of tanks already on the market. Feasibility of the titanium alloy for use alongside each substance is explored in individual sections and where possible alternatives are introduced.

4.3.1. Water tank

Main influence on water tank size is given by delta-v required to perform manoeuvres throughout the whole mission lifetime. Volume of the tank needs to be further increased for accommodation of pressurization mechanisms. For example storage of pressurizer gas for blow-down operated tanks.

Furthermore, as seen in Barlow's equation tank mass is driven by maximum pressure expected during operation. As FLEX utilizes blow-down system in its hydrazine tank with blow-down ratio of 4:1 [18], the same approach is chosen for the water tank. This sets volume of pressurizer gas and with initial pressure known mass of the pressurizer can be determined from an ideal gas equation shown in Equation (4.3) where p is pressure, ρ is density, $R_{specific}$ is specific gas constant and T is temperature. All gases in the analysis are assumed to be an ideal gas.

$$p = \rho \cdot R_{specific} \cdot T \quad (4.3)$$

Difference between conventional and water tank is in maximum pressure. As conventional propulsion subsystem is dependent on high pressure for efficient thruster operation its initial - maximum pressure is larger than for the case of water where a limit of 15 bar was assumed. This, alongside higher specific impulse of WEP leading to lower required propellant mass and similar densities of both substances, results in lower tank mass for water than for hydrazine if the same tank materials are used.

Water tank material selection

In the past storage of water in space was used for drinking and waste water on human missions. Materials used for this application vary but recently Thales Alenia Space was developing a tank for storage of drinking water with a shell made of titanium with bellow made of stainless steel [33]. Similarly, only off-the-shelf water tank, which is developed by MT-aerospace, is made of stainless steel [34]. These are the primary two materials which are considered.

With both materials being corrosion resistant selection is based on performance. If aerospace grade titanium alloys, such as Ti-6Al-4V, are considered they outperform stainless steel, such as AISI 316, by having both lower density and higher strength. With Ti-6Al-4V being one of the most used material for tanks availability of off-the-shelf tanks for use with water is high. With many manufacturers already confirming compatibility with de-ionized and distilled water [31].

Important consideration is operation of the water tank. In case of the original propulsion subsystem nitrogen is present inside the tank to work as pressurizer. Tank material needs to be compatible with these pressurizer gases. As for hydrazine blow-down mode is used for feeding of water and nitrogen is used as pressurizer with which Ti-6Al-4V is compatible. For tank materials incompatible with pressurizer gases alternative modes of operation need to be chosen.

Alternatively, composite tanks could be used for storage of water but no such tank has been found for space application. Due to this, Ti-6Al-4V is chosen as a material for water tank with composite offering reduction in tank mass in the future.

4.3.2. Intermediate tanks

Sizing of oxygen and hydrogen intermediate tanks is dependent on the largest required manoeuvre. Although products of electrolysis are in stoichiometric ratio, which based on their molar masses is ratio of oxygen to hydrogen of 7.94, their difference in density results in different sizing and masses of tanks. This causes that required volume for oxygen tank is half of volume required for hydrogen tank.

Intermediate tank volume needs to be larger than what is required for storage of propellants for maximum delta-v manoeuvre. With a required pressure output towards the thrusters more gases needs to be stored in the tanks to ensure that required maximum amount of propellant can be delivered above the required pressure. This additional propellant mass serves as a pressurizer as it is left behind to maintain pressure at all times. The larger the operating pressure of thrusters the larger the volume of the intermediate tanks is required to provide pressurization.

Tank mass is driven mainly by maximum pressure. With the assumption of maximum pressure of 100 bar, and the tanks being relatively small, mass calculated via Barlow's formula needs to be multiplied by a big factor, as shown in Figure 4.2, to find the actual mass which results in high tank masses.

Both gases are typically stored under cryogenic conditions in a liquid form for aerospace applications. Their storage in gaseous form provides challenges with tank material selection.

Hydrogen tank material selection

Hydrogen is typically stored in cryogenic conditions in space applications to prevent leakage of hydrogen atoms through lattice of tank material due to their small size. Application of gaseous hydrogen storage in space applications has not yet been sufficiently explored and the actual leak rates are unknown. Furthermore, titanium alloys such as Ti-6Al-4V suffer from a phenomena called hydrogen embrittlement which degrades mechanical properties of the alloy so protection layers need to be included in the tank for storage of hydrogen.

Alternative materials have been used for storage of gaseous hydrogen on Earth due to this issue so no data was found which would express degradation of titanium by hydrogen. Typical gaseous hydrogen storage on Earth is done in dedicated tanks which range from Type I, fully metallic vessels, to type IV, composite vessels with a plastic liner [35]. Type IV tanks are lighter thanks to use of composite materials and are generally used for storage of hydrogen in the range of hundreds of bar.

With the increased demand for hydrogen applications use of these tanks became more researched topic and Type V pressure vessel is currently being developed which would reduce tank mass even further. This is achieved by making the pressure vessel completely out of composites. This technology is believed to be the key for use in space applications [36].

If titanium alloys are deemed unfeasible for storage of gaseous hydrogen, difficulties with other components within the propulsion subsystem come up. As pipes, valves and other components within the system are made of titanium alloys alternative materials would have to be used for them too. Means of protecting the titanium walls from direct contact with hydrogen could be the solution.

Even though insufficient information is available about hydrogen permeation of both materials decision was made that due to uncertainty of compatibility of titanium and gaseous hydrogen for current generation of tanks, Type IV tank shall be used for storage of hydrogen on board of the reference satellite. An assumption is made that Type IV tanks are made completely of Carbon-Fiber-Reinforced Polymer (CFRP) to simplify determination of its mass.

Hydrogen permeation

As mentioned previously permeation is a phenomena that occurs when molecules, atoms or ions of a substance are sufficiently small to diffuse through lattice of a material. Permeation/leakage rate increases with increasing temperature and pressure. With small size of hydrogen ions permeation of hydrogen is a big problem which provides a challenge whose exploration intensified in recent years mainly thanks to increased demand for hydrogen storage in cars.

Permeation cannot be eliminated but there are means by which leakage of hydrogen through material lattice can be decreased. Selection of materials plays a significant role as more tightly packed lattice provides lower permeation rate. Alternatively use of coating or liners within the tanks enables use of conventional tank materials while providing required resistance to permeation [37].

With material of the hydrogen tank chosen as CFRP typical values of permeation were searched. Thanks to the aforementioned increase in interest due to utilization in land vehicles there are regulations in place which standardize leakage of hydrogen via permeation to protect users of such vehicles. Such regulations were introduced in regulation UN ECE 134 presented by Economic Commission for Europe of the United

Nations (UN/ECE). This permeation rate is introduced only for extreme temperatures, as permeation increases with increasing temperature, and they propose that maximum discharge of hydrogen can be 46 ml/l/hr. At the same time it needs to be ensured that maximum values of leakage do not reach higher values than 0.005 mg/hr [38]. As operation at high pressures is required leakage rate increases with increasing pressure and consideration of 46 ml/l/hr would result in values larger than 0.005 mg/hr. For this reason value of 0.005 mg/hr is taken as leakage rate at the maximum expected pressure of 100 bar. With known volume of considered tank and density of the gas at pressure of 100 bar value for permeation of 0.53 ml/l/hr can be found which results in fulfilment of the regulation.

Similarly, standards have been updated with the increasing use of hydrogen in vehicles. Currently the most recent standard is ISO 19881:2018(E) which states the maximum permeation rate of 6 ml/l/hr at any moment [39]. In comparison allowed tolerance for leakage of Helium for space systems given by ECSS standard ECSS-E-10-03A is $10^{-5} Pa \cdot m^3/s$ [40] or, after converting to common units by normalizing it with volume, 0.0009 ml/l/hr which is several orders of magnitude smaller indicating more strict requirements for leak tightness in space.

Ongoing research by Condé-Wolter et al. [41] explores different composites to use for tanks and proposes liners to prevent hydrogen permeation. Properties of multiple materials have been explored with varying degree of mean leakage rate from 0.091 to 0.904 ml/hr. For simplicity the lowest achieved leakage rate of 0.091 ml/hr is taken for comparison with previously introduced regulations and standards which, after normalizing, is equal to 0.022 ml/l/hr. All considered permeation rates are listed in Table 4.4.

Table 4.4.: Hydrogen permeation rates determined from literature search

Permeation case	Source	Original value	Common unit	Source
1	ISO standard	-	6 ml/l/hr	[39]
2	UN/ECE regulation	0.005 mg/s	0.53 ml/l/hr	[38]
3	ECSS Helium tolerance	$10^{-5} Pa \cdot m^3/s$	0.00088 ml/l/hr	[40]
4	Condé-Wolter et al.	0.091 ml/hr	0.022 ml/l/hr	[41]

Tolerated leakage rate of helium for space applications orders of magnitude lower than allowed leakage rate of hydrogen for Earth applications indicates that requirements for space applications of hydrogen will need to be set stricter than for Earth applications. However, it is uncertain whether hydrogen leakage can be reduced to values achieved by helium leakage as it is not known if both mechanisms are identical and also due to difference in size of atoms/ions for which permeation occurs. Therefore, use of helium leakage rate, as given by ECSS, cannot be used for the case of hydrogen to estimate permeation. With wide variation of allowed leakage rates proposed by Earth standards and with constant development of hydrogen storage, low permeation achieved by Condé-Wolter et al. provides an optimistic expectation for development of more leak tight hydrogen tanks in the future [41]. The value of 0.022 ml/l/hr determined in their research can be used for evaluation in preliminary design as a reasonable assumption of hydrogen permeation with expected permeation levels being reduced further in future applications. Chosen value is arbitrary as impact that the selected value has along with effects of varying permeation on satellite mass is explored in later sections in a sensitivity analysis.

With relation given by the ideal gas equation which states that with increasing pressure in the intermediate tanks hydrogen mass increases and so does density of the gas. With tank volume fixed density sets the mass leakage rate which means that pressure in the tank has an effect on the rate at which the hydrogen

permeates and this introduces a challenge to the gas generation schedule. In an ideal case the tanks would be kept at 100 bar at all times to provide required propellants on demand. This pressure would lead to high amounts of lost hydrogen so a smaller pressure has to be kept in the intermediate tanks to reduce hydrogen losses. To highlight the importance of reduction of permeation rate Table 4.5 shows yearly losses of hydrogen for permeation rates shown in Table 4.4. By reducing both pressure and permeation rate of the material less hydrogen is lost and less water needs to be carried onboard of the satellite to compensate for these losses as for each gram of hydrogen lost 8.94 grams of water need to be added to the propellant mass. With an assumption of long-term storage of hydrogen at 10 bar selected permeation rate of 0.022 ml/l/hr results in loss of only 0.66 g of hydrogen per year compared to 177.43 g for Earth applications given by the ISO standard but lacks in comparison with helium leakage rate.

Reduction of losses of hydrogen helps maintain hydrogen-oxygen ratio, that was generated during the electrolysis in intermediate tanks, without extensive venting of oxygen to make up for the lost hydrogen to keep pressure in both tanks equal.

Table 4.5.: Hydrogen losses due to permeation for different storage pressures

Permeation case	1	2	3	4
Pressure [bar]	Hydrogen permeation loss [g/year]			
1	17.74	1.58	0.003	0.066
10	177.43	15.77	0.026	0.66
50	887.15	78.84	0.13	3.30
100	1774.30	157.68	0.26	6.59

Amount of hydrogen lost needs to be calculated to determine additional water that needs to be carried onboard of the satellite to compensate for these losses. There are two contributions to permeation losses: idle, which accounts for losses in between manoeuvres when electrolyser is not running, and charging losses, which describe hydrogen loss due to increase of pressure during charging cycle of the electrolyser.

Calculation of idle losses is performed with the assumed intermediate tank pressure of 10 bar. Mass of gases corresponding to that pressure in tanks of known volume can be calculated from an ideal gas equation which enables calculation of density which can be used to determine permeation losses in unit of g/s. With total mission duration and charging duration for each manoeuvre known idle losses can be calculated.

The approach is identical for charging losses. However, as pressure varies so do the permeation losses and an iterative approach needs to be taken. This approach will be described further in later sections.

Oxygen tank material selection

As in the case of hydrogen, oxygen is typically stored in cryogenic conditions in aerospace industry which leads to different requirements on the tank material. This, along with typical use of liquid oxygen for launchers rather than satellite propulsion, results in use of aluminium-lithium alloys such as AA2195-T8 which was developed for the Space Shuttle mission and is still used today [42]. Even though the material was developed to perform best at cryogenic conditions it will be considered for storage of gaseous oxygen due to its light weight and corrosion resistance.

With common use of gaseous oxygen in medical applications on Earth an insight into means of storage in

this field shows that oxygen tanks are typically made of composites with carbon fiber providing a shell for a metallic liner. Possibility of use of composites for oxygen storage is supported by recent development of liner-less composite tanks, made purely of CFRP, for application in small launcher liquid oxygen storage which are comparable to Type V tanks in development for hydrogen storage [43].

Similarly as in case of water and hydrogen storage titanium alloy Ti-6Al-4V is considered for oxygen tank material too. With its corrosion resistance against oxygen, high strength to weight ratio and the availability of tanks of various sizes already on the market it is a safe choice for this application. However, with the recent developments in the field of composite tanks CFRP is a better choice than both AA2195-T8 and Ti-6Al-4V to achieve smaller mass. With Ti-6Al-4V being the second best choice over AA2195-T8 due to better performance and availability.

Properties of materials that were chosen for individual tanks along with considered ones are listed in Table 4.6. Even though CFRP tanks for required purpose are equipped with additional liners to improve their performance, the effect of the liners on the tank mass are neglected because their dimensions and material are unknown. Density of pure CFRP is therefore used. Performance of CFRP in terms of yield strength varies widely between individual types. In one research focusing on storage of hydrogen in aircraft applications National Aeronautics and Space Administration (NASA) determined yield strength of carbon composites to be up to 1900 MPa [44]. For the case of this thesis, more conservative value of 800 MPa is used based on data available from manufacturers [45].

Table 4.6.: Properties of considered materials for tanks

Material	Density [kg/m^3]	Yield strength [MPa]	Reference
Titanium alloy Ti-6Al-4V	4420	870	[46]
CFRP	1550	800	[45]
Aluminium alloy AA2195-T8	2720	517	[47]
Stainless steel AISI 347	7900	205	[48]

4.4. Electrolyser

Electrolyser sizing is the most important task in this feasibility analysis and it is dependent on the combination of required delta-v and time available for operation of the electrolyser prior to each manoeuvre. It needs to be ensured that the electrolyser is capable of producing propellants required to perform all manoeuvres.

The goal of this section is to determine performance of a satellite with an existing electrolyser. This approach is assumed valid only if relatively small number of cells is utilized because for higher number of cells it is more efficient to provide each cell with higher active area to reduce mass.

The existing electrolyser, later referenced as nominal, is being developed by Heizmann [8, 11] whose electrolyser cell provides 46.987 cm² of active area and it utilizes components shown in Table 4.7. The electrolyser always consists of two base plates and depending on the number of cells within the electrolyser corresponding number of H_2O , H_2 and O_2 plates is used with each cell separated by a separator plate.

Table 4.7.: Electrolyser components [8]

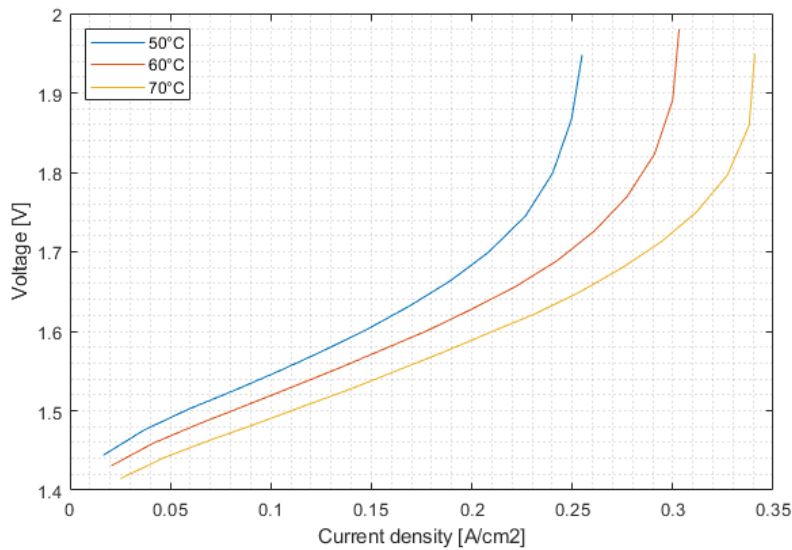
Part	Mass [g]
Base plate	324.1
Cell H_2O plate	59.5
Cell H_2 plate	21.9
Cell O_2 plate	57.2
Separator plate	133.0

4.4.1. Electrolyser performance

Sizing of the electrolyser relies on knowledge of its performance. In this section derivation of its performance is done from experimentally obtained data to be able to simulate electrolyser operation and aid in its sizing.

As the performance of the whole WEP system is driven by the electrolyser reliable data of its properties and behaviour are crucial for the upcoming steps. As a working prototype is already being developed electrolyser performance presented by Heizmann [11] can be used for system analysis which contains electrolyser performance at constant pressure of 1 bar at 3 temperatures - 50°, 60° and 70°C.

From this data dependence of current density on voltage, which is the electrolyser control variable that enables setting electrolyser performance, can be determined and it is shown in Figure 4.3. It can be seen that the higher the temperature the higher current densities can be achieved at the same voltage.

**Figure 4.3.:** Electrolyser current densities for voltage settings at different temperatures [11]

Based on data from Heizmann [11] and Harmansa [49] electrolyser efficiency increases with an increasing temperature. Temperature of 70°C is the most feasible to be set as an operating temperature as higher temperatures could damage the electrolyser. Data describing performance at 50°C and 60°C enable understanding of the dependency of individual properties on temperature.

Because an assumption was made in previous sections that the satellite temperature is 20°C electrolyser performance at this temperature shall be estimated to have whole operational range available. To obtain

these estimated values measured properties at 50 - 70°C were distributed in vectors of equal lengths and the difference between each point for each temperature were taken and gradients of each property with respect to temperature were found by averaging the gradients between the three measured temperatures.

Using these gradients for each property corresponding values at required temperatures were found. Both measured and estimated data can be seen plotted in Figure 4.4 for cell efficiency where it can be seen that not only cell efficiency decreases with temperature but also the available current density.

By deriving electrolyser behaviour at lower temperature boundary the whole operating range is available for analysis. It can be seen that estimated curves get more unreliable with decreasing temperatures although performance at lower temperatures is not important for electrolyser operation while it enables getting an insight into electrolyser behaviour during transient heating up of the electrolyser. Heating up duration and electrolyser performance during heat up will be analysed in a later stage.

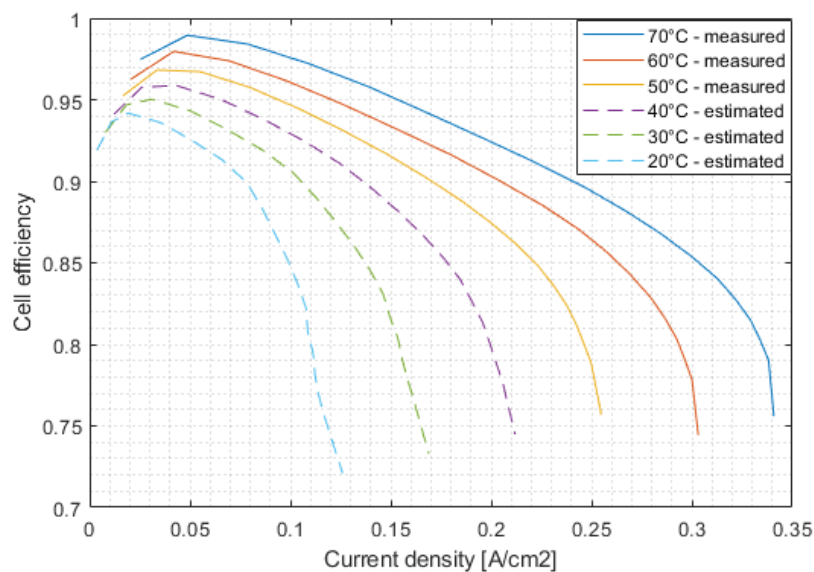


Figure 4.4.: Electrolyser performance at different temperatures [11]

Effects of pressure

As the experimental measurements were performed at a constant pressure of 1 bar there is no information about dependence of current density on pressure. No measurements can be performed at this time to study this dependency. Instead data from other electrolysers can be used for estimation. One such electrolyser developed by Harmansa [49] was tested in various conditions which explore dependency of current density on pressure and the results can be implemented for the electrolyser explored in this thesis.

As the measurements are available only in a graph form extraction of this data needs to be done first. MATLAB[®] script was developed which uses pictures in various formats as an input and as a result arrays of colour channels are generated for each pixel of a picture. Required curve from any plot can be extracted by setting a value of the curve in terms of Red-Green-Blue (RGB) colour channel. For example, if desired curve has a green colour each pixel which belongs to this curve will have the values of RGB as 0-255-0. This becomes more difficult if there are multiple curves in a plot or complex colours are used.

For the best results it is desirable to have a picture with as large resolution as possible and a curve which is distinct and consistent. These two requirements go together as sometimes, curves in low resolution pictures can have various fading colours and extraction is more difficult.

MATLAB[®] identifies all pixels where the green and blue channel are equal to 0 as belonging to the curve and extracts them. At this stage coordinates are given in terms of pixels, so assignment of property values is done to be able to use the extracted values. For this the input picture needs to be cropped right at the edges of the plot where the boundaries are. These can then be assigned on the first and last pixel for each axis and assigned linearly or logarithmically distributed values depending on what is required.

In the last step extracted data needs to be filtered. As curves are represented by multiple pixels corresponding to the same value they need to be reduced to have one value of y corresponding to each value of x . This can be done by finding values of y belonging to each value of x and keeping only the median value.

Although this approach does not enable getting the exact data it is a good estimation for the current stage of development. The process of extraction is shown in steps, which were described in previous sections, in Figure 4.5.

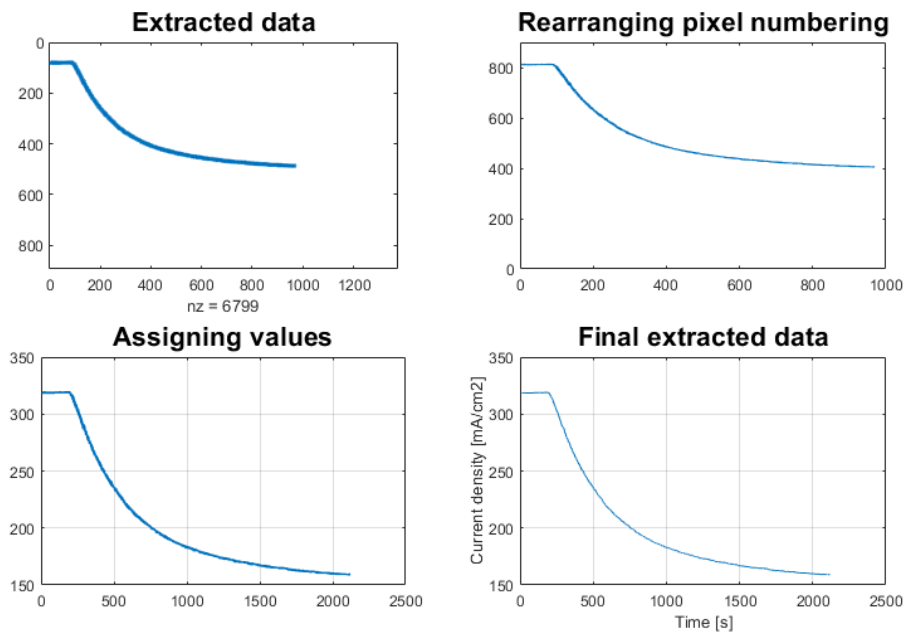


Figure 4.5.: Process of extraction of data for experimental measurements of [49]

With data extracted dependence of current density on pressure is now known in the original range analysed during the experiments of up to 22 bar [49]. Resulting curve is indicated in Figure 4.6 which shows dependency of current density on pressure derived from pressure and current density versus time curves.

Because required operating pressure goes beyond the measured one it is necessary to estimate current densities which are to be expected at the upper boundary of the pressure range - 100 bar. No research has performed electrolyser operations or experimental measurements at such a high pressure yet.

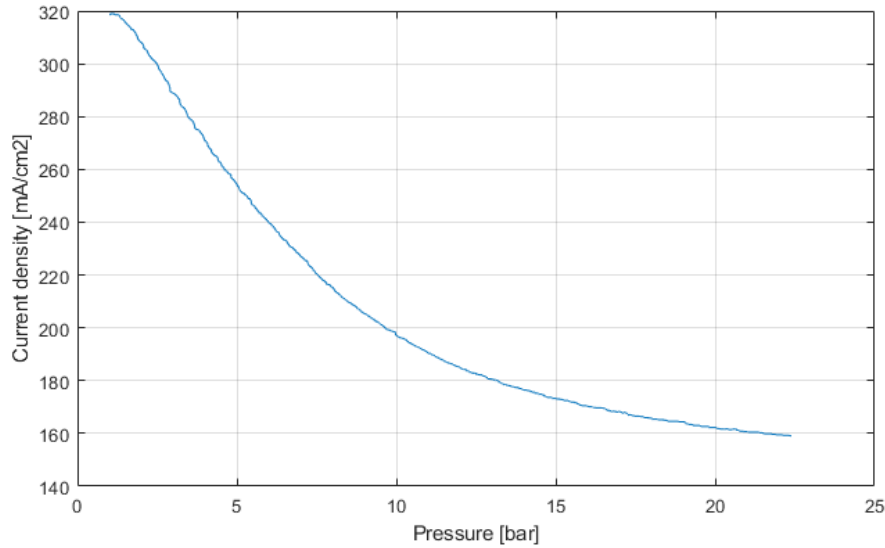


Figure 4.6.: Electrolyser performance dependency on pressure derived from [49]

To estimate behaviour beyond measured values curve fitting needs to be performed. Iterative approach based on trial and error was applied to find a correct representation of the pressure-current density curve. This approach resulted into representation of the current density-pressure curve via fifth order rational function shown in Equation (4.4).

$$j(p) = \frac{s_1 \cdot p^5 + s_2 \cdot p^4 + s_3 \cdot p^3 + s_4 \cdot p^2 + s_5 \cdot p + s_6}{p^5 + q_1 \cdot p^4 + q_2 \cdot p^3 + q_3 \cdot p^2 + q_4 \cdot p + q_5} \quad (4.4)$$

where j is current density, p is pressure, s_N , where $N = 1:6$, are numerator coefficients and q_n , where $n = 1:5$, are denominator coefficients. Corresponding coefficients were calculated via MATLAB[®] function "fit" and they are indicated in Table 4.8.

Table 4.8.: Coefficients for pressure-current density curve in Equation (4.4)

Coefficient	s_1	s_2	s_3	s_4	s_5	s_6	q_1	q_2	q_3	q_4	q_5
Value	143.6	-1590	17240	-167600	693900	-465400	-11.4	70	-474	2028	-1371

By applying the equation for original and extended ranges of pressure degree of accuracy of representation of the curve can be seen in Figure 4.7. Resulting curve, which can be called as a pressure-current density curve, shows the maximum available current density at each pressure level with significant reduction of current density at lower pressures and reducing importance of pressure at higher values.

Prior experiments observing dependency of current density on pressure indicated that there is a minimum value that the maximum available current density tends to with increasing pressure - an asymptote. Value of the asymptote can be calculated using limits at an infinite value of pressure in Equation (4.4). This results in a value of the lower boundary of current density of 143.59 mA/cm².

However, there are two limitations. The electrolyser used for experimental measurements differs from the one currently in development and the effect of temperature is not accounted for as the analysed data is for operation at 50°C while the intended operating temperature is 70° C.

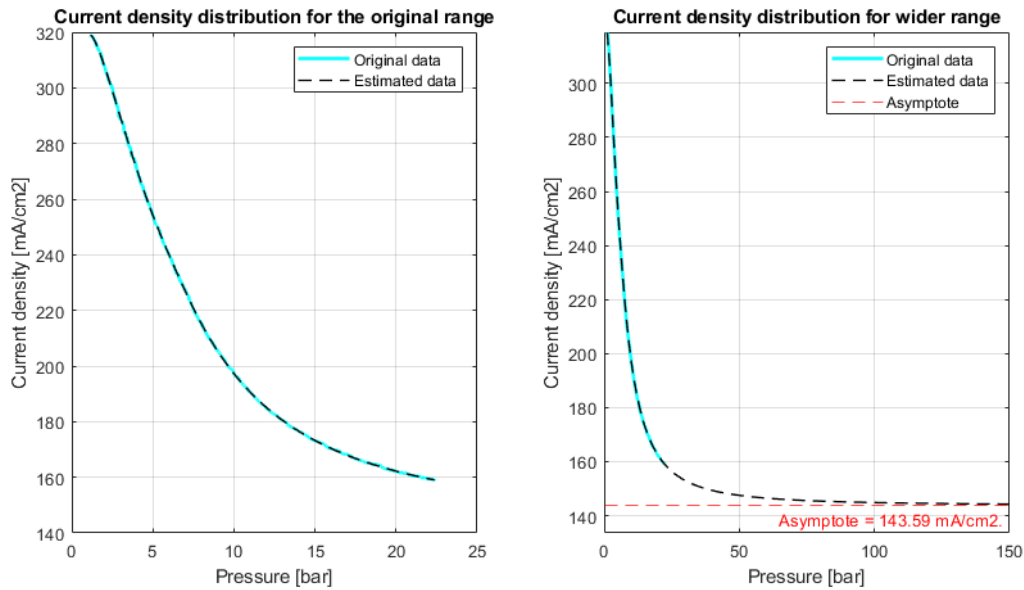


Figure 4.7.: Dependency of maximum available current density on pressure: pressure-current density curve [49].

Using value of current density at initial pressure and the asymptote a percentage decrease between initial and final current density can be found which is an indicator of performance of the electrolyser. Furthermore, the pressure-current density curve also provides an outlook towards the future in which higher pressures might be required and the value of the asymptote provides an estimation of lower current density boundary.

Resulting maximum available current densities at different pressure levels are shown in Table 4.9. These values enable derivation of the absolute current density drop between pressures of 0 bar and infinite to 42.31 % of the initial value. Once the required operating pressure range is known drop of maximum available current density across this range can be determined and applied to the performance data. It is assumed that this percentage drop is applicable to any electrolyser.

Table 4.9.: Maximum available current densities for various pressures

Pressure [bar]	Current density [mA/cm ²]
0	339.40
1	318.97
10	197.35
100	144.84
∞	143.59

To obtain pressure-current density curve for nominal electrolyser to be used in simulation of the electrolyser operation, the pressure-current density curve found in Figure 4.7 for the reference electrolyser can be used. Ratio of maximum available current densities for nominal and reference electrolysers at the same pressure can be found which when multiplied by current densities of the reference electrolyser enables determining the nominal electrolyser values for higher pressures. As measurements for the nominal electrolyser were performed at 1 bar this pressure is used to determine the ratio of nominal and reference electrolyser current density which resulted in a value of 1.076 that is used to obtain current density curve

as shown in Figure 4.8 for the nominal electrolyser. This approach leads to the same percentage drops of maximum available current density over the pressure range as in the case of the reference electrolyser. The reason why the available current density differs for the two electrolyser could be caused by the different temperatures at which the electrolysers were tested.

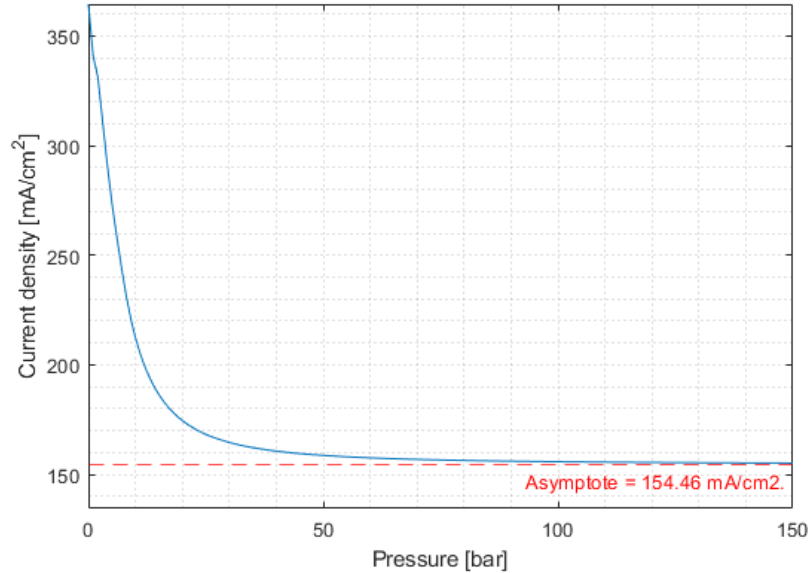


Figure 4.8.: Pressure-current density curve for the nominal electrolyser developed by [11]

Using pressure-current density curve performance of the nominal electrolyser can be adjusted to estimate effects that pressure has on electrolyser properties. In case of cell efficiency effect of pressure leads to a shift of the maximum available current density and position of the maximum efficiency point. This can be seen at various pressure levels in Figure 4.9. However, the point of maximum efficiency remains at the same voltage setting at all pressure levels even through degradation of current density.

Gas generation rate

With pressure-current density curve established dependency of mass flow rate on current density can be determined so that electrolyser sizing can be explored. Current density is directly connected to specific gas generation rates, which are independent of active area, via relationships in Equation (4.5) and Equation (4.6):

$$\Gamma_{H_2} = \frac{j}{2 \cdot F} \quad \left[\frac{\text{mol}}{\text{cm}^2 \cdot \text{s}} \right] \quad (4.5)$$

$$\Gamma_{O_2} = \frac{j}{4 \cdot F_c} = \frac{1}{2} \cdot \Gamma_{H_2} \quad \left[\frac{\text{mol}}{\text{cm}^2 \cdot \text{s}} \right] \quad (4.6)$$

where Γ_{H_2} is specific gas generation rate of hydrogen, Γ_{O_2} is specific gas generation rate of oxygen, j is current density and F_c is Faraday constant where $F_c = 96\,485 \text{ C/mol}$. To derive gas generation rate in terms of g/s specific gas generation rates can be expressed in the form of Equation (4.7) and Equation (4.8).

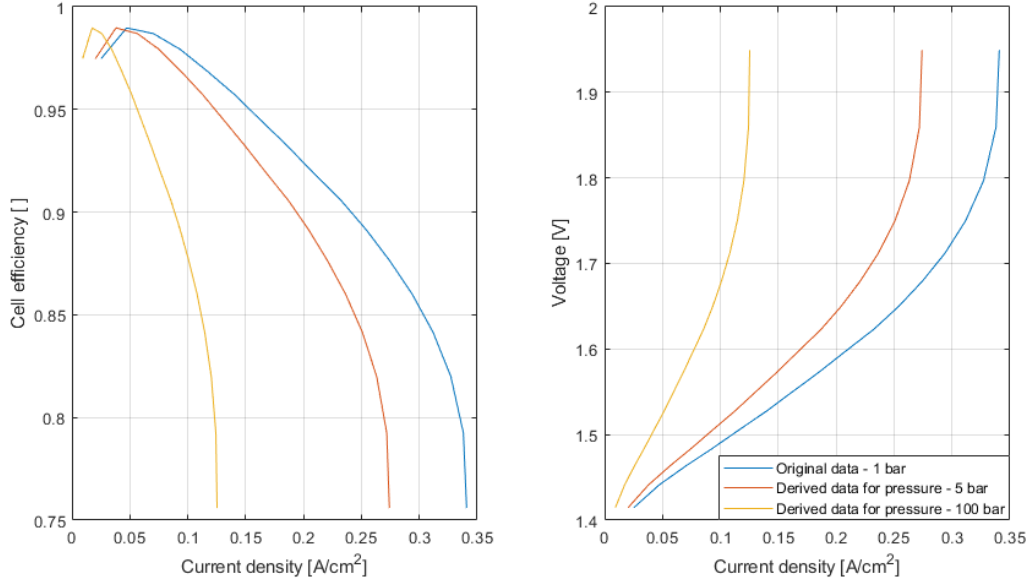


Figure 4.9.: Effect of pressure on electrolyser performance with original data from [11]

$$\Gamma_{H_2} = \frac{\dot{m}_H}{M_{H_2} \cdot A_{act}} \quad (4.7)$$

$$\Gamma_{O_2} = \frac{\dot{m}_O}{M_{O_2} \cdot A_{act}} \quad (4.8)$$

where \dot{m} depending on subscript is hydrogen or oxygen mass flow rate in g/s, M_{H_2} and M_{O_2} are molar masses of H_2 and O_2 molecule in g/mol and A_{act} is active area in cm^2 . By rearranging the equations the final expressions for hydrogen and oxygen generation are listed in Equation (4.9) and Equation (4.10).

$$\dot{m}_H = \Gamma_{H_2} \cdot M_{H_2} \cdot A_{act} = \frac{j}{2 \cdot F} \cdot M_{H_2} \cdot A_{act} \quad \left[\frac{g}{s}\right] \quad (4.9)$$

$$\dot{m}_O = \Gamma_{O_2} \cdot M_{O_2} \cdot A_{act} = \frac{j}{4 \cdot F} \cdot M_{O_2} \cdot A_{act} \quad \left[\frac{g}{s}\right] \quad (4.10)$$

To validate resulting gas generation rates Faraday law can be used which was previously shown in Equation (2.6). By replacing current with current density in this equation expression for determination of total generated gas from current density j can be found as Equation (4.11). The equation can be adjusted to express gas generated for each specie by assigning respective molar mass and it yields identical results to Equation (4.9) and Equation (4.10) for given period of time.

$$m = \frac{j \cdot A_{act} \cdot t \cdot M}{z \cdot F} \quad (4.11)$$

Both approaches provide only theoretical gas generation rate. To get the actual gas generation rate adjustment via Faraday efficiency, which expresses actual gas generation rate of hydrogen to the theo-

retical value, needs to be done. With theoretical value calculated and Faraday efficiency obtained from measurements the actual generation rate can be easily found for each setting of current density.

4.4.2. Electrolyser operation modelling

With behaviour and dependence of the electrolyser performance known from the previous sections modelling of its operation can be done. Purpose of this modelling is to create a mathematical model which is able to accurately depict operation of the electrolyser and the intermediate tanks to estimate gas generation rate at any point of operation. Voltage and corresponding current density at which the electrolyser is operated is important because it directly influences the performance. However, this topic is explored in later sections.

Propellants can be generated prior to each individual manoeuvre, or if there are manoeuvres with insufficient time in between them for complete propellant charge the charging process can be grouped as if the two manoeuvres were one. For the former case upper limit of current density is equal for all the manoeuvres as the initial pressure is always identical. For the latter the maximum permissible current density after the first manoeuvre depends on the remaining propellant in the tank and corresponding pressure. For simplicity, only the case of charging for a single manoeuvre is analysed.

By using the pressure-current density curve in combination with ideal gas equation gas generation rates can be determined for individual manoeuvres along with charging times. An iterative script was written which uses three inputs. Initial tank pressure, required propellant mass and step size. With step size being time increment during which gas generation rate is held constant. This enables simulation of process of gas generation which is divided into the following steps:

1. Determine pressure in the tank from mass inside using ideal gas equation
2. Determine maximum available current density corresponding to pressure from pressure-current density curve
3. Calculate gas generation rate for required voltage/current density
4. Calculate permeation rate
5. Subtract gas generation and permeation rates and multiply result with step size to get generated gas mass during this step
6. Sum generated gas mass with the mass in the tank
7. Check if required mass has been achieved, if not repeat

In short the script uses ideal gas equation to relate mass in the tank to pressure for which gas generation rate can be found from pressure-current density relation at each step. By adding up mass produced in each step into the tank pressure increases leading to change in gas generation rate. With sufficiently low step size gas generation can be accurately simulated and durations to achieve propellant masses for each manoeuvre can be found. Visualisation of the iterative process is shown in Figure 4.10. This script enables determination of the maximum available current density from the pressure-current density curve but any current density can be set for the operation using voltage.

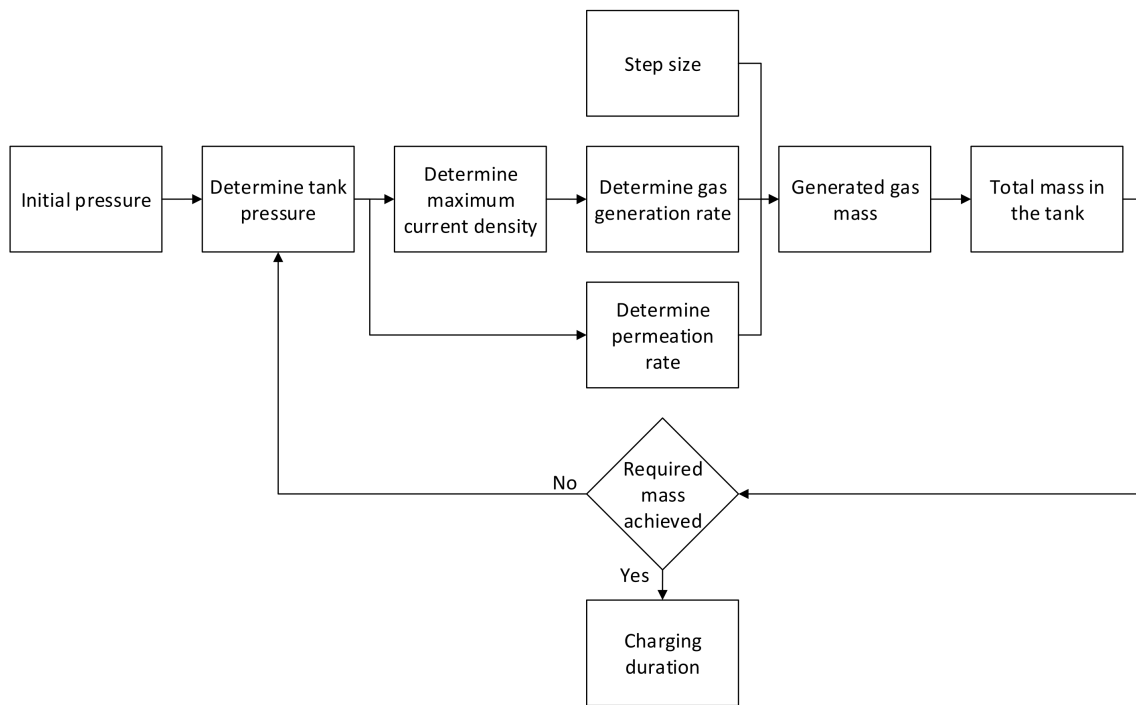


Figure 4.10.: Flowchart of simulation of electrolyser operation

To avoid running this script for all manoeuvres iteration can be run once for the largest manoeuvre to achieve maximum capacity of the tank to generate plots of pressure/mass dependency on time across the whole operating range. These curves, such as shown in Figure 4.11, describe electrolyser performance and can be created for varying number of cells to size the electrolyser to perform all manoeuvres.

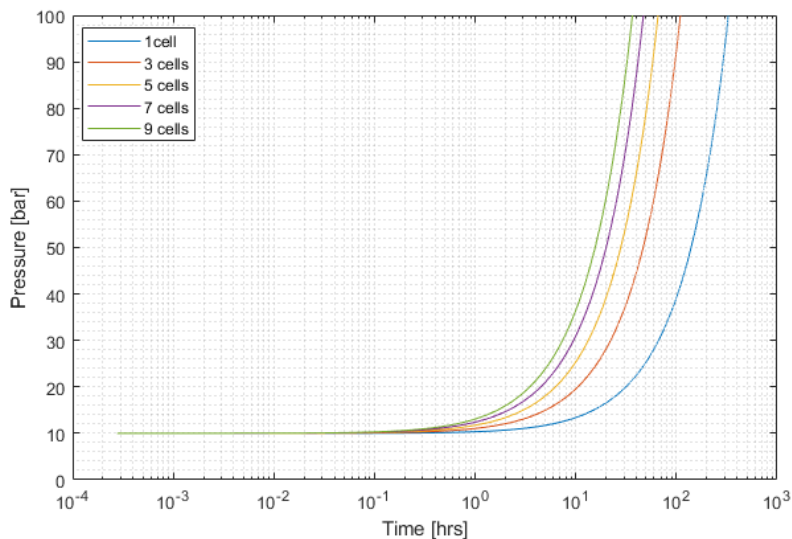


Figure 4.11.: Performance of electrolyser represented by charging curves for varying number of cells

With list of delta-v manoeuvres and corresponding charging time available and shown previously in Figure 3.7, this can be combined with the electrolyser performance plot to size the electrolyser directly for each considered case as shown in Figure 4.12 by ensuring all manoeuvres are below charging curve.

Based on this it can be seen that manoeuvres of the satellite Sentinel-3 are distributed in a way which would enable, with the exception of one manoeuvre, use of only 1 electrolyser cell to generate required propellants. However, for the sake of redundancy two cells would have to be included anyway. Wider distribution of manoeuvres for CALIPSO results in larger number of required cells.

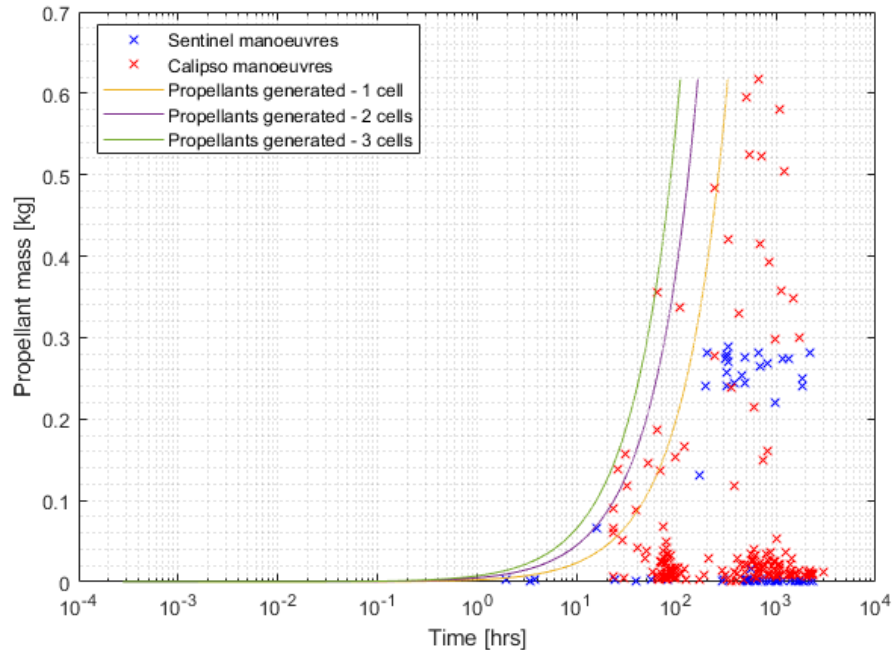


Figure 4.12.: Sizing of the electrolyser depending on delta-v requirements [16]

Charging cycle

Unlike in conventional propulsion propellants are not ready on demand and a charging timetable needs to be set up to provide time to generate propellants required for each manoeuvre. The simplest solution is operation of the electrolyser directly after each manoeuvre to fill the intermediate tanks fully. This approach is currently not investigated due to permeation which increases with pressure and results in high hydrogen losses.

With timetable of manoeuvres known an alternative approach is to calculate time required for generation of exact amount of gases required for each manoeuvre and setting the charging cycle in a way that the manoeuvre start coincides with charging cycle end. This approach is good for cases where each manoeuvre is scheduled but for spontaneous manoeuvres, such as collision avoidance, sufficient time is required to generate propellants to perform the manoeuvre on short notice. For cases considered in this thesis this is not a concern and this approach is chosen. Evolution of propellants in intermediate tanks during the mission for both approaches is shown in Figure 4.13 which uses CALIPSO delta-v budget.

4.4.3. Electrolyser thermals

Thermal behaviour of an electrolyser is a complex area whose exploration within the scope of this thesis is limited and a focus is given on top level thermal considerations; electrolyser start-up and electrolyser

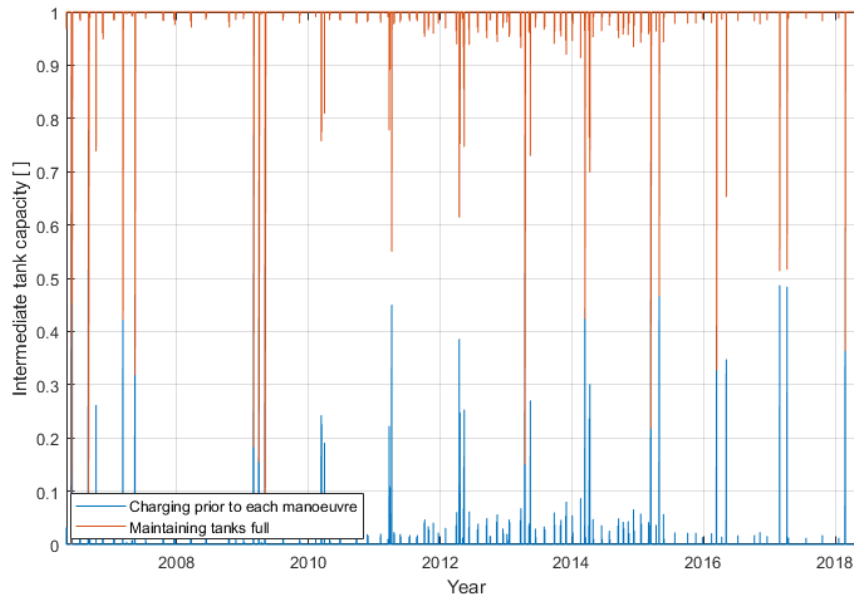


Figure 4.13.: Effect of charging cycles on propellants in intermediate tanks

nominal operations.

During the start-up of the electrolyser main focus is on duration of the heating up process. As it is necessary to achieve operating temperatures to ensure efficient performance. Nominal operations section focuses on heat that is generated by electrolyser and means of removing it.

Even though selected operating range of the electrolyser affects whole WEP for thermal aspects this is the most crucial consideration. With optimum current density at which nominal operations should be done unknown and no research indicating a global optimum two operating ranges are considered for the preliminary thermal analysis to show electrolyser thermal behaviour. These two operating points, which are shown in Figure 4.14, are both extreme points on the current density curve - point of maximum efficiency and point of maximum voltage - maximum available current density.

Optimisation process needs to be carried out between these two points depending on optimization goal as one point enables highest efficiency while the other provides higher gas generation rates which results in lower system mass at the cost of efficiency. Optimization for the case of this thesis, where matching performance of conventional propulsion whilst minimizing wet mass is the goal, is performed in later sections.

Electrolyser start-up

During start-up transient processes reduce electrolyser performance until the temperature of 70°C, which is set as the nominal operating temperature, is achieved. Reduction of heat up duration is desired to utilize full potential of the electrolyser mainly in terms of gas generation rate.

To find time required to heat up the electrolyser to operational temperature, thermal energy needs to be found first. This can be done using Equation (4.12).

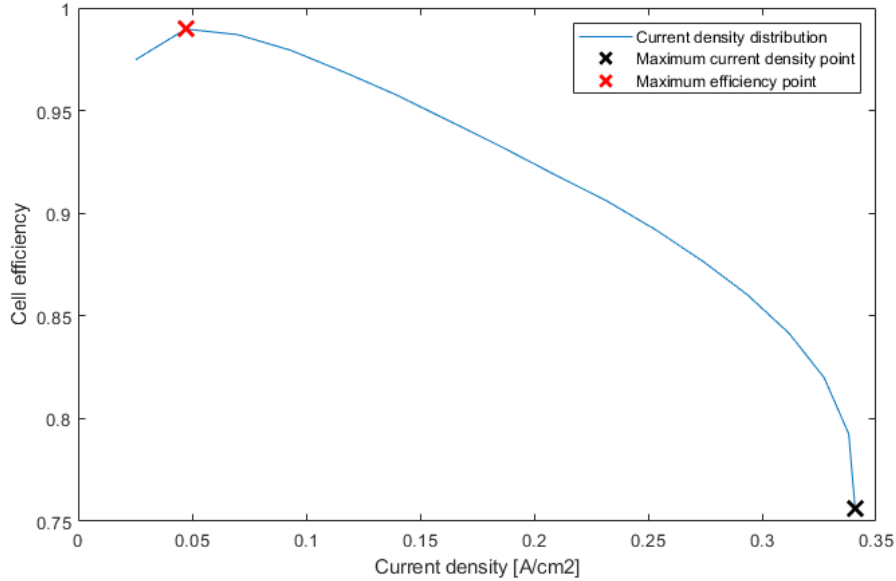


Figure 4.14.: Operating points considered for thermal analysis on current density curve obtained by [11]

$$Q_{th} = m_{EL} \cdot c_p \cdot \Delta T \quad (4.12)$$

where Q_{th} is thermal energy, m_{EL} is mass of the electrolyser, c_p is specific heat capacity in and ΔT is difference between initial and final temperature.

An assumption is made that full mass of the electrolyser is made of titanium to simplify calculations. Hence, specific heat capacity of titanium is $0.523 \text{ J/g}^\circ\text{C}$. Heating time depends on power of the electrolyser which increases with increasing current density that results from increasing temperature. Operating point in terms of power or current density is important during heat up because it affects speed at which the operating temperature is achieved. For fastest heat up electrolyser should be operated at maximum available current density - maximum power. But an assumption is made that heat up process has the same operational range or point as is chosen for nominal operation. Equation used to find heating time is given by Equation (4.13).

$$t = \frac{Q_{th}}{P} \quad (4.13)$$

where t is heating time, Q_{th} is thermal energy and P is power the electrolyser is supplied with.

To calculate time required to bring the electrolyser from initial temperature to the operating temperature iterative approach can be taken similarly how it was done in case of electrolyser in Figure 4.10. With data available for temperatures between 20° and 70°C only in increments of 10°C simplifications need to be made to enable this approach. The assumptions are the following:

- During heat up increase in pressure is negligible and pressure is assumed to be held at the initial value

- Current density and power variation between 20°C and 70°C are distributed linearly
- Constant voltage operation

Based on the assumptions effect of increasing pressure on current density is neglected and current densities corresponding to initial and final temperatures are considered at the initial pressure.

Fixed time step size chosen during which power, current density and gas generation rate are held constant. Equation (4.13) can be rearranged to enable determination of heat transferred to the electrolyser during this step size. Similarly, Equation (4.12) is rearranged to enable calculation of final temperature upon heat transfer which leads to Equation (4.14) where T_1 is initial and T_2 is final temperature for one step. Iteration then repeats at new initial temperature for which corresponding current density and power are calculated from the linear distribution and new thermal energy transfer for one step found. This repeats until the required temperature of 70°C is achieved.

$$T_2 = \frac{Q_{th}}{m_{EL} \cdot c} + T_1 \quad (4.14)$$

Since current density at each step is known gas generation rate can be calculated. By multiplying gas generation rate with the step size and adding them up in each iteration total generated gas during heat up can be calculated. Current density corresponding to initial pressure at the operating temperature can then be used to find gas generated for nominal operation during the time it takes to heat the electrolyser up to compare the values. Time required for additional nominal operation of electrolyser can be found that is needed to make up for lower gas generation during heat up.

Dependence of number of cells on heating time was considered alongside the two considered operating points. Heating time increases with increasing number of cells but overall added time per cell reduces in greater amounts of cells. Selection of operating point affects heating time significantly especially for lower current density settings. In these cases best solution might be higher current density setting during heat up to reduce heating time and to increase generated gases during this period even at a costs of reduced cell efficiency. Heating process for both operating points is shown in Figure 4.15.

Electrolyser performance with different number of cells for the two considered operating points is shown in Table 4.10. The table compares gas generated during heat up with gas generated during nominal operation for the same duration at the same pressure. Even though generated masses in both cases increase with increasing number of cells ratio of these two values stays constant. Between the two considered operating points the ratio differs by 1 %. Similar case occurs for the time required to compensate for heat up, which considers duration of nominal electrolyser operations that needs to be added to each manoeuvre to compensate for smaller gas generation rate during heat up. As the heating time and compensation time increase with more cells, their ratio remains the same.

Electrolyser nominal operations

During nominal electrolyser operations primary thermal effects occur due to heat which is dissipated by the electrolyser that comes as a result of inefficiencies in electrolyser performance. This heat is expressed via heat dissipation rate \dot{Q}_{diss} which can be determined via equation derived by Heizmann [8], which is shown in Equation (4.15).

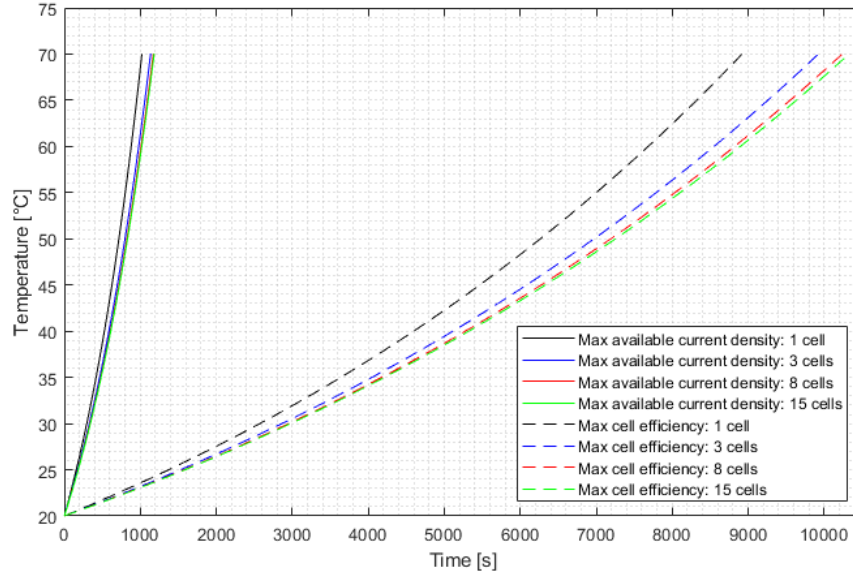


Figure 4.15.: Evolution of temperatures during electrolyser heat up for different operating points

Table 4.10.: Performance of electrolyser during heat up with varying number of cells

Case	Max available current density			Max cell efficiency		
	1	8	15	1	8	15
Number of cells						
Mass generated - heat up [g]	0.96	8.83	16.73	1.23	11.31	21.40
Mass generated - nominal [g]	1.52	13.94	26.39	1.98	18.14	34.30
Heat up vs. nominal mass fraction	63.35 %	63.35 %	63.38 %	62.37 %	62.37 %	62.38 %
Heating up time [s]	1021	1172	1183	8918	10237	10325
Time to compensate heat up [s]	374.21	429.48	433.17	3355.45	3851.68	3884.76
Fraction of time to compensate	36.65 %	36.65 %	36.62 %	37.63 %	37.63 %	37.62 %

$$\dot{Q}_{diss} = \frac{A_{act} \cdot \Psi}{\eta_F} \cdot (\eta_{cell} - 1) \quad (4.15)$$

where A_{act} is active area, Ψ is power density, η_F is Faradaic efficiency and η_{cell} is cell efficiency.

Heat dissipation rate is dependent on pressure as pressure affects current and power densities which are primary influence on \dot{Q}_{diss} . The lower the pressure the higher current densities are available and correspondingly highest heat dissipation rate occurs. Therefore, consideration of the operating range is important as it heavily influences released heat. Figure 4.16 shows resulting heat dissipation rate for pressures of 1 and 100 bar. Heat dissipation rate in this figure is normalized as the non-normalized value depends on number of cells which at this stage is unknown. However, ratio of heat dissipation rates in the selected pressure range remains the same at any number of cells.

To counter released heat it is necessary to remove it which can be achieved by absorption of heat by satellite structure. To describe thermal relationship between electrolyser and satellite structure it is first necessary to calculate capability of structure to absorb this heat. Equation (4.16) describes calculation of heat rate that can be absorbed by satellite structure.

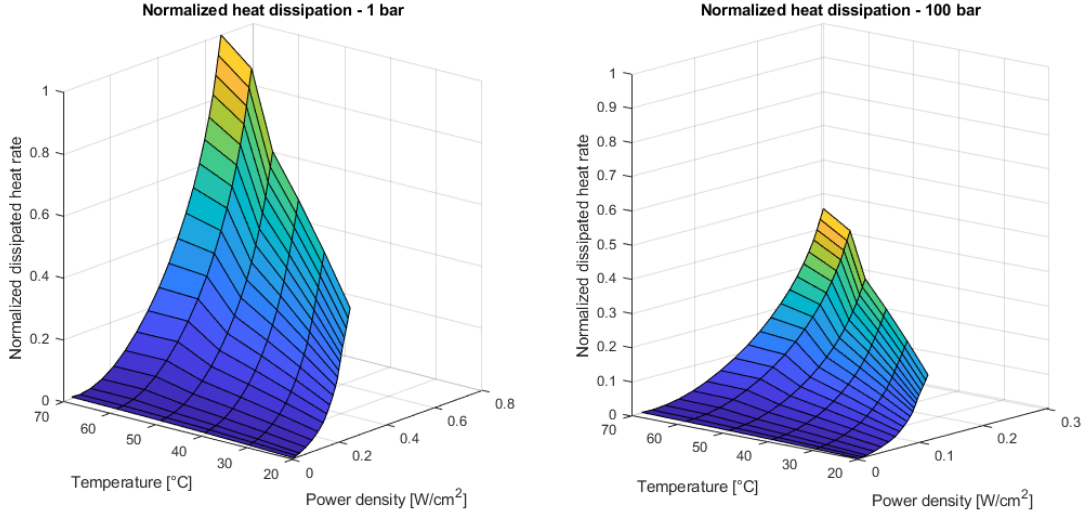


Figure 4.16.: Heat dissipation rate dependence on electrolyser performance and pressure

$$\dot{Q}_{abs} = \frac{T_{op} - T_{SAT}}{R_{\lambda}} \quad (4.16)$$

where \dot{Q}_{abs} is absorbed heat rate, T_{op} is electrolyser operating temperature, T_{sat} is satellite structure temperature and R_{λ} is thermal resistance.

To adjust amount of heat absorbed by satellite structure thermal resistance R_{λ} plays crucial role. Its selection determines effects of heat released by electrolyser on its performance and heating of satellite structure. The value can be determined by assuming that heat dissipation rate \dot{Q}_{diss} is equal to \dot{Q}_{abs} . An equilibrium temperature, which indicates balance of generated and absorbed heat, can be achieved. However, \dot{Q}_{diss} depends on an operating point of the electrolyser and selected thermal resistance will lead to desired thermal behaviour only at this one operating point where there is equality of \dot{Q}_{diss} and \dot{Q}_{abs} .

Setting thermal resistance

When selecting thermal resistance an optimization process that is beyond scope of this thesis is required. Simplified approach is taken to determine main implications of the selection.

As two operating ranges were chosen optimal R_{λ} is different for both of them. The simplest approach to select R_{λ} is to set it based on the initial operating pressure which is present at the start of each charging sequence. The reason why this is assumed to be a valid approach is because it is necessary to ensure that the electrolyser does not generate heat rate that would cause it to reach temperatures higher than 70°C which would result in damage. By setting \dot{Q}_{diss} and \dot{Q}_{abs} equal at this initial point thermal resistance can be found for which the equilibrium temperature of 70°C at this initial operating point can be achieved. By setting \dot{Q}_{diss} and \dot{Q}_{abs} equal Equation (4.15) and Equation (4.16) can be combined to achieve Equation (4.17) to find R_{λ} for required power density Ψ .

$$R_\lambda = (T_{op} - T_{SAT}) \cdot \frac{\eta F}{A_{act} \cdot \Psi \cdot (\eta_{cell} - 1)} \quad (4.17)$$

However, as pressure increases power density and corresponding heat dissipation rate decrease. Selected thermal resistance no longer leads to the equilibrium temperature of 70°C. Instead it is at lower values because heat rate absorbed by the satellite structure is higher than electrolyser heat dissipation rate. This means that the electrolyser heat is not sufficient to maintain its temperature at required value which leads to degradation of its performance. It would therefore be necessary to provide alternative means of maintaining electrolyser temperature above the equilibrium temperature or vary electrolyser current density.

Alternatively thermal resistance could be chosen at the final operating point of 100 bar. This approach would remove ability to operate the electrolyser at high current densities because the equilibrium temperature of 70°C occurs only at the end of the operating range and at any other point it is above it. Instead current density would have to be chosen at lower values to reduce achievable temperatures and reduce gas generation rate.

An example of heat dissipation rates for the case of maximum available current density at expected pressures of 1 and 100 bar, for which R_λ was set at the initial pressure of 1 bar, is shown in Figure 4.17. Orange plane in both plots represents absorbed heat rate by the satellite structure. Intersection of the heat dissipation rate and absorbed heat rate indicates equilibrium temperature for different power densities. At 1 bar, at which R_λ was chosen to achieve 70°C, this equilibrium temperature is achieved. By the time pressure increases to 100 bar the equilibrium temperature drops to values below 40°C.

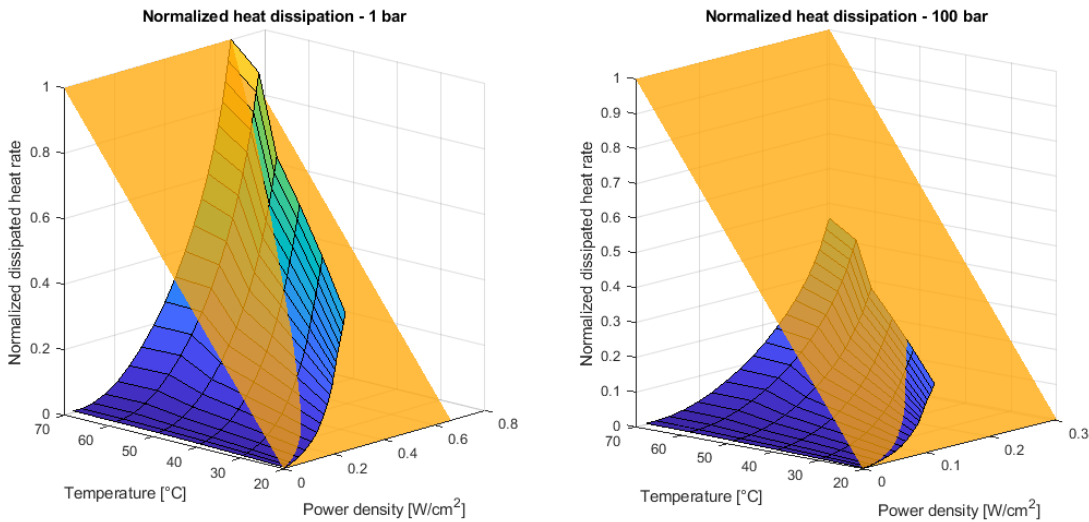


Figure 4.17.: Heat dissipation rate (blue) with satellite absorbed heat rate (orange) at different pressures for operating case of maximum available current density. Thermal resistance R_λ was set for maximum current density at 1 bar. Intersection of surfaces shows equilibrium temperature.

As variation of heat dissipation rate is dependent on operating range it should be part of optimization. But because heat dissipation rate is not target of the optimisation in this thesis it is assumed R_λ is set at 1 bar at required power density Ψ and alternative means of maintaining electrolyser temperature at 70°C at higher pressures are used.

4.5. Power subsystem

Power subsystem designed for satellite with conventional propulsion needs to be adjusted to account for power increase required for operation of the electrolyser. To simplify redesign of the subsystem it is assumed that power available for the satellite with conventional propulsion is fixed and is all used for nominal operations of the satellite.

To obtain power required for operation of the electrolyser size of the power subsystem needs to be increased. To simplify this, scaling of the existing power subsystem is used to obtain mass of power subsystem for a satellite with WEP. To resize all components maximum power at EoL is used for scaling. Scaling formula used is shown in Equation (4.18) where m_{new} is component mass for WEP case, $m_{original}$ is component mass for conventional propulsion, P_{new} is EoL power required for WEP system and $P_{original}$ is EoL power for conventional propulsion system.

$$m_{new} = P_{new} \cdot \frac{m_{original}}{P_{original}} \quad (4.18)$$

Simplified power subsystem is divided into three main components: solar array, Power Conditioning and Distribution Unit (PCDU) and battery. Masses of individual components used for FLEX is known and is shown in Table 4.11. Equation (4.18) is applied to each component separately to resize it.

Table 4.11.: Masses of components used in power subsystem of FLEX [50]

Component	Mass [kg]	Capability
Solar array	24.98	Power at EoL: 700 W
PCDU	14.99	Peak power: 1000 W
Battery	15	Capacity: 45 Ah
Power subsystem	54.97	

To provide sufficient power for nominal operations and electrolyser operation power needs to be increased which leads to increase of solar array and battery masses. If total required power is larger than 1000 W, which is the peak power of the PCDU, it needs to be resized too.

4.6. De-orbit

Due to how propellant is treated in WEP compared to conventional propulsion subsystem single burn cannot be performed to lower periapsis of a satellite's orbit to begin de-orbit. This is caused by size of the intermediate tanks which are sized according to the largest manoeuvre during nominal lifetime. Although de-orbit manoeuvre is the largest, sizing the tanks according to it is inefficient. De-orbit manoeuvre is therefore split into number of smaller manoeuvres to reduce altitude while using tanks sized according to nominal operation manoeuvres.

Two primary factors which affect WEP de-orbit are the starting altitude and the gas generation rate of the chosen electrolyser. Similarly to how heat-up of the electrolyser was treated it is assumed that no special setting of electrolyser in terms of current density is used for de-orbiting to simplify the analysis. Delta-v required for de-orbiting for both orbits was previously found in Table 3.17.

By determining velocity at apoapsis of the final orbit and subtracting delta-v required for de-orbit final velocity at apoapsis is determined. De-orbit manoeuvre duration can then be determined iteratively. With performance of the electrolyser modelled and duration of one full orbit known this time can be used to generate as much of propellant as possible for use upon reaching the apoapsis. With duration of each orbit for both cases of around 100 minutes this process needs to be repeated until the required de-orbit delta-v is achieved.

4.7. Mathematical model solver

To determine effects of individual components and subsystems on the complete system, means of combination of all the contributions needs to be developed. This is done in MATLAB[®] where all considerations from previous sections are implemented to produce a solver for performing preliminary design. Primary goal of the solver is to achieve the optimisation target which for the WEP system is to match performance of the conventional propulsion subsystem and minimizing mass of the satellite.

Main challenge of such solver are interconnections between individual components which result in the need for iterative approach. Coupled components can be split into two categories; primary and secondary. Primary category are components which are changed depending on delta-v budget and dry mass of current iteration, such as the electrolyser and tanks. Secondary category concerns subsystems which need to be resized to accommodate primary category components' needs, such as power subsystem which needs to be resized to provide power required by the electrolyser.

Top level overview of mass iteration is shown in Figure 4.18 and it consists of components which are described in previous sections. It contains following inputs:

- Initial dry mass - dry mass of the satellite with conventional propulsion subsystem which serves only for initialization of the iteration
- Delta-v budget - list of delta-v for manoeuvres with corresponding charging times
- Propulsion subsystem added mass - masses of all non-varied components within WEP - all components excluding tanks, electrolyser and propellants
- Electrolyser performance - experimentally obtained data for derivation of electrolyser properties

The reason why propulsion subsystem added mass is not iterated is because it consists of components of the propulsion subsystem which are fixed. The propulsion subsystem is designed in a way that number of components such as thrusters, valves and others are fixed and are not iterated. The fluid diagram indicating all of these components was introduced in Figure 4.1.

The most important parameter for iteration is delta-v budget. It is used along dry mass to estimate total mass of required propellant to size primary tank. It is used to determine propellant required for each manoeuvre to find the largest manoeuvre to size intermediate tanks. And each manoeuvre in combination with charging time is used to determine size of the electrolyser and power subsystem required to operate it. Once all masses are added up to create new dry mass the iteration repeats until mass difference between iterations goes below required value.

5. Optimization

Focus of this section is on finding optimal operating range of WEP which enables matching performance of the conventional propulsion subsystem while achieving minimum mass. Main challenge of the optimization is caused by interconnections between individual components of the WEP system. Current density is the main variable that influences performance of WEP and its selection becomes the target of the optimization effort. Selection of current density has the following effects:

- Change of gas generation rate
 - Affects electrolyser mass
 - Longer charging results in higher propellant loss via permeation at higher pressures
- Change of power for electrolyser operation
 - Affects power subsystem mass
- Change of electrolyser efficiency
 - Affects heat dissipation rate
 - Affects gas generation

Because it affects all of the different aspects of the satellite operating point/range cannot be defined globally and it needs to be tailored for the needs of each mission.

5.1. Current density optimization

Previously two cases were considered as an operating point for thermal analysis: point of electrolyser maximum efficiency and point of maximum available current density. Target of this chapter is not only analyse satellite performance at these two extreme points but also to analyse the whole current density range to determine whether there are any other optima.

Delta-v budget for Sentinel-3 is taken to show difference in satellite properties for the two cases. This helps in determining where different optimization goals should be focused. Some of these properties, which come from preliminary design introduced in previous chapter, are shown in Table 5.1. They indicate that if the optimization goal is mass reduction, higher current density is desirable. However, decrease in efficiency causes that more power is required for operation which leads to higher heat dissipation rate and heavier power subsystem. Power and heat dissipation rate shown are for conditions at the start of charging cycle - 1 bar. As pressure increases power and heat dissipation rate decrease.

It also indicates that if efficiency is the main goal of optimization process, operation at point of maximum cell efficiency brings small losses but more electrolyser cells cause that the whole system is heavier.

Table 5.1.: Satellite properties for extreme operating points for Sentinel-3 delta-v budget

	Max cell efficiency	Max voltage
Number of electrolyser cells	12	2
Wet mass [kg]	462.859	454.113
Propellant mass [kg]	17.905	17.566
Electrolyser mass [kg]	10.90	1.71
Power subsystem mass [kg]	56.339	57.195
Cell efficiency	0.99	0.76
Electrolyser power [W]	23.97	38.96
Electrolyser heat dissipation rate [W]	0.26	9.56
Time to heat up [s]	10300	1108

Important consideration is also time to heat up the electrolyser which due to its size and small current density is significantly longer for maximum efficiency case. If short charging cycles are present during a mission this would cause poor performance of the electrolyser.

To determine performance of the system at various operating points, data obtained experimentally is used. It consists of measurements of different properties of the electrolyser at various voltage settings at pressure of 1 bar which lead to different values of current density. Voltage is a control variable that determines current density of the electrolyser depending on electrolyser temperature and intermediate tank pressures. This is possible because, as shown previously in Figure 4.3 and Figure 4.9, voltage range stays constant at any pressure and temperature and only current density and efficiencies degrade. Chosen operating point in terms of voltage is therefore assumed constant during the complete operation cycle. For this reason voltage is used to characterise individual operating points and it ranges from values of 1.41 V to 1.95 V for 70°C [11].

Each point in the measured data, which consists of 17 different voltages, would be set as the operating point and preliminary design would be performed for each voltage to size components according to electrolyser performance at given voltage. This resulted in a plot of wet mass dependence on voltage shown in Figure 5.1. During this optimization it was determined that the maximum voltage setting does not produce system with minimum wet mass. For both delta-v budgets minimum wet mass voltage was determined to be 1.65 V. It cannot be deemed that this voltage represents the minimum wet mass globally and in other systems it can vary. Wide variation in mass come as a result of varying number of cells required to match performance given by delta-v budget.

The reason why maximum voltage setting does not correspond to minimum system mass is given by electrolyser power. As voltage is increased beyond optimum mass point number of cells does not change but it results in higher current density, which leads to higher power, and lower efficiency leading to higher heat dissipation rate. To generate more power power subsystem becomes heavier leading to higher satellite mass than in the optimum case.

Optimization confirmed that maximum efficiency point leads to optimum power and heat dissipation rate. As voltage increases both heat dissipation rate and power increase. This is shown in Figure 5.2. Similarly to wet mass power and heat dissipation rate rise and fall due to varying number of cells. Optimum mass point results in low power and heat dissipation rate, thanks to small number of cells, which increase with higher voltage requiring more power. Normalizing the values with respect to number of cells shows that power and heat dissipation rate increase with increasing voltage in a clear manner as shown in Figure 5.2.

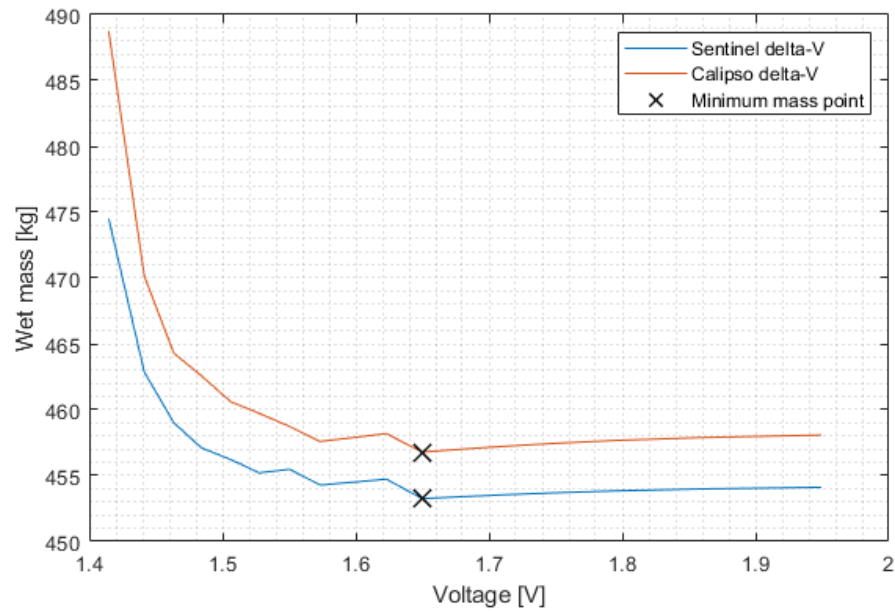


Figure 5.1.: Satellite mass optimisation via electrolyser operating voltage with constant voltage operation

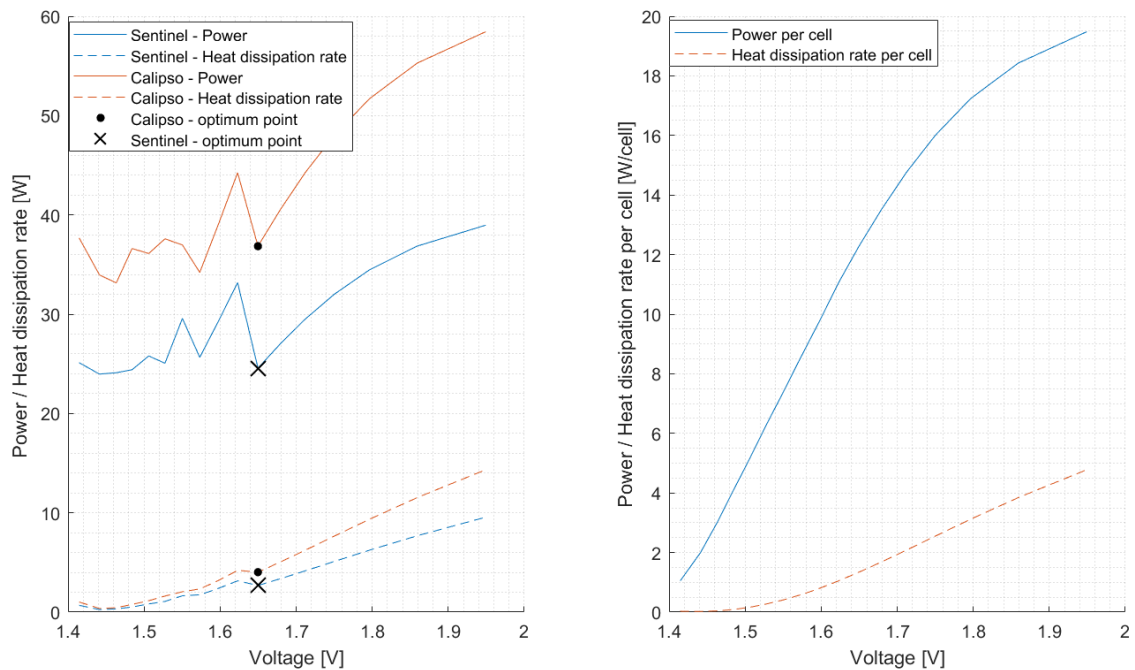


Figure 5.2.: Power and heat dissipation rate for different voltage settings (left). Power and heat dissipation rate for different voltage settings per cell (right).

To see how performance of the satellite changes for the optimum wet mass voltage Table 5.2 was compiled for Sentinel delta-v budget from the newly found optimum and the extreme points which were introduced in Table 5.1. Compared to the two extreme points not only the point of optimum mass provides smallest mass but also provides reduced power, good gas generation and a reasonable heat dissipation compared to maximum voltage case thanks to increase in efficiency. Detailed information about performance of the optimum case is shown in the next chapter.

Table 5.2.: Satellite properties for different operating ranges for Sentinel-3 delta-v budget

	Max cell efficiency	Max voltage	Optimum mass
Number of electrolyser cells	12	2	2
Wet mass [kg]	462.859	454.113	453.250
Propellant mass [kg]	17.905	17.566	17.533
Electrolyser mass [kg]	10.90	1.71	1.71
Power subsystem mass [kg]	56.339	57.195	56.373
Cell efficiency	0.99	0.76	0.89
Electrolyser power [W]	23.97	38.96	24.57
Electrolyser heat dissipation rate [W]	0.26	9.56	2.68
Time to heat up [s]	10300	1108	1552

Operating range for the two extreme cases, initially introduced in Figure 4.14 for single pressure, along with the newly found optimum, is shown in Figure 5.3 with voltage in the full possible operating range of 1 bar to 100 bar. Like voltage cell efficiency is constant during the whole charging cycle.

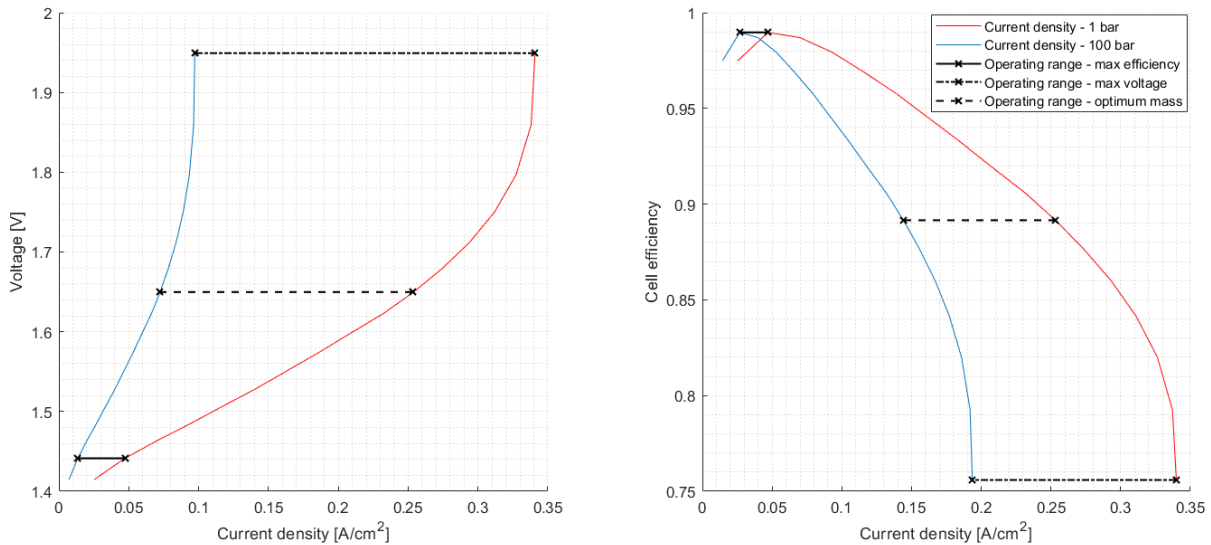


Figure 5.3.: Operating ranges for maximum voltage, maximum efficiency and optimum mass cases in voltage (left) and cell efficiency (right), original data from [11].

6. System performance

With electrolyser performance optimized to achieve minimum system mass performance of WEP can be compared with conventional propulsion. This overview consists of nominal performance of WEP where analysis inputs are assumed to be ideal and where each subsection contains performance of individual subsystems whose operation and modelling were introduced in the preliminary design section. Both delta-v budgets were considered to see their effects. However, variation of system properties is expected and sensitivity analysis is part of this chapter to determine effects of deviation from nominal conditions on satellite performance.

6.1. Nominal performance

6.1.1. Tanks

With water tank size driven by total delta-v, specific impulse and pressure of the tank these parameters are identical for both considered delta-v cases. However, due to different sizes of the intermediate tanks, required amount of water for the two cases is different mainly by inclusion of water that replaces permeated hydrogen which had higher losses in larger intermediate tank.

Intermediate tanks are restricted by small density of hydrogen and high pressure at which the gases are stored. This affects mass budget significantly since in conventional propulsion only a single tank is necessary. Properties of the tanks are shown in Table 6.1. Depending on delta-v budget all three tanks for WEP can weigh between 4.53 and 6.19 kg which is an increase in comparison with tank originally used for storage of hydrazine which weighs 3.9 kg [31]. Due to higher specific impulse WEP requires between 17.539 and 17.785 kg of propellant compared to 28 kg for hydrazine. Such reduction of propellants enables reduction in tank volume from 37.3 liters for hydrazine to combined volume of 29.92 liters for Sentinel and increase to 37.63 liters for CALIPSO orbit.

Table 6.1.: Properties of tanks chosen for WEP

	Sentinel	Calipso
Propellant mass [kg]	17.534	17.785
Pressurizer mass [kg]	0.101	0.103
Water mass to counter permeation [kg]	0.0494	0.169
Water tank volume [l]	23.448	23.784
Hydrogen tank volume [l]	4.314	9.233
Oxygen tank volume [l]	2.157	4.617
Water tank mass [kg]	2.360	2.384
Hydrogen tank mass [kg]	1.376	2.361
Oxygen tank mass [kg]	0.793	1.441

6.1.2. Electrolyser

Target of the optimization required minimizing satellite mass and operating range puts an emphasis on this. With sizing of the electrolyser given by size of one cell sizing is done by delta-v requirements. Resulting active area of the electrolysers along with their masses for the two considered delta-v budgets is shown in Table 6.2.

Table 6.2.: Electrolyser properties for considered delta-v budgets

	Sentinel	Calipso
Number of electrolyser cells	2	3
Electrolyser active area [cm^2]	93.974	140.961
Electrolyser mass [kg]	1.707	2.626
Electrolyser cell efficiency [%]	89.16	89.16

6.1.3. Power subsystem and thermals

Target of optimisation and corresponding operating range are most crucial factors in power subsystem and thermal management. With minimum power demand and minimum heat dissipation rate being on the opposite side of optimisation, minimization of mass results in higher power demand and heat losses which results in heavier power subsystem. Selection of thermal resistance was done at 1 bar to enable operation of the electrolyser at required current density without dangers of achieving temperatures above 70°C. This however results to decreasing operating temperature of the electrolyser to temperatures of 42.9°C for both considered delta-v budgets at pressure of 100 bar. Means of maintaining temperature at 70°C would have to be implemented to prevent efficiency reduction. At this stage it is neglected and constant operating temperature is assumed.

Values for both delta-v budgets are shown in Table 6.3. Power and heat dissipation rate are indicated in ranges because current density decreases with increasing pressure and so do these parameters. Even with high power demand due to priority of wet mass minimization power subsystem mass does not deviate much from the original mass of 54.97 kg used for the conventional propulsion. Heating time difference between the cases comes from different size of the electrolyser. Time to compensate heat up represents additional nominal electrolyser operation to counter smaller gas generation during heat up.

Table 6.3.: Power subsystem and thermal properties for electrolyser for considered delta-v budgets

	Sentinel	Calipso
Electrolyser power range [W]	18.000 - 24.566	26.995 - 36.849
Satellite power range [W]	718.000 - 724.566	726.995 - 736.849
Heat dissipation rate range [W]	1.226 - 2.682	1.840 - 4.024
Power subsystem mass [kg]	56.373	57.075
Solar array mass [kg]	25.857	26.295
PCDU mass [kg]	14.990	14.990
Battery mass [kg]	15.526	15.790
Time to heat up [s]	1552	1592
Time to compensate heat up [s]	570	584

6.1.4. De-orbit

Factor affecting de-orbit is mainly altitude which makes CALIPSO de-orbit simpler. Sentinel-3 orbit has an advantage of longer orbital period which provides more time for charging per orbit. This advantage is not sufficient enough to compensate for difference in altitude. As indicated in Table 6.4 de-orbit duration for the two considered orbits, which differ in altitude by around 100 km, is significantly different. This duration needs to be considered when planning de-orbit manoeuvres to manage satellite de-orbit within the required 25 years. Alternatively, these de-orbit manoeuvres can still be considered as a part of satellite nominal operations and only after performing them the period of 25 year de-orbit would commence.

Table 6.4.: De-orbit performance of considered orbits

	Sentinel	Calipso
Number of orbits to perform de-orbit manoeuvre	1287	443
Duration of de-orbit manoeuvres [days]	88.829	30.166

6.1.5. Propellant charging cycles

Previously it was mentioned that delta-v budget of Sentinel-3 is more feasible for application of WEP than CALIPSO's delta-v budget. To emphasize why a representation of charging cycle for each manoeuvre was created for both budgets. These charging cycles use required timing given by delta-v budget but as the electrolyser was sized to produce sufficient propellants for all manoeuvres there is a delay necessary between each propellant generation to ensure that charging ends right as a manoeuvre is started to prevent long storage of high pressure hydrogen to avoid high permeation losses. This leads to creation of Figure 6.1 which shows capacity of intermediate tanks during nominal mission lifetime. It shows that Sentinel-3 delta-v budget is more feasible for WEP due to regular distribution of manoeuvres and similar delta-v required for each manoeuvre. While in the case of CALIPSO delta-v for manoeuvres vary widely and their timing is irregular. Satellite mass determined using Sentinel-3 delta-v budget is therefore a better approximation of WEP propelled satellite due to more favourable properties.

6.1.6. System nominal mass

With nominal performance of individual subsystems known total wet mass of a satellite which uses WEP can be determined. With target of the thesis on matching performance of the conventional propulsion system whilst minimizing satellite mass, mass plays the most significant role as it directly provides information on feasibility of the proposed system for use in LEO. Table 6.5 contains masses of individual subsystems, components and propellants required for carrying out the selected reference mission for both WEP and conventional propulsion.

Proposed WEP provides savings in mass compared to conventional propulsion system in range of 0.7 % to 1.47 % depending on chosen delta-v budget. Lower boundary of the range corresponds to a conservative delta-v budget as it is more demanding due to more frequent and varying manoeuvres. Upper boundary belongs to a delta-v budget, designed for the target altitude of FLEX, which is more feasible for application of WEP as was explained in the previous section.

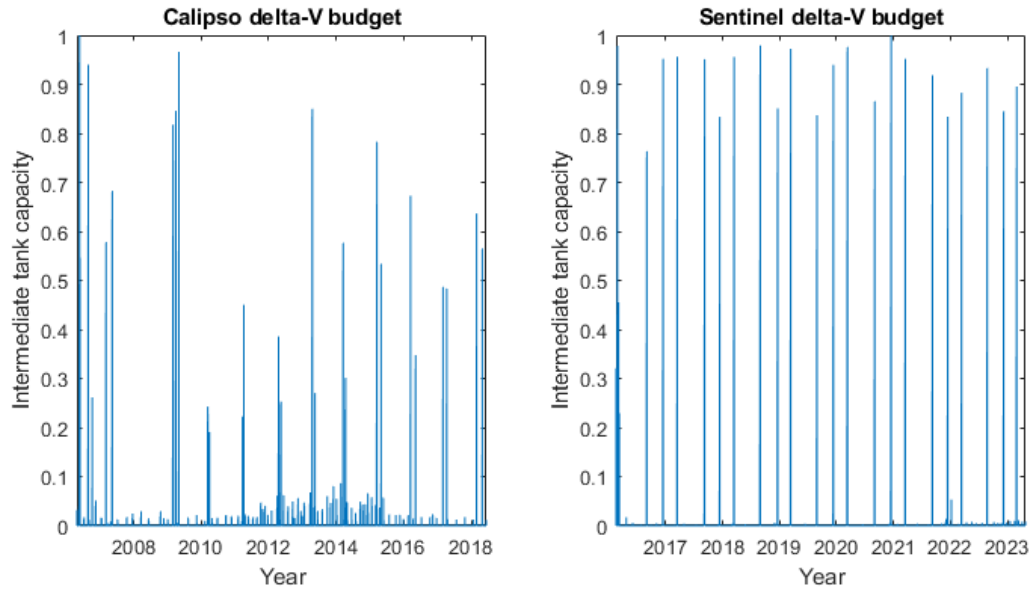


Figure 6.1.: Intermediate tank capacity during nominal mission lifetime for the two considered delta-v budgets

Table 6.5.: Comparison of mass budget of FLEX with WEP and conventional propulsion system

Delta-v budget	WEP		Conventional propulsion
	Sentinel	Calipso	
Propellant & pressurizer mass [kg]	17.635	17.887	28.343
Electrolyser mass [kg]	1.707	2.626	-
Propulsion system components [kg]	2.535	2.535	2.315
Tank masses [kg]	4.529	6.187	3.900
Power subsystem mass [kg]	56.373	57.075	54.970
Payload and other subsystems [kg]	370.472	370.472	370.472
Wet mass [kg]	453.250	456.782	460.000

6.2. Sensitivity analysis

As inputs used in the solver are based on target values and outputs of other researches it is necessary to validate how well the system performs if input parameters change to counter uncertainties that might occur and also to see trends and hints for potential improvements of WEP operation.

Inputs were not given in terms of range so an arbitrary deviation from nominal value can be used instead. For the purpose of this thesis following parameters are investigated:

- Specific impulse I_{sp}
- Maximum intermediate tank pressure
- Intermediate tank outlet pressure
- Combination of intermediate tank outlet pressure and minimum intermediate tank pressure
- Permeation rate

These parameters are the main building blocks on which preliminary design of WEP is based. Specific

impulse sets the amount of propellant required, pressures set requirements for electrolyser performance in terms of gas generation rate and tank size and permeation rate sets propellant losses and added mass to replace these losses. With focus of this thesis on minimizing satellite wet mass, mass is primary performance indicator in the sensitivity analysis.

To perform sensitivity analysis Monte Carlo methods are used. This approach uses random sampling - parameter values are randomly distributed across chosen range. It enables probing of the whole design space while keeping analysis simple as results of individual simulation runs can be merged to get a larger data set. Alternatively an approach of "full factorial design" could be taken which uses equal spacing of data points which offers more organized but more computationally heavy approach whose benefits cannot be used at this stage of development. Random sampling is used instead.

6.2.1. Specific impulse

Specific impulse is given by thruster performance, which was not the focus of this thesis, which at this stage is assumed to be 340 seconds. With theoretically achievable values for combination of hydrogen and oxygen above this value deviation of specific impulse was set to 20 % to see how the thruster improvement could result in larger propellant savings and lower mass and how performance below the target could do the opposite. Results of the analysis are shown in Figure 6.2. Sensitivity analysis confirmed expected trend of decreasing wet mass with increasing specific impulse and the figure indicates that depending on chosen delta-v budget even lower values of Isp can still lead to smaller wet mass than conventional propulsion. Sudden drops in wet mass are caused by reduction in number of cells required to generate sufficient propellants thanks to better performance of the thrusters - less propellant is needed.

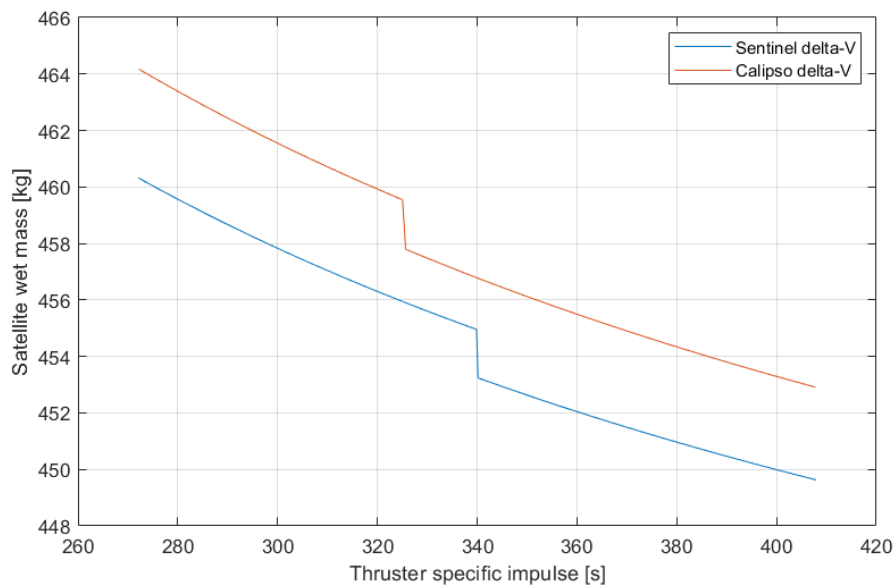


Figure 6.2.: Sensitivity analysis results for specific impulse

6.2.2. Pressure

With thruster design yet to be finished its operating pressure is uncertain. Intermediate tank outlet pressure can change in the future correspondingly. Dependence of variation of pressure on wet mass is explored in this section. Analysis is separated into three sections to explore dependence of satellite mass on considered pressures while exploring their coupling. The explored cases are:

- Case 1: Variation of intermediate tank outlet pressure while keeping the intermediate tank storage pressure constant at 10 bar
- Case 2: Variation of intermediate tank outlet pressure while setting the intermediate tank storage pressure equal to it
- Case 3: Variation of both intermediate tank outlet and intermediate storage pressures

Case 1

This case explores situation in which long term propellant storage is done at pressures below required outlet pressure. This approach is undesirable as pressure difference causes that longer charging cycles are required prior to each manoeuvre to accumulate propellants in intermediate tanks and this puts constraints on timing of manoeuvres. However, if hydrogen tanks cannot reduce permeation rate sufficiently long term storage might need to be done at smaller pressures to reduce leakage and this case aims to determine how pressure difference affects wet mass. For this case long term storage pressure was fixed at 10 bar while intermediate tank outlet pressure is varied.

Figure 6.3 shows effects of variation of intermediate tank outlet pressure on wet mass. Wet mass increases with increasing gap between outlet and storage pressures in a steady manner. Major mass increases come from an increasing number of cells required to provide sufficient gas generation rates to overcome pressure gap and generate required propellants. In case of Sentinel-3 delta-v budget number of cells required increases rapidly with increasing pressure difference indicating potential issues in timing of manoeuvres.

Case 2

This case was explored to determine if there is an optimum when both pressures are kept equal. Sensitivity analysis results are shown in Figure 6.4 and they indicate that pressure affects mass optima. As pressure changes for both delta-v budgets variation in number of cells is necessary for operation. In the case of Sentinel-3 delta-v budget additional cell is needed above 10 bar, which was considered in the nominal case, making 10 bar the optimum above which wet mass increases. While for CALIPSO higher pressure could be used to provide better satellite mass. However, selection of pressure depends on thruster design and this mass variation should be taken into account when aiming for smallest satellite mass.

Case 3

This case disregards coupling between the two pressures and explores effects of their variation on wet mass. Results are shown in Figure 6.5 and they indicate complex relationship between wet mass and the two pressures which goes beyond scope of this thesis. It is assumed that different groupings of masses are caused by number of cells with some pressures requiring more cells to operate than other ones. A trend

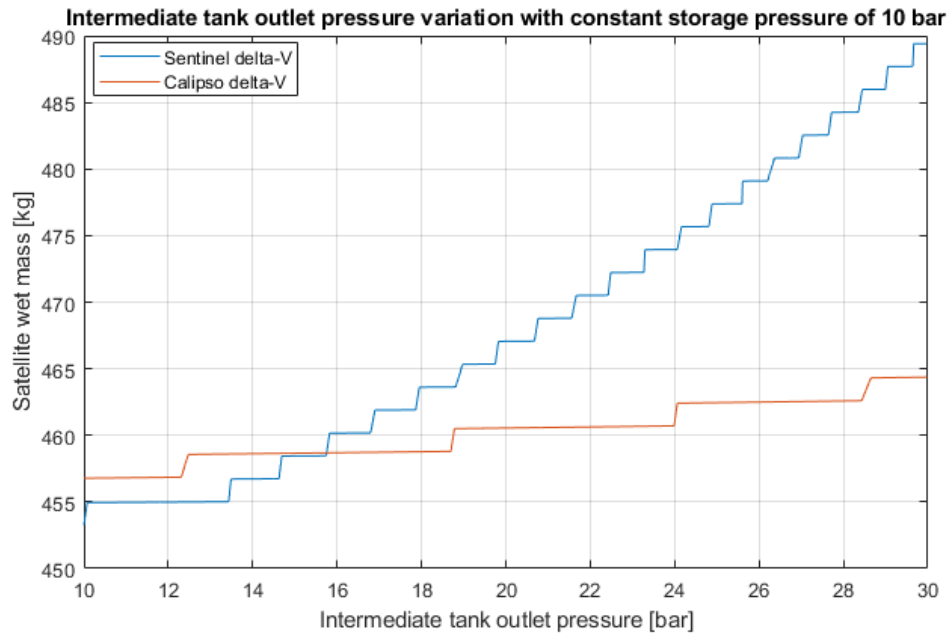


Figure 6.3.: Sensitivity analysis for pressure case 1 - variation of intermediate tank outlet pressure with intermediate tank storage pressure of 10 bar

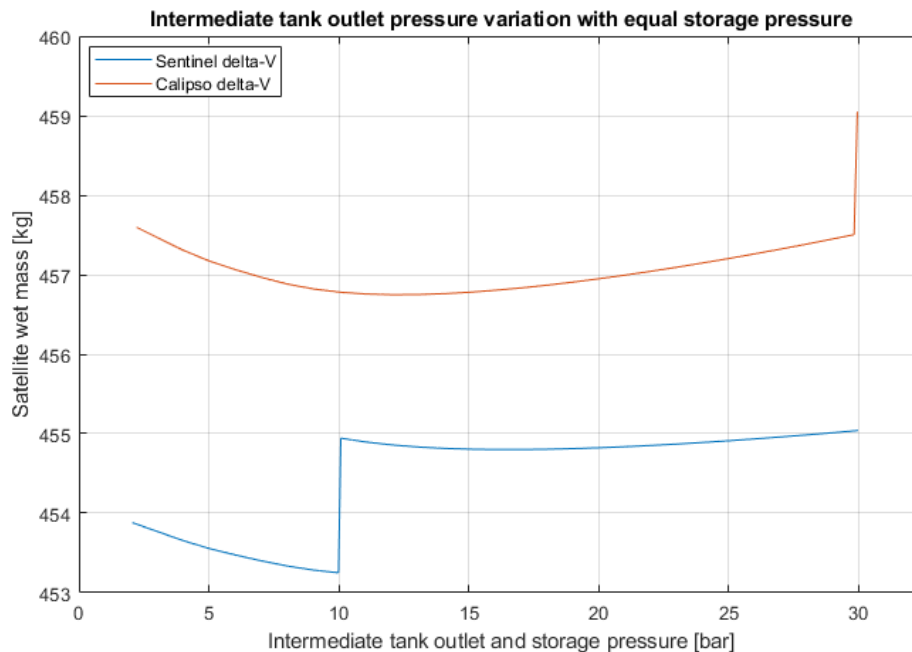


Figure 6.4.: Sensitivity analysis for pressure case 2 - variation of intermediate tank outlet pressure with intermediate tank storage pressure equal to it

from this complex behaviour was determined that lowest mass can be achieved when both pressures are equal which was considered in nominal simulation. With Case 2 exploring area where both pressures are equal it provides all information that is necessary.

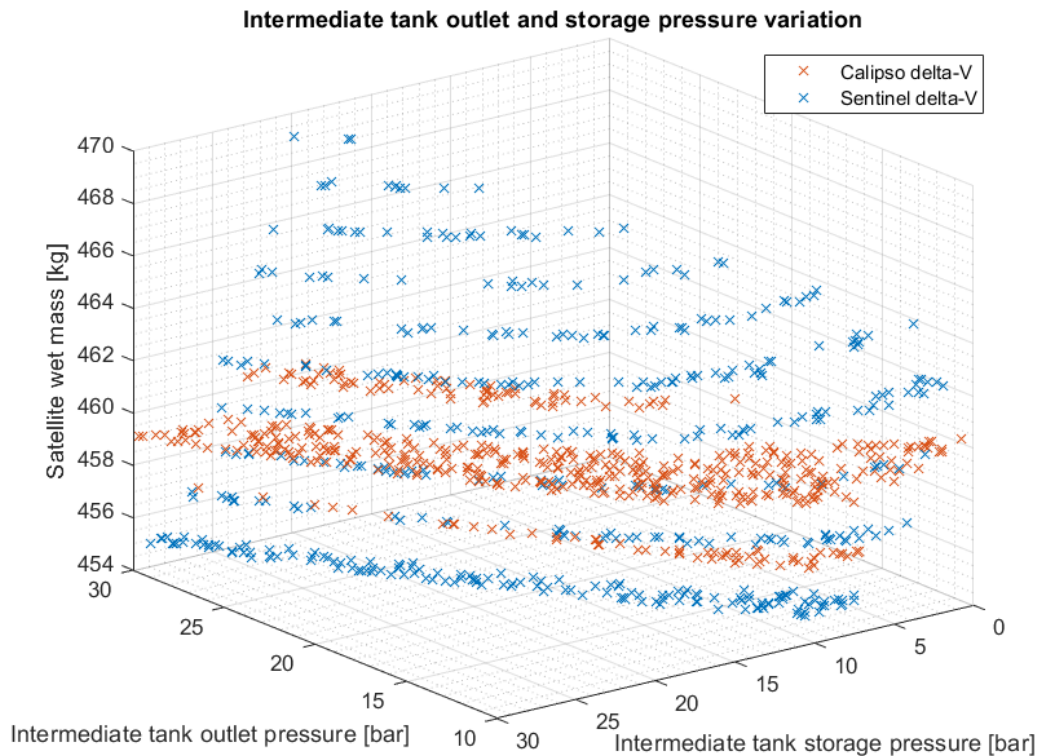


Figure 6.5.: Sensitivity analysis for pressure case 3 - variation of intermediate tank outlet and storage pressures

6.2.3. Permeation

With permeation driving amount of propellant lost and necessity to carry additional propellant to replace it its variation influences wet mass significantly. Propellant loss rate is driven by tank size so minimizing maximum delta-v manoeuvre needs to be done to minimize leakage rate.

Figure 6.6 shows effect of varying permeation on wet mass. Increase of wet mass is linear with increasing permeation for the same number of cells. Sudden increases of mass are caused by increasing number of electrolyser cells that are necessary to provide sufficient gas generation rate to counter leakage rate of propellants in between manoeuvres and during generation of propellants when pressure increases and so does leakage rate which can reach values higher than gas generation rate. This limits maximum achievable tank pressure and more cells are required to overcome this.

It can be seen that wet mass for CALIPSO delta-v budget increases more rapidly than for Sentinel-3 delta-v budget which is caused by larger tanks required for CALIPSO orbit. This shows necessity of optimization of delta-v budget for WEP if sufficiently small permeation rate cannot be achieved.

6.3. SWOT analysis

With properties of satellite with WEP quantified the system can be described via SWOT analysis which consists of listing strengths, weaknesses, opportunities and threats of WEP system for LEO satellites.

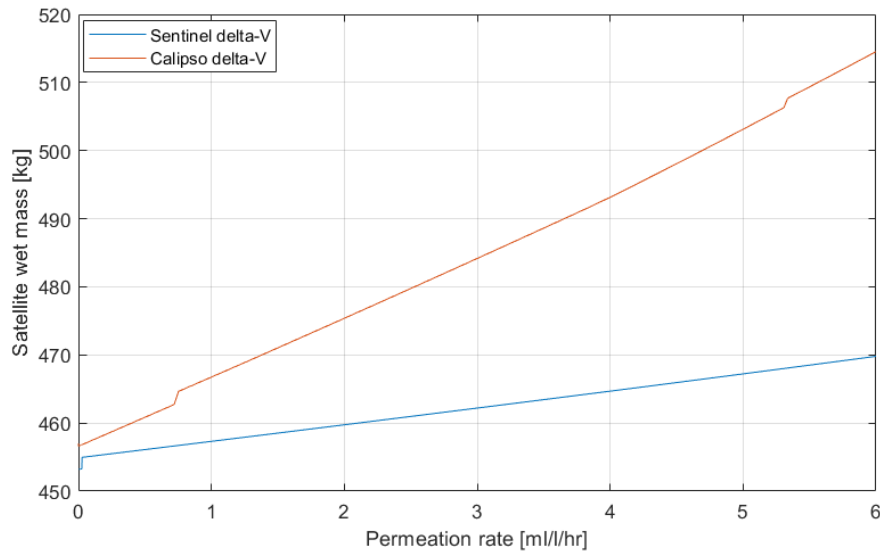


Figure 6.6.: Sensitivity analysis results for permeation

6.3.1. Strengths

Strengths of WEP system can be seen at all stages of LEO mission lifetime. In early stages WEP, unlike conventional propulsion subsystems, provides a propellant which is sustainable and it is not hazardous to environment and humans. This provides benefits during initial phases of satellite lifetime as Assembly, Integration and Testing (AIT) processes can be done simpler without necessity of protecting operators from danger in case of propellant leakage. This provides reduction of costs that go towards such precautions. In cases of launcher failure and return of satellite into atmosphere with residual propellants no harm to environment will be done from WEP propellants and as water has no chemical energy it is safe for storage. Furthermore, as water requires only minor treatment prior to its use as a propellant, unlike conventional propellants, it also promotes sustainability through reduced carbon footprint.

Performance of WEP compared to conventional monopropellant propulsion is represented by higher specific impulse, which results in lower propellant mass. This thesis confirmed that overall system mass for WEP is lower than for conventional propulsion which in turn results in lower launch costs. As WEP can be considered as bi-propellant propulsion, even though it uses a single primary propellant, in comparison with conventional bi-propellant propulsion it provides comparable performance to storable propellants while providing less complex and lighter storage than cryogenic propellants.

6.3.2. Weaknesses

Primary weaknesses of WEP are in mission planning and operations. As propellants are generated on demand higher degree of planning is required ahead. Manoeuvres have to be planned with sufficient delays between them to provide sufficient charging time. Charging of propellants too ahead of a manoeuvre leads to higher losses of hydrogen due to permeation. Permeation occurs at any point of mission and additional measures need to be taken to reduce this leakage. High permeation causes that there is an imbalance in propellants and oxygen needs to be vented, to maintain stoichiometric ratio and to maintain equal pressure in both tanks, or alternative means of oxygen reduction need to be used. Gaseous hydrogen

introduces additional challenge in terms of compatibility with titanium, which is commonly used in propulsion subsystems, that leads to hydrogen embrittlement.

Need for storage of highly pressurized gases in intermediate tanks results in high tank masses even for smaller propellant capacity. This, along with small density of hydrogen results in large tanks and creates a challenge for manoeuvre design as larger manoeuvres need to be split into smaller impulses with sufficient charging time between them. This challenge is not crucial as for LEO only higher delta-v manoeuvres which are affected are satellite commissioning and de-orbit which are not time-critical and can be split into smaller manoeuvres.

Effect of varying pressure on electrolyser operation results in challenging thermal management of the electrolyser. As equilibrium temperature decreases with pressure, either heating mechanisms that keep the electrolyser at operating temperature need to be included, which leads to increasing complexity, or more advanced operating range needs to be designed which adjusts current density to maintain temperature, which leads to varying efficiency and gas generation which need to be accounted for.

To counter effect of a potential cell failure, redundant but heavy design of the electrolyser needs to be maintained to reduce effects of such failure on capability of the satellite to complete its mission

6.3.3. Opportunities

With increasing motivation to promote sustainability WEP provides a way of promoting this trend in the segment of space propulsion on LEO. Unlike other green propellants it provides a performance improvement over hydrazine giving an incentive to change from a well proven hydrazine technology.

As water is easily accessible and requires only minor processing for use in propulsion compared to production of other propellants, it provides assurances of low costs towards future as it is not dependent on other chemicals nor industries.

In future WEP is intended for use alongside In-Situ Resource Utilization (ISRU) for missions to celestial bodies where water is present to refuel a spacecraft. This technology is not available for use in LEO however as water is safe and it provides high density and good performance it could be used for on-orbit refuelling for frequented orbits such as SSO.

Another strength WEP has is its possible synergy with other spacecraft subsystems:

- Thermal subsystem - temperature regulation in thermal subsystem with water as a working liquid [51]
- Power subsystem - using reversible fuel cell where chemical energy of electrolysis products can be stored and energy used on demand [52]
- Attitude control system - using water to distribute mass as required

6.3.4. Threats

With prices of propellants for WEP stable it suffers from prices of materials for development of electrolysers. As electrolyser catalysts are often made of precious metals, such as platinum, which already are expensive, increase in prices could affect cost of such propulsion system further.

Permeation was previously mentioned as a challenge that needs to be solved in future implementation. If no way of sufficiently reducing hydrogen leakage is found this could be seen problematic in some implementations and other type of propulsion system might be more feasible.

A threat to WEP is development of an alternative propulsion system which would promote sustainability while providing a better performance. This could be the case of a new development in electrical propulsion with sufficiently high thrust that would be incompatible with hydrogen and oxygen. This would make implementation of WEP for use in propulsion more challenging.

Lastly, if sustainability efforts are disregarded in future, this might affect use of WEP in favour of less sustainable, yet more tested, propulsion systems. However, even in such cases the fact that WEP provides better performance should be recognized.

Results of the SWOT analysis are shown in a tabular for in Figure 6.7.

	Helpful	Harmful
Internal origin	<p style="text-align: center;"><u>Strengths</u></p> <ul style="list-style-type: none"> • Sustainable and safe propellant • Simpler and cheaper AIT • Better performance than conventional propulsion • Lighter satellite design 	<p style="text-align: center;"><u>Weaknesses</u></p> <ul style="list-style-type: none"> • More complex planning of manoeuvres • Compensation of lost propellant via permeation • Material compatibility due to hydrogen embrittlement • Maximum delta-V per impulse limited by heavy tanks due to high pressures • Thermal management of electrolyser
External origin	<p style="text-align: center;"><u>Opportunities</u></p> <ul style="list-style-type: none"> • Promotes sustainability • Cheap and available propellant whose price will not fluctuate • Propellant good for refuelling missions • Synergy with other subsystems – thermal, power and attitude control 	<p style="text-align: center;"><u>Threats</u></p> <ul style="list-style-type: none"> • Price increase of electrolyser materials • Inability to reduce permeation • Alternative propulsion system with better performance and incompatibility with hydrogen/oxygen • Lack of interest in sustainability

Figure 6.7.: Results of SWOT analysis

7. Outlook

This thesis provided a look at a design of a WEP system to analyse its feasibility for use in LEO. This look, however, was top level and studies of individual parts of this thesis need to be performed in more detail in future.

When it comes to materials, exploration of compatibility of space-grade materials with gaseous hydrogen is necessary to ensure successful operation of the system. Increased demand for hydrogen propelled cars could help with solving the first problem - permeation. Tanks which are capable of reducing permeation rates need to be developed to ensure that propellant loss is not significant and it does not endanger a mission. Experimental measurements of permeation at higher pressures need to be conducted for various materials to enable modelling of this behaviour so that it can be accounted for during mission planning.

Hydrogen embrittlement is the second material issue. Titanium suffers from this condition and it needs to be determined how this affects conventional propulsion components such as valves and tanks which are made from titanium alloys. Means of reducing these effects need to be found if harmfulness of hydrogen embrittlement is not negligible.

With behaviour of the electrolyser affecting all different components of WEP more in depth optimization needs to be carried out to determine how best to operate the system. Part of this must be manoeuvre optimization that designs manoeuvres in a way which is best for operation of the electrolyser and enables minimization of number of cells. While considering permeation charging cycle should be optimized alongside manoeuvre design to minimize propellant losses while enabling quick reaction time of the propulsion subsystem.

Once these are considered optimization of electrolyser operating range needs to be performed to achieve required gas generation rate while simplifying thermal management of the electrolyser. As its equilibrium temperature varies with changing pressure adjustments to current density, and gas generation rate, or inclusion of additional components to maintain temperature might be required. Furthermore, exploring alternative ways of ensuring electrolyser operation in case of a cell failure that does not require inclusion of heavy components is desirable.

Lastly effects of humidity should be considered. At low temperatures both hydrogen and oxygen gases are dry but humidity increases with increasing temperature [7]. Effects of humidity on storage in intermediate tanks and on performance of the thruster should be considered as it can lead to degradation of I_{SP} .

8. Conclusion

The objective of this thesis was to determine whether WEP is feasible for application on LEO and to validate if it is a competitive alternative to conventional propulsion currently in use. Target of the analysis was to match performance of the conventional propulsion while minimizing the mass. Results suggest that application of WEP in LEO is feasible and it enables reduction of mass of up to 1.47 % for a satellite in mass category of 460 kg due to higher performance than the most commonly used conventional propulsion system which uses hydrazine.

More importantly this research identified critical parameters that need to be considered and optimized to ensure best performance of WEP. With mass of the propulsion subsystem components comparable to ones in hydrazine propulsion primary parameter that affects mass is delta-v budget. Two delta-v budgets for altitudes of 705 km and 814 km were considered and frequency of manoeuvres and delta-v allocated for each manoeuvre affects sizing of electrolyser and intermediate tanks which are primary mass contributors of WEP system. Reduction of maximum delta-v per manoeuvre is crucial for reducing mass. Required gas generation rate given by duration between manoeuvres poses requirements on electrolyser sizing whose operation needs to be optimised not only to produce sufficient gas generation rate but to also ensure that thermal management of the satellite can handle its dissipated heat and that sufficient power is allocated to operate it.

Even though WEP system is more complex than hydrazine system its pros outweigh the cons. It provides better performance which leads to lower mass, it promotes sustainability and propellant is easily accessible and it simplifies AIT by avoiding manipulation with toxic propellants which reduces costs.

Further research needs to be carried out in certain areas, as outlined in previous chapter, for the system to be ready to replace hydrazine propulsion on LEO.

Bibliography

- [1] Inter-Agency Space Debris Coordination Committee: IADC Space Debris Mitigation Guidelines, orbitaldebris.jsc.nasa.gov/library/iadc-space-debris-guidelines-revision-2.pdf (accessed 2023-06-03), 2002.
- [2] European Chemicals Agency: Inclusion of Substances of Very High Concern in the Candidate List: ED/31/2011, 2011.
- [3] HERBERTZ, A.: Theoretical Performance and Application Cases of Water Electrolysis Propulsion. TRANSACTIONS OF THE JAPAN SOCIETY FOR AERONAUTICAL AND SPACE SCIENCES, AEROSPACE TECHNOLOGY JAPAN, Vol. 19, No. 2, pp. 199–204, 2021.
- [4] Dengler, S.; Ebert, F.; Manfletti, C.; Leichtfuß, S.: WATER ELECTROLYSIS PROPULSION IN CUBESATS: A CASE STUDY. In: SPACE PROPULSION 2022. ESTORIL, PORTUGAL, (cit. on p. 2), 2022.
- [5] Shiva Kumar, S.; Himabindu, V.: Hydrogen production by PEM water electrolysis – A review. Materials Science for Energy Technologies, Vol. 2, No. 3, pp. 442–454, 2019.
- [6] Schiller, G.; Ansar, A.; Lang, M.; Patz, O.: High temperature water electrolysis using metal supported solid oxide electrolyser cells (SOEC). Journal of Applied Electrochemistry, Vol. 39, No. 2, pp. 293–301, 2009.
- [7] Mitlitsky, F.; Myers, B.; Weisberg, A. H.; Leonida, A.: Applications and Development of High Pressure PEM Systems. In: Portable Fuel Cells Conference. Lucerne, Switzerland, (cit. on pp. 4, 5, 79), 1999.
- [8] Heizmann S., B.: Development of a Miniaturized PEM Electrolyzer for a Small Satellite Application, Stuttgart: Institut für Raumfahrtssysteme, 2018.
- [9] Lettenmeier, P.: Efficiency – Electrolysis: White paper, 2021.
- [10] Yodwong, B.; Guilbert, D.; Phattanasak, M.; Kaewmanee, W.; Hinaje, M.; Vitale, G.: Faraday’s Efficiency Modeling of a Proton Exchange Membrane Electrolyzer Based on Experimental Data. Energies, Vol. 13, No. 18, p. 4792, 2020.
- [11] Heizmann, S.; Herbertz, A.; Saryczew, J.; Manfletti, C.: Investigation of a Cathode-Vapour-Feed Electrolyser for a Water Electrolysis Propulsion System. In: Aerospace Europe Conference 2023 - 10th EUCASS and 9th CEAS Conference. Lausanne, Switzerland, (cit. on pp. 7, 43–45, 49, 50, 55, 64, 66), 2023.
- [12] Walter, U.: Astronautics: The physics of space flight, Cham, Switzerland: Springer, ISBN 978-3-319-74373-8, 2018.

- [13] The CubeSat Program, Cal Poly SLO: CubeSat Design Specification Rev. 14.1, static1.squarespace.com/static/5418c831e4b0fa4ecac1bacd/t/62193b7fc9e72e0053f00910/1645820809779/CDS+REV14_1+2022-02-09.pdf (accessed 2023-05-20), February 2022.
- [14] Kulu, Erik: Nanosatellite Launch Forecasts - Track Record and Latest Prediction. In: 36th Annual Small Satellite Conference, (cit. on p. 12), 2022.
- [15] UCS Satellite Database, www.ucsusa.org/resources/satellite-database (accessed 2023-05-20), 2005.
- [16] United States Space Command: Space-track.org: Query builder, space-track.org (accessed 2023-01-26).
- [17] European Space Agency: Facts and figures: Fluorescence Explorer (FLEX), esa.int/Applications/Observing_the_Earth/FutureEO/FLEX/Facts_and_figures (accessed 2023-06-02).
- [18] Pollard, Mark; Pitera, Andrea; Stiles, Peter; Hunter, Chris: QUALIFICATION OF THE MHT-1N MONOPROPELLANT THRUSTER FOR THE FLEX PROGRAMME. In: SPACE PROPULSION 2022. ESTORIL, PORTUGAL, (cit. on pp. 23, 35, 36, 38), 2022.
- [19] ESA Space Debris Mitigation WG: ESA Space Debris Mitigation Compliance Verification Guidelines, [esamultimedia.esa.int/docs/spacesafety/ESSB-HB-U-002-Issue2\(14February2023\).pdf](https://esamultimedia.esa.int/docs/spacesafety/ESSB-HB-U-002-Issue2(14February2023).pdf) (accessed 2023-06-03), 2015.
- [20] Space Standardization, E. C. for: Space engineering: Space environment, ECSS-E-ST-10-04C, 2020.
- [21] Standardization, I. O. for: Space systems: Estimation of orbit lifetime, ISO 27852:2016, 2016.
- [22] ESA-ESTEC: Margin philosophy for science assessment studies, sci.esa.int/documents/34375/36249/1567260131067-Margin_philosophy_for_science_assessment_studies_1.3.pdf (accessed 2023-06-04), 2012.
- [23] Wertz, J. R.; Larson, W. J.: Space mission analysis and design. Space technology library, Torrance, Calif.: Microcosm, Dordrecht, and London : Kluwer Academic, ISBN 1-881883-10-8, 1999.
- [24] ESA-ESTEC: CDF STUDY REPORT COMET INTERCEPTOR: Assessment of Mission to Intercept a Long Period Comet or Interplanetary Object, esamultimedia.esa.int/docs/cdf/CometInterceptor_CDF_Study_Report.pdf (accessed 2023-06-09), 2019.
- [25] Wurdak, M.; Harmansa, N.-E.; Gotzig, U.; Deck, J.: LATEST DEVELOPMENTS OF THE WATER PROPULSION SYSTEM – THRUSTER. In: SPACE PROPULSION 2022. ESTORIL, PORTUGAL, (cit. on p. 34), 2022.
- [26] Fill and Drain Valve, nammo.com/wp-content/uploads/2021/03/2021-Nammo-Cheltenham-Fill-and-Drain-Valve.pdf (accessed 2023-06-10).
- [27] PRESSURE TRANSDUCERS, ariane.group/wp-content/uploads/2020/06/Pressure_Transducers_2017_10_PS_EN_Web.pdf (accessed 2023-06-10).
- [28] MINI PRESSURE TRANSDUCER, static1.squarespace.com/static/603ed12be8847300%2013401d7a/t/6054f4c51001e742aa4111b0/1616180422980/be_datasheet_minipt_2018apr.pdf (accessed 2023-06-10).
- [29] PYROVALVES; FILL, DRAIN AND VENT VALVES ;LATCH VALVES; FLOW CONTROL VALVE: ORBITAL PROPULSION FLUIDIC EQUIPMENT, space-propulsion.com/brochures/valves/space-propulsion-valves.pdf (accessed 2023-06-10).

-
- [30] Mechanical Pressure Regulator, nammo.com/product/mechanical-pressure-regulator/ (accessed 2023-06-10).
- [31] Rafael Space Systems: Rafael Space Propulsion: CATALOGUE, rafael.co.il/wp-content/uploads/2021/07/RAFAEL-SPACE-PROPULSION-2021-CATALOGUE-2.pdf (accessed 2023-06-05), 2021.
- [32] Humble, R. W.; Henry, G. N.; Larson, W. J.: Space propulsion analysis and design. College custom series, New York and London: McGraw-Hill, ISBN 0-07-031320-2, 1995.
- [33] Julien: Working on the water tank, blogs.esa.int/orion/2017/12/18/working-on-the-water-tank/ (accessed 2023-06-09), 2017.
- [34] MT Aerospace AG: Spacecraft Propellant Tanks, mt-aerospace.de/files/mta/tankkatalog/MT-Tankkatalog.pdf (accessed 2023-06-09).
- [35] Sloan J.: : Composites end markets: Pressure vessels (2023), compositesworld.com/articles/composites-end-markets-pressure-vessels-2023 (accessed 2023-06-06), 2023.
- [36] National Composites Centre: Demonstrating the future of composite space tank technology, nccuk.com/media/0i5b10jw/space-tank.pdf (accessed 2023-06-06), 2023.
- [37] Hydrogen Permeation: Pressure Transmitters, Diaphragm Seals, web-material3.yokogawa.com/2/4563/files/AN-P-20220616-02_Hydrogen_Permeation.pdf (accessed 2023-06-22), 2022.
- [38] Economic Commission for Europe of the United Nations: Regulation No 134 of the Economic Commission for Europe of the United Nations (UN/ECE): Regulation No 134, 2018.
- [39] International Organization for Standardization: Gaseous hydrogen — Land vehicle fuel containers, ISO 19881:2018(E), 2018.
- [40] European Cooperation for Space Standardization: Space engineering: Testing, ECSS-E-10-03A, 2020.
- [41] Condé-Wolter, J.; Ruf, M. G.; Liebsch, A.; Lebelt, T.; Koch, I.; Drechsler, K.; Gude, M.: Hydrogen permeability of thermoplastic composites and liner systems for future mobility applications. Composites Part A: Applied Science and Manufacturing, Vol. 167, p. 107446, 2023.
- [42] Niedzinski, Michael: The Evolution of Constellium Al-Li Alloys for Space Launch and Crew Module Applications, lightmetalage.com/news/industry-news/aerospace/article-the-evolution-of-constellium-al-li-alloys-for-space-launch-and-crew-module-applications/ (accessed 2023-09-06), 2019.
- [43] Nehls, Grace, ed.: HyImpulse, Adamant Composites linerless CFRP tank passes hydrostatic burst test, compositesworld.com/news/hyimpulse-adamant-composites-linerless-cfrp-tank-passes-hydrostatic-burst-test (accessed 2023-06-09), 2023.
- [44] Colozza, A. J.: Hydrogen Storage for Aircraft Applications Overview, ntrs.nasa.gov/api/citations/20020085127/downloads/20020085127.pdf (accessed 2023-06-19), 2002.
- [45] SGL TECHNOLOGIES GmbH: The Weight Optimizers: Composite Solutions, sglcarbon.com/data/pdf/SGL-Broschuere-The-Weight-Optimizers-EN.pdf (accessed 2023-06-09), 2021.
- [46] S+D METALS: DATA SHEET: TI-6AL4V — WL 3.7164, sd-metals.com/files/web/PDFs2021/titanlegierungen/SD-METALS_Data-Sheet_Titanium-alloys_TI-6AL4V.pdf (accessed 2023-06-09), 2023.

- [47] Stanford Advanced Materials: LM1774 Aluminum Lithium (Al-Li) Alloy 2195, samaterials.com/aluminium/1774-2195-aluminum-lithium-alloy.html (accessed 2023-09-06).
- [48] S+D METALS: DATA SHEET: AISI 347 — 1.4546.9, sd-metals.com/files/web/PDFs2021/luftfahrt-sonderedelstahl/SD-METALS_Data-Sheet_AISI-347.pdf (accessed 2023-06-09), 2023.
- [49] Harmansa, N.-E.: Entwicklung und Charakterisierung eines Satellitenantriebssystems basierend auf Wasserelektrolyse. Raumfahrt, München: Verlag Dr. Hut, ISBN 9783843946193, 2020.
- [50] Salcedo, C.; Lelong, P.; Aigle, F.: DEVELOPMENT OF EFFICIENT AND INNOVATIVE EQUIPMENT FOR THE MYRIADE EVOLUTIONS PLATFORM, (accessed 2023-06-26).
- [51] Stenger, F. J.: Experimental feasibility study of water-filled capillary-pumped heat-transfer loops, Cleveland, Ohio: NASA, 1966.
- [52] Brey, J.; Muñoz, D.; Mesa, V.; Guerrero, T.: Use of Fuel Cells and Electrolyzers In Space Applications: From Energy Storage To Propulsion/Deorbitation. E3S Web of Conferences, Vol. 16, p. 17004, 2017.

A. Appendix

A.1. Market research data

Table A.1.: Mission types on LEO for considered satellites [15, 16]

Mission type	Mission number	Percentage of total
Earth Observation	358	70.89 %
Communications	37	7.33 %
Space Science	46	9.11 %
Technology development	28	5.54 %
Technology demonstration	24	4.75 %
Space Logistics	12	2.38 %
Total	505	

Table A.2.: Mission orbit types on LEO for considered satellites [15, 16]

Orbit type	Mission number	Percentage of total
SSO	405	80.20 %
Drifting orbit	57	11.29 %
Unknown orbit	22	4.36 %
Near equatorial orbit	11	2.18 %
Polar orbit	8	1.58 %
Cross-magnetosphere orbit	1	0.20 %
Equatorial orbit	1	0.20 %
Total	505	

Table A.3.: Propulsion types in use on LEO for considered satellites

Propulsion type	Mission number	Percentage of total
Unknown	282	55.84 %
Chemical propulsion (Monopropellant)	112	22.18 %
None	55	10.89 %
Electric propulsion	36	7.13 %
Chemical propulsion (Bipropellant)	11	2.18 %
Cold gas propulsion	6	1.19 %
Chemical (Monopropellant) + Electric	2	0.40 %
Chemical (Monopropellant) + Cold gas	1	0.20 %
Total	505	

Table A.4.: Mission propulsion use on LEO for considered satellites

Propulsion use	Mission number	Percentage
Orbit control	159	92.98 %
Maintenance	72	42.11 %
Attitude control	36	21.05 %
Manoeuvres	36	21.05 %
Number of propulsion systems	171	

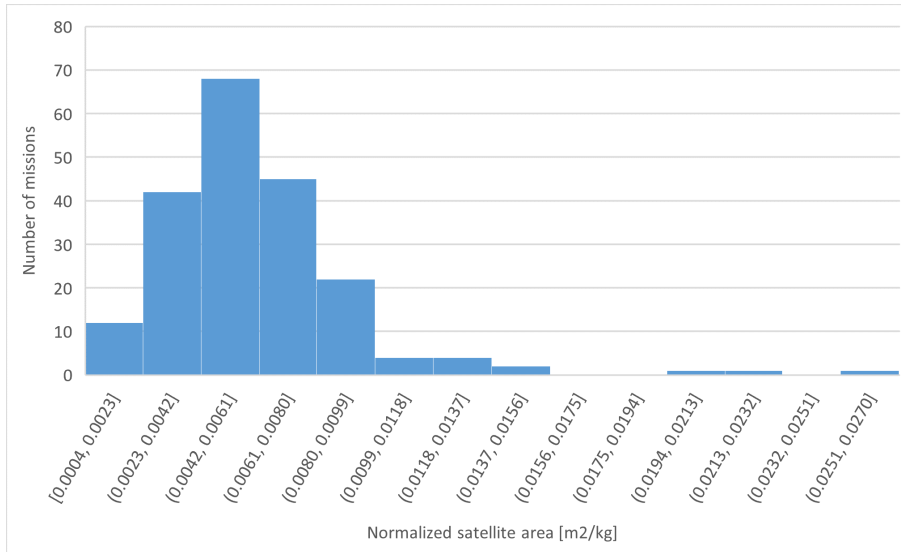


Figure A.1.: Distribution of satellite normalized area on LEO

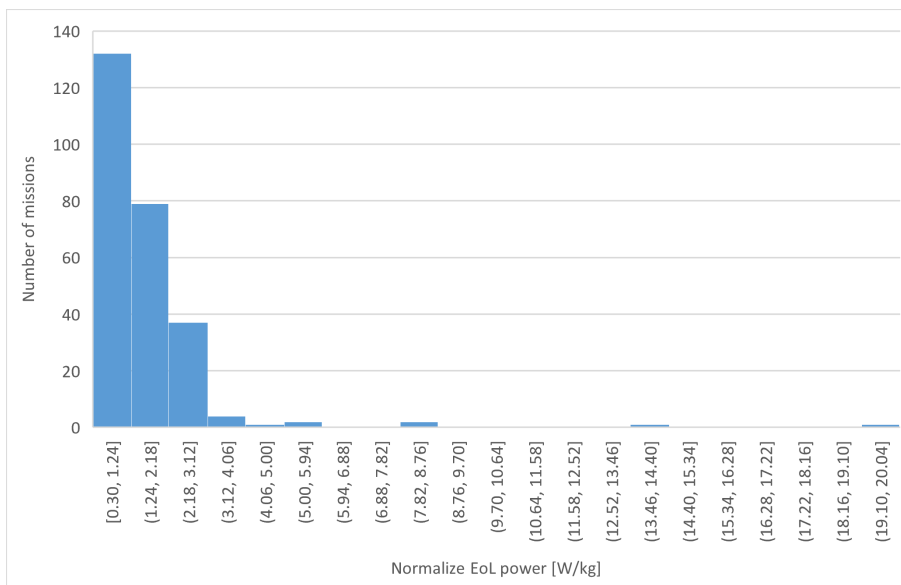


Figure A.2.: Distribution of satellite normalized EoL power on LEO

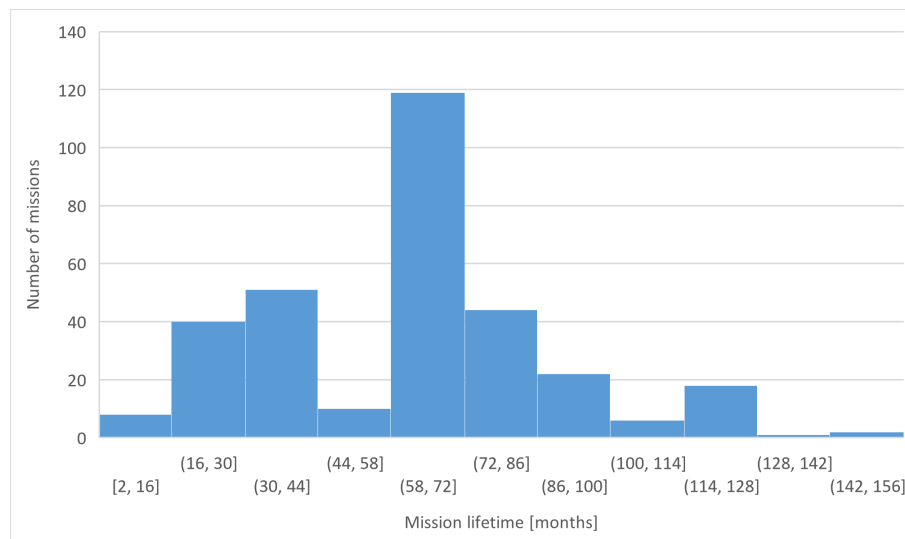


Figure A.3.: Distribution of satellite lifetime on LEO